

**ADSORPTION AND PHOTOCHEMICAL TRANSFORMATIONS OF  
POLYCYCLIC AROMATIC HYDROCARBONS ON  
ATMOSPHERIC WATER FILMS**

A Dissertation

Submitted to the Graduate Faculty of the  
Louisiana State University and  
Agricultural and Mechanical College  
in partial fulfillment of the  
requirements for the degree of  
Doctor of Philosophy

in

The Department of Chemical Engineering

by  
Jing Chen  
B.S., Fudan University, Shanghai, China, 2003  
August 2008

## **ACKNOWLEDGMENTS**

I would like to express my deep and sincere gratitude to my major advisor, Dr. Kalliat T. Valsaraj, for his insightful guidance and full support. Without his continuous support and encouragement this work would not have been possible.

I would like to thank Dr. Mary Julia Wornat, Dr. Kerry M. Dooley, Dr. Karsten E. Thompson, Dr. Francisco R. Hung, Dr. Evgueni E. Nesterov, and Dr. Yijun Xu for serving in my graduate committee. I would also like to thank Dr. Wornat for giving me valuable suggestions and insights into this project.

I would like to thank Dr. Ravikrishna and Dr. Raja for sharing with me their expertise and experience. I would like to thank Paul Rodriguez and Joe Bell for helping me with the design and construction of the reactor. I would like to thank my collaborator, Franz Ehrenhauser, for insightful discussion on this project. I would also like to thank all my colleagues in the group for providing a comfortable and friendly environment for my research.

My special thanks to my mother CHEN Huifang, my father CHEN Yuping, and my husband DENG Xiong for their unconditional love. I would also like to thank my 5-year-old nephew CHEN Zhuoyang for being a lovely child.

I would like to acknowledge the funding provided by the National Science Foundation (ATM 0355291).

# TABLE OF CONTENTS

ACKNOWLEDGMENTS .....	ii
LIST OF TABLES .....	vi
LIST OF FIGURES .....	vii
ABSTRACT.....	x
CHAPTER 1	
INTRODUCTION .....	1
1.1 Polycyclic Aromatic Hydrocarbons.....	1
1.2 Atmospheric Water Films.....	3
1.3 Chemodynamic Behavior of PAHs at the Air-Water Interface in the Atmosphere .....	6
1.4 Adsorption of PAHs at the Air-Water Interface in the Atmosphere .....	7
1.5 Photooxidation of PAHs at the Air-Water Interface in the Atmosphere.....	9
1.6 Model PAHs Chosen for This Study .....	10
1.7 Dissertation Overview .....	11
CHAPTER 2	
EXPERIMENTAL SETUP.....	13
2.1 Basic Experimental Setup.....	13
2.1.1 Flow-Tube Photo-Reactor .....	15
2.1.2 PAH Vapor Generator .....	16
2.1.3 Online GC-MS .....	17
2.2 Analytical Apparatus for Sample Analysis .....	17
CHAPTER 3	
ADSORPTION OF PAHS AT THE AIR-WATER INTERFACE .....	19
3.1 Introduction .....	19
3.2 Adsorption of Naphthalene on Thin Water Films .....	21
3.2.1 Experimental Section .....	22
3.2.2 Results and Discussion.....	23
3.2.2.1 Data Analysis.....	23
3.2.2.2 Effect of Water Film Thickness on Partitioning to the Film .....	25
3.2.2.3 Effect of Temperature on Uptake into the Film.....	27
3.3 Adsorption of Phenanthrene on Thin Water Films.....	29
3.3.1 Experimental Section .....	29
3.3.1.1 Interfacial Partitioning at the Air-Water Interface.....	29
3.3.1.2 Measurement of Henry's Law Constant .....	30
3.3.1.3 Sample Analysis in HPLC .....	31
3.3.2 Results and Discussion.....	31
3.3.2.1 Equilibrium Uptake of Gas-Phase Phenanthrene on Water Films.....	31
3.3.2.2 Effect of Water Film Thickness on Partitioning to the Film .....	32
3.4 Molecular Dynamics Simulation .....	33
3.4.1 Systems and Computational Method.....	34

3.4.2 Computational Results .....	35
3.4.3 Comparison of Computational Results and Experimental Observations .....	38
CHAPTER 4	
EFFECTS OF DISSOLVED SURFACTANTS ON PAH ADSORPTION AT THE	
AIR-WATER INTERFACE .....	41
4.1 Introduction .....	41
4.2 Experimental Section.....	42
4.2.1 Materials.....	42
4.2.2 Adsorption of PAHs on Thin Water Films Containing Surfactants.....	42
4.2.3 Surface Tension of SRFA Solutions .....	43
4.3 Results and Discussion .....	44
4.3.1 Surface Excess of SRFA .....	44
4.3.2 Uptake of Naphthalene into Surfactant Films .....	46
4.3.3 Adsorption of Phenanthrene on Surfactant Films .....	48
CHAPTER 5	
UV PHOTO-OXIDATION OF GAS-PHASE NAPHTHALENE ON ATMOSPHERIC WATER	
FILMS.....	50
5.1 Introduction .....	50
5.2 Photooxidation of Naphthalene on Pure Water Films .....	51
5.2.1 Experimental Section .....	51
5.2.2 Results and Discussion.....	53
5.2.3 Atmospheric Implications .....	60
5.3 Photooxidation of Naphthalene on Surfactant Aqueous Films .....	61
5.3.1 Experimental Section .....	63
5.3.1.1 Photooxidation of Naphthalene.....	63
5.3.1.2 Light Absorption by SRFA.....	64
5.3.1.3 Fluorescence Measurements .....	64
5.3.2 Results and Discussion.....	65
5.3.2.1 Photochemical Reactions of Naphthalene in SRFA Aqueous Films .....	65
5.3.2.2 Photochemical Reactions of Naphthalene in SDS Aqueous Films.....	76
5.3.3 Atmospheric Implications .....	78
CHAPTER 6	
UV PHOTO-OXIDATION OF GAS-PHASE PHENANTHRENE ON ATMOSPHERIC	
WATER FILMS.....	79
6.1 Introduction .....	79
6.2 Experimental Section.....	79
6.2.1 Photooxidation of Phenanthrene on Thin Aqueous Films .....	79
6.2.2 Measurement of Singlet Oxygen.....	80
6.2.3 Photooxidation of Phenanthrene on Aqueous Films Containing D <sub>2</sub> O .....	80
6.2.4 Sample Analysis.....	80
6.3 Results and Discussion .....	81
6.3.1 Photochemical Reactions of Phenanthrene on Thin Aqueous Films .....	81
6.3.2 Effect of Film Thickness on Reaction Rates.....	83
6.3.3 Effect of SRFA on Reaction Rates.....	84
6.3.4 Photooxidation Pathways of Phenanthrene .....	87

6.3.5 Comparison of Reaction Rates via Radical Cations, $^1\text{O}_2$ , and $\cdot\text{OH}$ .....	90
6.4 Conclusions .....	91
CHAPTER 7	
SUMMARY AND RECOMMENDATIONS FOR FUTURE RESEARCH .....	93
7.1 Summary.....	93
7.2 Recommendations for Future Work .....	95
REFERENCES .....	96
APPENDIX I SUPPORTING INFORMATION FOR SECTION 5.3.2 .....	107
APPENDIX II COPYRIGHT PERMISSION FOR PUBLISHED MATERIAL .....	110
VITA.....	112

## LIST OF TABLES

<b>Table 1.1.</b> Physicochemical properties of naphthalene and phenanthrene.....	11
<b>Table 3.1.</b> Literature values of the physico-chemical properties of naphthalene.....	22
<b>Table 3.2.</b> Experimental and literature values of air-water partition constants for naphthalene at 293K.....	26
<b>Table 3.3.</b> Literature values of the physico-chemical properties of phenanthrene.....	29
<b>Table 3.4.</b> Experimental and literature values of air-water partition constants for phenanthrene at 296K.....	33
<b>Table 3.5.</b> Aqueous bulk concentrations and the highest and averaged values in the interfacial region, compared to the gas phase value (normalized to 1.0).....	38
<b>Table 4.1.</b> Physicochemical properties of SRFA and SDS.....	43
<b>Table 4.2.</b> Bulk and Interface Air-water Partition Constants of Phenanthrene.....	49
<b>Table 5.1.</b> Kinetic rate constants for product formation in water films in the reactor.....	58
<b>Table 5.2.</b> Kinetic rate constants for product formation in SRFA solution films and pure water films.....	67
<b>Table 5.3.</b> Parameters obtained by fitting the formation rate constant data to Eqn. 5.13.....	73
<b>Table 6.1.</b> Observed Product Formation Rate Constants in Water Films (T=296 K).....	85

## LIST OF FIGURES

<b>Figure 1.1.</b> Typical structures of PAHs.....	2
<b>Figure 1.2.</b> Average contributions of various organic compound classes to the total dissolved organic carbon (DOC) contents of fog water collected in Baton Rouge and Houston.....	5
<b>Figure 1.3.</b> Physicochemical processes occurring at the air-water interface.....	7
<b>Figure 2.1.</b> Schematic of the horizontal flow-tube photo-reactor and ancillaries used for carrying out the adsorption and photooxidation experiments.....	14
<b>Figure 2.2.</b> Cross-sectional view of the flow-tube photo-reactor assembly.....	15
<b>Figure 2.3.</b> In-line stainless steel tube mixer.....	17
<b>Figure 2.4.</b> Two-position 6-port valve.....	18
<b>Figure 3.1.</b> Equilibrium partition relationships between the interface and the bulk phases.....	20
<b>Figure 3.2.</b> MS signal of naphthalene for the two cases involving control and water film experiments.....	24
<b>Figure 3.3.</b> The effect of water film thickness on the partition constant for naphthalene.....	26
<b>Figure 3.4.</b> The effect of temperature on naphthalene partitioning to the thin water film. The thickness of the water film was 150 $\mu\text{m}$ .....	28
<b>Figure 3.5.</b> Uptake of phenanthrene from the gas phase on aqueous films with varying thicknesses.....	33
<b>Figure 3.6.</b> Potential of mean force for moving benzene through an aqueous slab defined via the water density profile.....	36
<b>Figure 3.7.</b> Potential of mean force for moving naphthalene through an aqueous slab defined via the water density profile.....	36
<b>Figure 3.8.</b> Potential of mean force for moving anthracene through an aqueous slab defined via the water density profile.....	37
<b>Figure 3.9.</b> Potential of mean force for moving phenanthrene through an aqueous slab defined via the water density profile.....	37
<b>Figure 3.10.</b> Comparison of the experimental and MD-simulated free energy of adsorption from the gas phase for benzene, naphthalene and phenanthrene.....	40

<b>Figure 4.1.</b> Surface tension change of the aqueous solution of SRFA. Also shown is the surface excess of SRFA at the air-water interface fitted to a Langmuir isotherm.....	45
<b>Figure 4.2.</b> Uptake of naphthalene from the gas phase on an aqueous film (450 $\mu\text{m}$ ) with different surfactant (SRFA and SDS) concentrations.....	47
<b>Figure 4.3.</b> Uptake of phenanthrene from the gas phase on aqueous films with varying thicknesses.....	49
<b>Figure 5.1.</b> Detailed HPLC trace of the aqueous film sample after 16 h exposure to UV light...54	
<b>Figure 5.2.</b> Mechanisms for the formation of main products identified in the HPLC trace of the aqueous film samples.....	54
<b>Figure 5.3.</b> Photooxidation of naphthalene vapor on a 450 $\mu\text{m}$ water film.....	57
<b>Figure 5.4.</b> Photooxidation of naphthalene vapor on a 22 $\mu\text{m}$ water film.....	57
<b>Figure 5.5.</b> Effect of SRFA on the observed formation rate constants for phthalide and coumarin in a 450 $\mu\text{m}$ aqueous film.....	68
<b>Figure 5.6.</b> Mechanistic interpretation of naphthalene oxidation by singlet oxygen via (a) self-sensitized and (b) SRFA-sensitized pathways.....	69
<b>Figure 5.7.</b> Fluorescence excitation spectrum of SRFA (4.4 $\text{mg}\cdot\text{L}^{-1}$ , detection emission wavelength: 432 nm) and fluorescence emission spectrum of naphthalene (6.5 $\text{mg}\cdot\text{L}^{-1}$ , excited at 286.5nm).....	72
<b>Figure 5.8.</b> Effect of SRFA on the observed formation rate constants for phthalide and coumarin in a 22 $\mu\text{m}$ aqueous film.....	75
<b>Figure 5.9.</b> Effect of SDS on the observed formation rate constants for phthalide and coumarin in a 450 $\mu\text{m}$ aqueous film.....	77
<b>Figure 6.1.</b> HPLC trace of a 515 $\mu\text{m}$ aqueous film sample after 12 hours exposure to UV light.82	
<b>Figure 6.2.</b> Accumulation of the three main photooxidation products of phenanthrene in a 515 $\mu\text{m}$ water film.....	82
<b>Figure 6.3.</b> Effect of film thickness on the observed formation rate constants of 9,10-phenanthrenequinone, 3, 4-benzocoumarin, and 9-fluorenone.....	85
<b>Figure 6.4.</b> Effect of SRFA on the observed formation rate constants of 9, 10-phenanthrenequinone, 3, 4-benzocoumarin, and 9-fluorenone in a 515 $\mu\text{m}$ aqueous film.....	86
<b>Figure 6.5.</b> Scheme of photooxidation pathways of PAHs in the $\text{O}_2/\text{H}_2\text{O}$ system.....	87

**Figure 6.6.** Observed formation rate constants of 9, 10-phenanthrenequinone, 3,4-benzocoumarin, and 9-fluorenone in 515  $\mu\text{m}$  100%  $\text{H}_2\text{O}$ , 50/50  $\text{H}_2\text{O}/\text{D}_2\text{O}$ , and 100%  $\text{D}_2\text{O}$  films.....89

## ABSTRACT

Atmospheric water films affect the processing of chemicals in the atmosphere and have potential effects on human health and the environment. In this work, adsorption and photochemical transformations of gas-phase PAHs were studied in a flow-tube photo-reactor with a view to understanding the behavior of gas-phase PAHs occurring in thin water films such as those of aerosols and fog. Naphthalene and phenanthrene were chosen as model PAHs for this study.

Bulk water-air and air-to-interface partition constants of naphthalene and phenanthrene were estimated from the experiments based on the dependence of the equilibrium uptake on the water film thickness. Theoretical computations of molecular dynamics (MD) of PAHs showed a deep free energy minimum at the air-water interface for PAHs entering water phase from the air. The MD-simulated hydration free energy was in agreement with experimental data.

Suwannee River fulvic acid (SRFA) was chosen as a surrogate for the surface active substances present in atmospheric water films. The effect of SRFA in the aqueous phase on the equilibrium partitioning of PAHs to the air-water interface were investigated. To compare with SRFA, the effect of a conventional surfactant, sodium dodecyl sulfate, was also studied.

Several photooxidation products of naphthalene and phenanthrene were identified in the water films and the mechanism of photooxidation was assessed. The effect of singlet oxygen on PAH photooxidation was ascertained. The photooxidation of PAHs can be very complex, especially for PAHs with several aromatic rings. It was proposed that phenanthrene photodegraded via three different pathways: through radical cation intermediates, via reaction with singlet oxygen, and via reaction with hydroxyl radical. The reaction rate constants were also

determined and were substantially higher in the thin water film as compared to the bulk phase reaction.

Effects of SRFA on the photooxidation of naphthalene and phenanthrene were investigated to give insight into the photooxidation process of PAHs in fog droplets in which surface active compounds are present. The presence of SRFA in the water led to multiple effects on the rate of reaction. These were characterized via a dual mechanism of self-sensitized and surfactant-sensitized pathways for reaction.

# CHAPTER 1

## INTRODUCTION

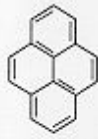
### 1.1 Polycyclic Aromatic Hydrocarbons

Polycyclic aromatic hydrocarbons (PAHs) are a class of very stable organic molecules built up of fused aromatic rings. They range from the basic 2-ring naphthalene to multi-ring compounds of very large molecular weight. Figure 1.1 shows some typical structures of PAHs. PAHs are ubiquitous contaminants in the environment. They are the most abundant class of carbon-bearing compounds in the universe [1]. PAHs are a standard survivor of incomplete combustion of almost any kind of organic material. They arise from a variety of sources including fossil fuel combustion, biomass burning, coal gasification, smelting operations, petroleum cracking, forest fires, volcanic eruptions and even organism biosynthesis [2]. PAHs are one group of the main components of anthropogenic emissions and industrial wastes. Worldwide total concentrations of PAHs in air vary from 0.01 to 100 ng.m<sup>-3</sup> and exhibit a linear increase with human population, indicating their anthropogenic origin [3].

PAHs are hydrophobic and they accumulate in organic rich environments such as lipids, aerosols, and soil particles [4]. Most of the PAHs have very low vapor pressure but high aqueous activity coefficients. PAHs and their derivatives comprise half of all known carcinogens [5]. Many PAHs exhibit carcinogenic, mutagenic, or teratogenic activities. It is also suspected that oxidation products of PAHs are more toxic than the parent molecules [6]. Hence, studying the chemodynamics behavior and fate of PAHs in the environment has become an important topic of research.

# PAH Structures

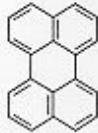
## Pericondensed



Pyrene  
 $C_{16}H_{10}$



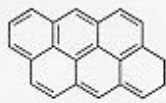
Coronene  
 $C_{24}H_{12}$



Perylene  
 $C_{20}H_{12}$



Benzo[ghi]perylene  
 $C_{22}H_{12}$

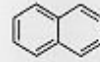


Antanthrene  
 $C_{22}H_{12}$

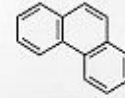


Ovalene  
 $C_{32}H_{14}$

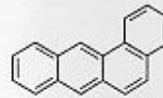
## Catacondensed



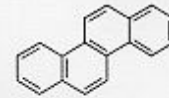
Naphthalene  
 $C_{10}H_8$



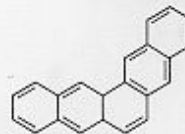
Phenanthrene  
 $C_{14}H_{10}$



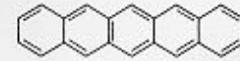
Tetraphene  
 $C_{18}H_{12}$



Chrysene  
 $C_{18}H_{12}$



Pentaphene  
 $C_{22}H_{14}$



Pentacene  
 $C_{22}H_{14}$

**Figure 1.1.** Typical structures of PAHs.

## 1.2 Atmospheric Water Films

Field measurements have shown significant fractions of hydrophobic organic compounds (PAHs, pesticides) in fog droplets and ice surfaces in the atmosphere [7-9]. Fogs are formed by condensation of water vapor onto an aerosol particle that serves as a cloud condensation nucleus (CCN). Sizes of fog droplets range from a few micrometers to several tens of micrometers [10]. The chemical compositions of particles acting as CCN determine the initial compositions of fog droplets, which can be further altered by uptake of soluble gases and by aqueous phase chemical reactions. As fog droplets settle to the ground, the pollutants contained within them are deposited. This is termed “wet deposition”. Some of the aqueous droplets that do not undergo wet deposition evaporate and leave behind a portion of the scavenged pollutants on residual aerosol particles that could undergo dry deposition. The enhancement of fog formation by high aerosol concentrations, followed by the growth of these aerosol particles during fog processing, has been referred to as a smog-fog-smog cycle [9]. In a collaborative work undertaken by our group and the research group directed by Prof. Collett of the Department of Atmospheric Science of Colorado State University, fog water from several fog episodes in two different Gulf Coast regions, Baton Rouge and Houston, were collected and analyzed. Figure 1.2 shows the organic composition of fog water samples collected from the two sampling sites. A considerable amount of PAHs have been detected in the fog water samples from both sampling sites. PAHs detected include naphthalene, phenanthrene, 9-10 anthracenedione and other methyl derivatives of naphthalene [9].

Deviations from Henry’s Law of gas-water partitioning have been observed for hydrophobic organic compounds in fog droplets. Earlier work by a number of investigators shows that large composition differences exist in fog droplets of varying sizes [11-13]. Hydrophobic organic compounds tend to accumulate in fog droplets as their sizes decrease.

Since the ratio of surface area to bulk volume of fog droplets increases as their sizes decrease, it is suggested that deviations from Henry's Law for hydrophobic organic compounds in fog droplets and ice surfaces in the atmosphere result from the accumulation of hydrophobic organic compounds at the gas-water interface [14].

Water films on aerosol particles and in the form of atmospheric droplets (fog, rain, and mist) have been known to affect the processing of organic compounds in the atmosphere [15, 16]. Uptake of gas-phase chemicals takes place on atmospheric water films and the uptake depends on the air-to-interface partition constant of the compound, its hydrophobicity and the presence of other surface-active compounds in thin films. In a recent work, Sumner et al [17] summarized the interactions of thin films of water with various substrates of atmospheric interest and showed that on most surfaces water films can support a variety of heterogeneous reactions. Reactions that occur at very low rates in the homogeneous gas phase are known to proceed much faster on film surfaces via heterogeneous processes [18], for which the determining factor is the concentration of compounds in thin films. Reactions of organic vapors on the surface of thin films can also lead to the production of secondary organic aerosols (SOA) [19]. A major fate process for chemicals in both bulk and interface regions is the photochemical reaction initiated by solar UV radiation. For example, during a smog-fog-smog cycle, photoreactions on water films can be driven by UV light and transform the chemicals contained in fog droplets. Then the photo-transformation products are either released to the atmosphere or remain with the particles left behind in the smog. There have also been recent reports on the photochemistry of several compounds in ice and snow [20-22].

In order to improve our understanding of PAH processing occurring on atmospheric water films and the potential effects on human health and the environment, the interfacial behavior of PAHs at the air-water interface in the atmosphere was investigated in this work.

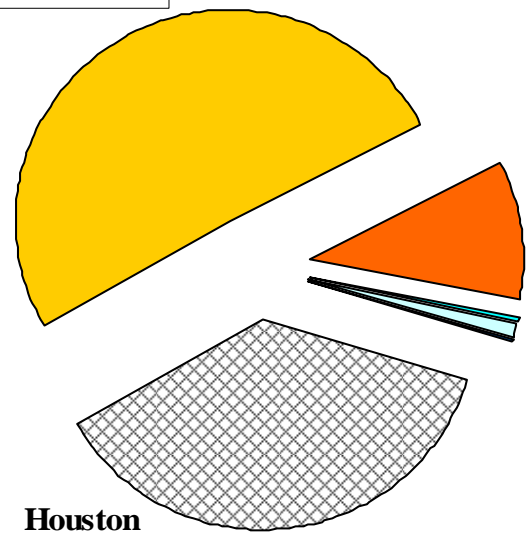
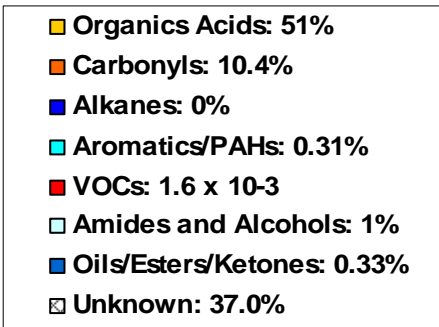
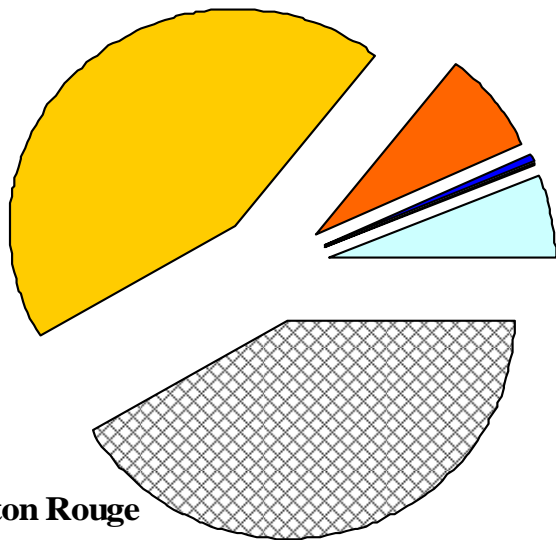
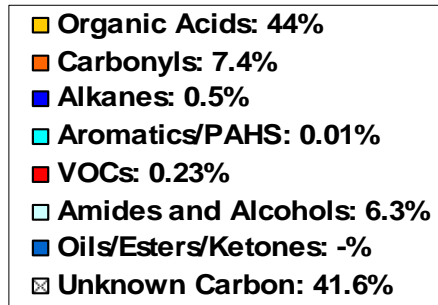


**Figure 1.2.** Average contributions of various organic compound classes to the total dissolved organic carbon (DOC) contents of fog water collected in Baton Rouge and Houston. Data obtained from Raja et al [9].

### **1.3 Chemodynamic Behavior of PAHs at the Air-Water Interface in the Atmosphere**

PAHs in the atmosphere exist as gases, or are adsorbed onto aerosols or dust particles. The aerosols are composed of solid particles and liquid water as thin films. PAHs can be distributed between the solid and liquid phases of the aerosols. PAHs are considered persistent organic pollutants since they do not degrade easily in the environment unless external stimuli are given. The extensive  $\pi$ -orbital systems of PAHs allow them to absorb sunlight in the visible (400 – 700 nm) and the ultraviolet (290-400 nm) range of the solar spectrum [23]. As a result, they undergo numerous photochemical reactions initiated by solar radiation. PAHs are hydrophobic and of low vapor pressure and they also display a tendency to adsorb at soil-water, sediment-water, and the air-water interfaces in the environment.

A number of important transport and transformation processes occur at the air-water, air-soil, and water-soil interfaces in the atmosphere. This work focuses on the transport and photochemical transformation characteristics of PAHs at the air-water (fog and ice) interface. The air-water interface, including both bulk air-bulk water interface and bulk air-water dispersoid (rain, fog, mist, snow, ice, and aerosol) interface, is the largest interface in the atmosphere. Figure 1.3 shows an outline of the main physicochemical processes concerning PAHs that occur at this interface.

As shown in Figure 1.3, two major processes occur at the air-water interface: mass partitioning and photochemical reactions. Under the specific conditions (air-fog or air-ice) that we are interested in, the ratio of surface area to bulk volume for the water phase can be quite large. As a result, the interfacial effects become significant for the transport and reactions of PAHs. At ambient and sub-ambient temperatures the adsorption of PAHs at the air-water interface is considerable and the concentration at the interface is much higher than that in the

bulk phase for high surface area dispersoids [24]. Since surface reaction rate is proportional to the number of moles on the surface, the heterogeneous photochemical reactions of PAHs initiated by solar UV radiation become more noticeable in these cases.

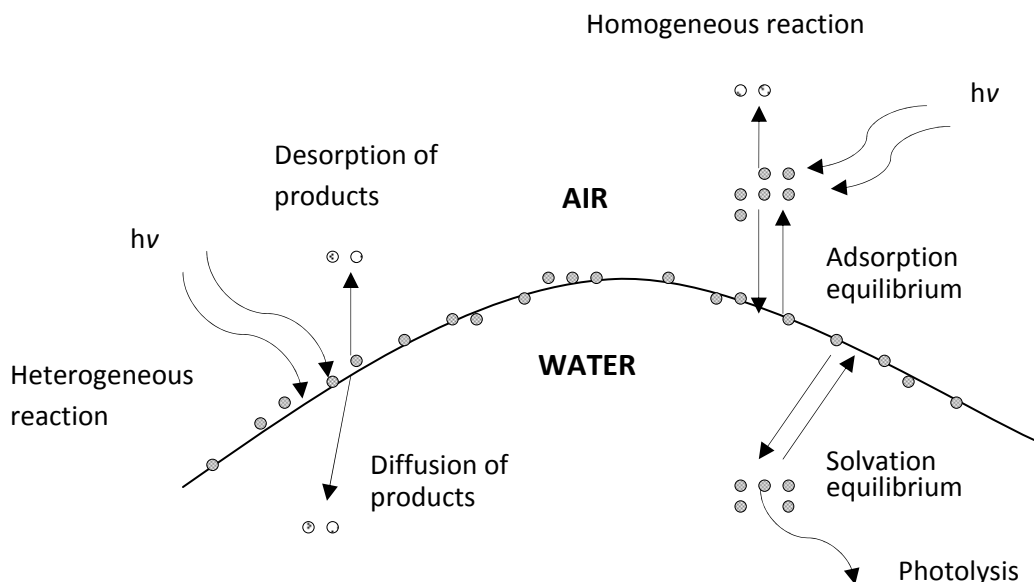


**Figure 1.3.** Physicochemical processes occurring at the air-water interface.

#### 1.4 Adsorption of PAHs at the Air-Water Interface in the Atmosphere

Theoretical computations of molecular dynamics at interfaces have shown that a free energy minimum exists at the air-water interface for most organic molecules entering water phase from its vapor state [25]. In other words, there exists a free energy barrier to the desorption of most organic compounds from the air-water interface to the bulk water and the chemical species tend to concentrate at the interface. The amount of the chemical species increases till the chemical potentials at the interface and in the bulk water are equal (Eqn. 1.1).

$$\mu_w^0 + RT \ln C_w = \mu_l^0 + RT \ln C_l \quad \text{Eqn. 1.1}$$

In Eqn. 1.1,  $\mu_l^0$  and  $\mu_w^0$  denote the standard-state chemical potential at the interface and in the bulk water respectively;  $C_w$  is the concentration in the water phase and  $C_l$  is the

concentration at the interface. Rearranging Eqn. 1.1, we obtain the equilibrium surface concentration at the interface as shown in Eqn. 1.2:

$$C_I = C_W \exp\left(\frac{\mu_W^0 - \mu_I^0}{RT}\right) \quad \text{Eqn. 1.2}$$

As mentioned above, a free energy minimum exists at the interface, which means  $\mu_W^0 > \mu_I^0$ . Therefore,  $C_I > C_W$  as determined by Eqn. 1.2. Adsorption of organic vapors to thin water films have been conducted since the 1920s [26-30]. Davidovits and co-workers proposed a “critical cluster” model to explain the dynamics of the entry of molecules from the gas phase to the water phase [31]. According to this model, gas-water interface is a dynamic region where aggregates are continually forming, dissipating, and reforming. As gas molecules enter this region, they are adsorbed at the interface and are interconnected or bound to the aqueous phase by various configurations and aggregations. When the cluster reaches a critical size, the gas molecules are finally incorporated into the bulk solution phase. The number of molecules required to form the cluster depends on the structure of the specific molecule undergoing the adsorption process.

Due to the accumulation of hydrophobic organic molecules at the interface, it is hypothesized that deviations from Henry’s law for hydrophobic organic compounds in fog-water and cloud-water samples are attributed to the interfacial adsorption phenomena. Partitioning of PAHs between air and water has been well investigated and reported in the literature, however, most of the research is concerned with bulk phase partitioning. Only recently has the behavior of PAHs at the gas-water interface been a focus of attention [32]. In this work, adsorption of PAHs on atmospheric water films was studied to give insight into the behavior of PAHs in a foggy environment.

## 1.5 Photooxidation of PAHs at the Air-Water Interface in the Atmosphere

Bulk phase photochemical reactions of dissolved PAH compounds with OH radicals generated by UV radiation are well documented and result in ring cleavage [33, 34]. Generally, PAHs are stable due to their delocalized  $\pi$ -electron cloud and large resonance energies. In spite of their intrinsically low chemical reactivities, PAHs strongly absorb UV light (300-420nm) and undergo numerous photochemical reactions. The photoreactions of PAHs can be broadly classified into two categories: (i) homogeneous reactions in bulk phases (air, water), and (ii) heterogeneous reactions involving adsorbed PAHs. Homogeneous photoreactions of PAHs have been widely studied, among which the reactions of PAHs with oxygen or ozone in the presence of UV radiation is the most extensively studied [35-38]. Beltran and co-workers investigated the reactions of PAHs dissolved in water under four different conditions (UV radiation, ozonation, oxidation by UV radiation combined with hydrogen peroxide, oxidation by ozone combined with hydrogen peroxide) and reported their kinetics and reaction products [35-37]. Photoreactions of PAHs and alkanes have also been studied under conditions relevant to the prebiotic Earth and the interstellar medium where carbon-carbon bonds have been found to form in the photochemical alkylation of PAHs [39]. Although there are a large number of studies on homogeneous photoreactions of PAHs, there is surprisingly little data on the photooxidation of PAHs under environmentally relevant conditions. Some PAH photoproducts have been obtained using light sources containing high levels of UVC (<280 nm), which is not present in sunlight. McConkey et al [40] studied the photooxidation of naphthalene in aqueous solution under natural sunlight and determined its photooxidation pathway, but not the kinetics of product formation. Some of the products of UV photolysis are often more toxic than the parent compound [40, 41]. The photolysis of PAH compounds adsorbed to ice and water-ice is also reported in the literature [42].

There is some evidence that under stratospheric conditions PAHs react to form higher molecular weight proteinaceous compounds [39].

The presence of thin water films, or so-called “adlayers”, on particulates in the atmosphere opens up the possibility of reactions occurring on the water surface, via adsorption of reactive gases onto the water film; within the water layer, via dissolution of reactive compounds into the condensed phase; and at the solid/water interface. Thus, the presence of water can potentially influence the reactivity at the surface of the aerosol and the extent to which it is able to participate in heterogeneous atmospheric reactions. Recent studies indicate that even small amounts of strongly bound surface adsorbed water may play a critical role in the interaction of gases with surfaces traditionally presumed to be solids [17]. Compared to gas-phase homogeneous photoreactions, data on heterogeneous photoreactions of PAHs are sparse, especially those at the air-water interface. Mmereki and Donaldson detailed the first study of heterogeneous chemical reactions of PAHs with ozone at the air-aqueous interface [43, 44]. There is, however, a lack of data on the photochemical reactivity of PAHs in thin films of water under ambient conditions of temperature and pressure. Hence, this work was undertaken to understand the adsorption and photochemical reactivity of PAHs on atmospheric water films under simulated sunlight conditions.

## **1.6 Model PAHs Chosen for This Study**

Two Model PAHs were chosen to study the adsorption and photochemical transformation processes at the air-water interface under environmentally relevant conditions, namely, naphthalene and phenanthrene. The reason for choosing these two compounds is that they stay mainly in the gas phase in the atmosphere at 25°C thus facilitating our study on their air-water interfacial behavior. Most of the other PAHs, such as benzo[a]pyrene and coronene, have relatively low vapor pressure and are present predominantly in the solid phase under ambient

conditions [5]. Table 1.1 shows some of the physicochemical properties of naphthalene and phenanthrene.

**Table 1.1.** Physicochemical properties of naphthalene and phenanthrene [45].

Compound	Molecular Weight	Melting Point, °C	Vapor Pressure, Pa at 25°C	Aqueous Solubility, $\mu\text{g}\cdot\text{L}^{-1}$	$\log K_{ow}^a$
Naphthalene	128.16	80.5	10.4±0.2	31,700	3.36
Phenanthrene	178.22	100.5	$(1.6\pm 0.04)\times 10^{-2}$	1,290	4.57

a.  $K_{ow}$  is the octanol-water partition constant and it is a measure of the “hydrophobicity” of a compound.

## 1.7 Dissertation Overview

The objective of this work is to study the transport and photochemical transformations of PAHs at the air-water interface in the atmosphere with a view to understanding the behavior of PAHs on thin atmospheric water films such as those of aerosols and fog.

In Chapter 2, the basic experimental setup used throughout our adsorption and photo-oxidation experiments, the flow-tube photo-reactor, is described in detail. Description of the analytical apparatus used for analyzing photo-oxidation products of PAHs is also given.

Chapters 3 and 4 describe the adsorption behavior of PAHs on thin water films, with Chapter 3 focusing on the adsorption of PAHs on pure water films and Chapter 4 on water films containing surfactants Suwannee River fulvic acid (SRFA) and sodium dodecyl sulfate (SDS). Partition constants of naphthalene and phenanthrene at the air-water interface on water films with and without surfactants are reported. The results of molecular dynamics (MD) simulations of the aqueous solvation of PAHs are given in Chapter 3 and comparison is made between the MD simulation results and the experimental results.

Chapters 5 and 6 describe the photo-oxidation processes of PAHs on thin water films under simulated sunlight conditions, with Chapter 5 focusing on naphthalene and Chapter 6 on

phenanthrene. Photooxidation products of both naphthalene and phenanthrene are reported and possible reaction mechanisms are given. Heterogeneous photoreactions of PAHs are revealed and comparison is made between the heterogeneous reactions taking place at the air-water interface and the homogeneous reactions in the bulk water phase. Effects of SRFA, a good surrogate for surface-active polycarboxylic acids found in fog waters, on the photooxidation of naphthalene and phenanthrene on water films are reported. Atmospheric implications of the results are also given.

The major conclusions of this work and recommendations for future work are given in Chapter 7.

## **CHAPTER 2**

### **EXPERIMENTAL SETUP**

#### **2.1 Basic Experimental Setup**

The adsorption and photochemical reactions of PAH vapor at the air-water interface of water films were studied in a horizontal flow-tube reactor. The flow-tube photo-reactor was constructed based on the conventional flow-tube assembly that is often employed in atmospheric chemistry for surface behavior study [46-48]. Currently, the techniques that are used to study interfacial behaviors are basically various forms of flow tube apparatus. Droplet-train flow reactor is among the types of flow tube reactors commonly used. Droplet-train flow reactor generally consists of a vertical flow tube in which droplets are generated and interact or react with the gas phase species passing through the reactor [49]. Sub-micron particles can be easily generated in the reactor thus interfacial study can be achieved. Interactions of solid or liquid surfaces with gas phase species can also be performed in a horizontal flow tube apparatus by coating the tube wall with the material of condense phase and introducing the gas phase species using a movable injector. The horizontal flow-tube reactor used in this work is constructed on the basis of this type of flow tube reactor. However, instead of coating water on the wall of the tube, a glass trough is employed on which the water film is coated. This way the cumbersome procedure of coating condense phase materials on tube walls is avoided. Also, by using a glass trough we can extend the water film thickness and easily switch between the surface study and bulk phase study. The schematic of the experimental apparatus is shown in Figure 2.1.

The experimental setup consists of three major components: the flow-tube photo-reactor, a PAH vapor generator and an online GC-MS.

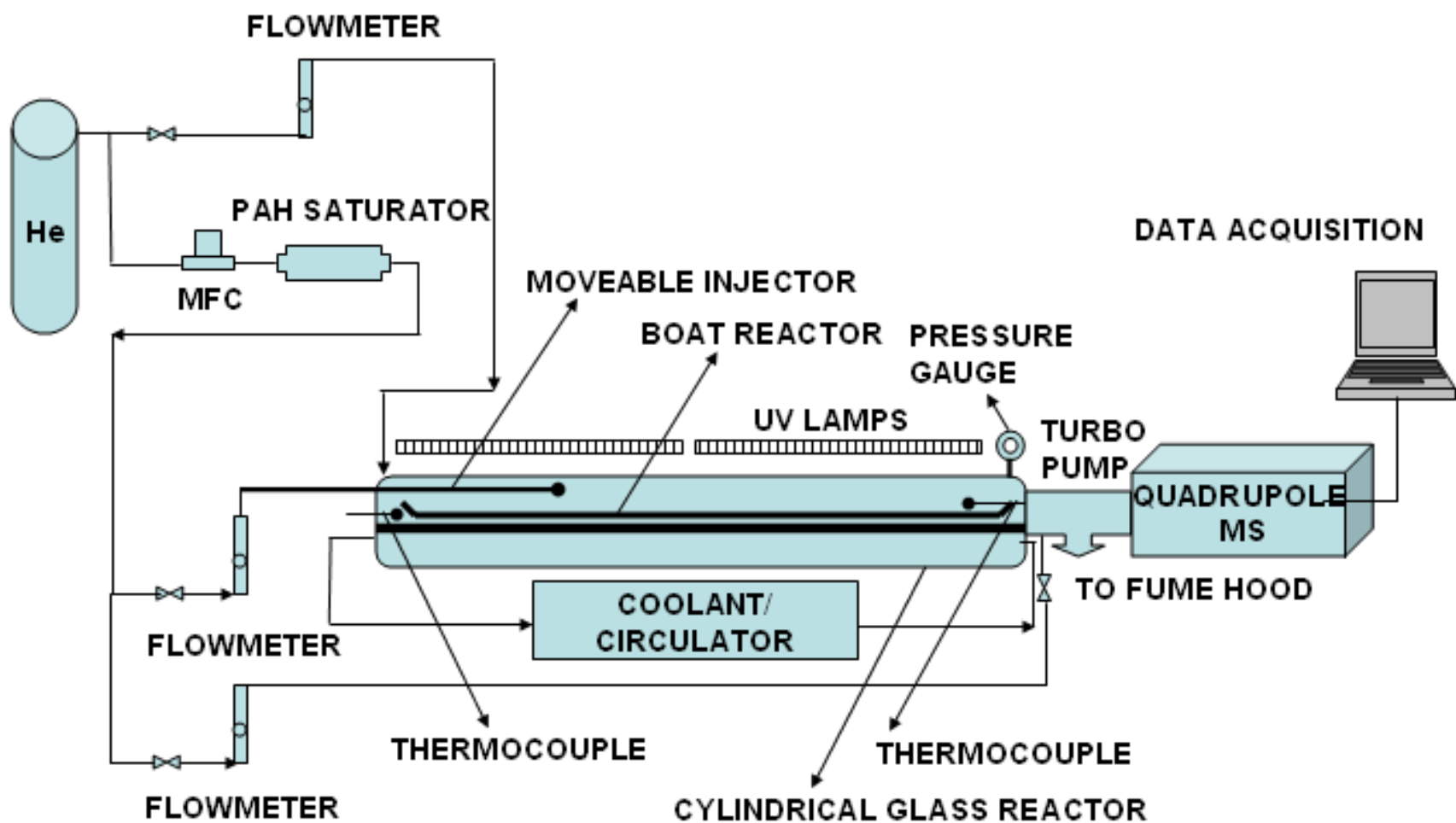


**Figure 2.1.** Schematic of the horizontal flow-tube photo-reactor and ancillaries used for carrying out the adsorption and photooxidation experiments.

### 2.1.1 Flow-Tube Photo-Reactor

The flow-tube photo-reactor assembly is comprised of a Pyrex tube, a rectangular borosilicate glass channel, a half-circular cooling tube and a removable aluminum block with UV lamps fixed inside of it. Figure 2.2 shows the cross-sectional view of the reactor assembly.

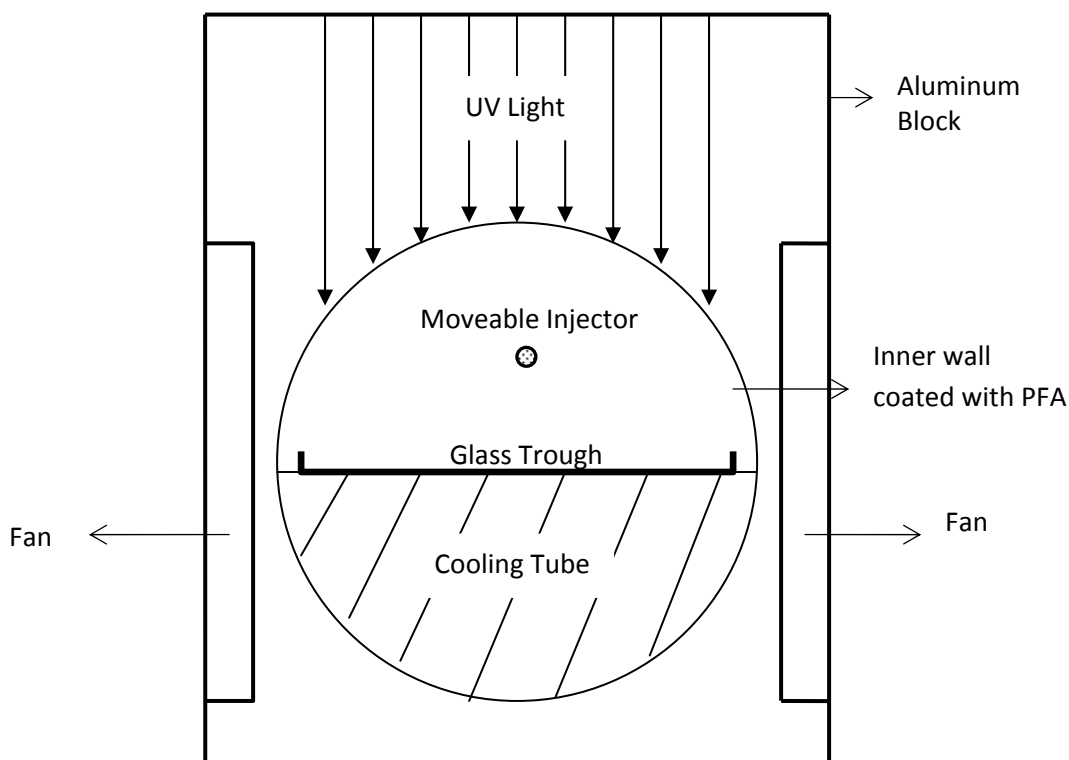


**Figure 2.2.** Cross-sectional view of the flow-tube photo-reactor assembly.

A thin film of water on which naphthalene was adsorbed and heterogeneous photochemical reactions took place was coated on the bottom surface of the low-edge glass trough (length 0.92 m, width 0.035 m, height 0.005 m, wall thickness 0.0018 m), which was obtained by cutting a rectangular borosilicate glass tubing (Wale Apparatus Co., Hellertown, PA) into halves. The temperature of the water film was maintained by the half-circular copper cooling tube that was placed under the glass trough. A fluid mixture of laboratory grade ethylene glycol (50%) and water (50%) was circulated through the cooling tube by a circulating bath (Model 12101-31, Cole-Parmer Co., Vernon Hills, Illinois) that is capable of controlling temperature in a range of

-30°C to 150°C. The glass trough and the cooling tube were both contained in the Pyrex tube (length 1m, O. D. 0.0508m, wall thickness 0.0032m, Chemglass, Vineland, NJ) through which two UV-B lamps (UVP Inc., Upland, CA) delivered UV light of appropriate wavelength (mid range,  $\lambda$  302nm). Two fans on the wall of the aluminum block circulated outside air into the block to keep the temperature of the air around the Pyrex reaction tube from getting too high when the UV-B lamps were turned on. Two thermocouples (copper-constantan, SS 304 sheath, 1/16" sheath diameter, Omega Engineering Inc., Stamford, Connecticut) embedded in the cooling tube were in contact with the bottom of the glass trough. They were used to measure the temperature of the water film.

### **2.1.2 PAH Vapor Generator**

The naphthalene vapor generator (naphthalene saturator), shown in Figure 2.1, was made of two serially connected tubular stainless steel columns (SS 316, 0.013m O. D., 0.37m long each), each of which was packed with 15 g of Chromosorb P (60/80 mesh size, acid washed, Supelco Inc., Bellefonte, PA)<sup>34</sup>. The Chromosorb P was coated with naphthalene (99.9% purity, Fisher Scientific Co., St. Louis, MO) by mixing it with naphthalene-hexane solution, and then evaporating hexane. The average loading obtained this way was about 0.02g naphthalene per gram of support. For phenanthrene, which has a lower vapor pressure than naphthalene, six serially connected tubular columns were needed to make the phenanthrene saturator. Each saturator column was packed with 15 g of Chromosorb P coated 10 percent by weight with phenanthrene. The coated packing was loaded into the vapor generation columns with glass wool on both ends of the columns to keep the powder from flowing outside.

Air was used as the carrier gas and a mass flow controller (0 - 200 mL/min, Aalborg Inc., Orangeburg, NY) was used to obtain reproducible gas flow rates. An in-line stainless steel tube mixer (15 elements, 0.013m O. D., Cole-Parmer Co., Vernon Hills, Illinois), shown in Figure 2.3,

was connected with the PAH vapor generator to provide efficient mixing of the PAH vapor and carrier gas. Water vapor was introduced into the reactor to keep the relative humidity 100% in the air and reduce water evaporation during the experiment. A moveable injector (SS 316, O. D. 32 cm) was used to introduce the PAH vapor into the glass boat reactor. The temperatures of the liquid and gas were monitored using thermocouples placed close to the surface. The top surface of the half-circular copper cooling tube and the inner top surface of the Pyrex tube were coated with a PFA film (2 mil thick, Berghof America, Coral Springs, FL) to avoid the adsorption of PAH onto these surfaces.



**Figure 2.3.** In-line stainless steel tube mixer.

### **2.1.3 Online GC-MS**

A Hewlett Packard 5890 Series II Gas Chromatograph with a Hewlett Packard Mass Selective Detector (MSD) was used to analyze the gas stream on-line. A 6-port injection valve (Valco Instrument Co., Houston, TX) and a digital valve sequence programmer (Valco Instrument Co., Houston, TX) were connected to the GC-MS such that the gas-phase sample was injected into the GC-MS automatically. The two-position 6-port valve is shown in Figure 2.4. An untreated fused silica tubing (Supelco Inc., Bellefonte, PA) was used as the GC column and the retention time of naphthalene inside the column was reduced to about 0.8 min. With this blank column installed, the gas phase was sampled every 3 minutes. The injection volume of the gas phase samples was 100 $\mu$ l, determined by the volume of the sample loop.

## **2.2 Analytical Apparatus for Sample Analysis**

Identification of the photooxidation products of naphthalene and phenanthrene were accomplished using a combination of GC-MS and HPLC-MS.

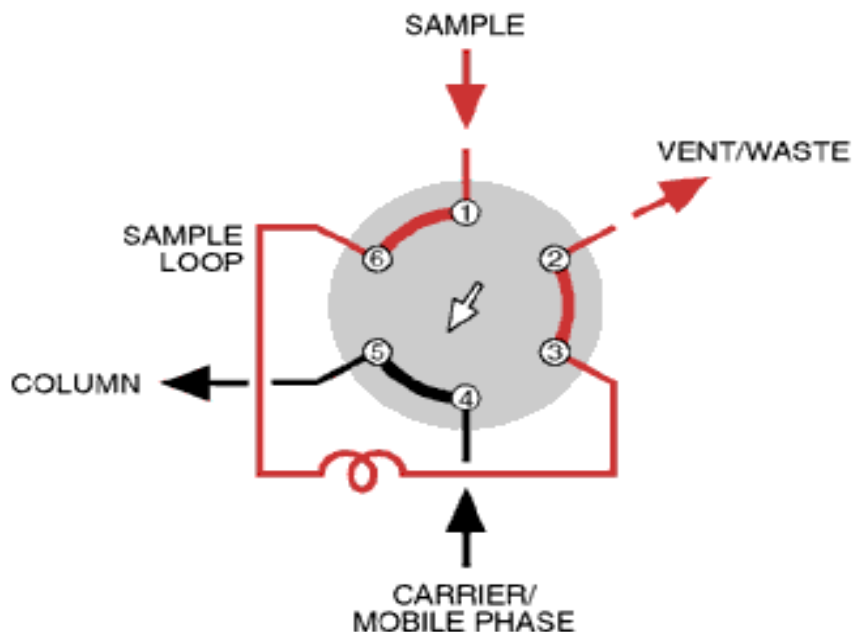


**Figure 2.4.** Two-position 6-port valve (<http://www.vici.com/support/app/app11j.php>).

The water samples of the photooxidation experiments were collected and extracted by hexane. The extract was concentrated under a stream of nitrogen and analyzed in a different GC-MS (Hewlett Packard 6890 Network GC and 5973 Network MSD) from the online GC-MS. The temperature of the GC column started at 100°C and ramped to 200 °C within 20 min, then held at this temperature for 14 min.

Because of the uncertainty introduced during the extraction and concentration processes of the reaction sample, the composition analysis of the reaction sample in GC-MS was only used as a reference. Identification of the products was further confirmed using HPLC. Detailed description of the HPLC is given in the following chapters.

## CHAPTER 3

### ADSORPTION OF PAHS AT THE AIR-WATER INTERFACE\*

#### 3.1 Introduction

The behavior of a gaseous PAH molecule at the air-water interface is important in determining its fate and transport in the environment. Air-water interface exists in different forms: (i) bulk phase contact (e.g. air-sea), (ii) air dispersed in bulk water (e.g., air bubbles in water), (iii) water droplets in bulk air (e.g., fog, mist) and, (iv) thin water films on solids (e.g., water films coating aerosols and water coating soil particles in the unsaturated soil zone). In all these cases, the air-water interfacial area can be large and provides an important venue for adsorption and reaction. Although much is known about the partitioning of PAH molecules between bulk air and water phases, much less is known about the adsorptive behavior at the air-water interface [50]. Only recently has this become a focus of research [51-56]. For example, adsorption parameters for a few PAH molecules have been recently reported [57]. Similarly, a few recent papers have shed light on the reactions occurring between adsorbed PAH molecules and ozone on both planar and highly curved interfaces [54, 55, 58-62].

The equilibrium partition relationships between the interface and the bulk phases (air and water) can be described by Gibbs surface excess model. Figure 3.1 shows the equilibrium partition relationships between the interface and the bulk phases. Equilibrium partition relationship between the two bulk phases is determined by the Henry's law constant,  $K_{WA}=C_W/C_A$ . The Gibbs surface excess,  $\Gamma_S$  identifies the equilibrium concentration at the surface.

---

\* Reproduced in part with permission from Journal of Physical Chemistry A, 2006, Volume 110, Pages 9161-9168, J. Chen, F. S. Ehrenhauser, K. T. Valsaraj, M. J. Wornat, *Uptake and UV-photooxidation of Gas-phase PAHs on the Surface of Atmospheric Water Films. I. Naphthalene*. Copyright 2006 American Chemical Society.

Equilibrium partition between the interface and bulk water is defined by the partition constant,  $K_{IW}=\Gamma_s/C_w$ . Similarly  $K_{IA}=\Gamma_s/C_A$  defines the equilibrium partition between the interface and bulk air [63]. According to the Gibbs surface excess model, the standard state Gibbs free energy for the transfer of molecules from air to the interface can be obtained by [4]

$$\Delta_A^I G^0 = -RT \ln \left( \frac{K_{IA}}{\delta_0} \right) \quad \text{Eqn. 3.1}$$

where  $\delta_0$  is the standard surface thickness ( $=6 \times 10^{-10}$  m), which is the ratio of the standard state pressure for the gas phase ( $= 101.325$  kPa) and the standard state Kemball-Rideal surface pressure ( $= 0.06084$  mN.m<sup>-1</sup>). The Kemball-Rideal standard state for the surface is the exact equivalent of the 1 atm pressure standard state for the bulk gas phase.

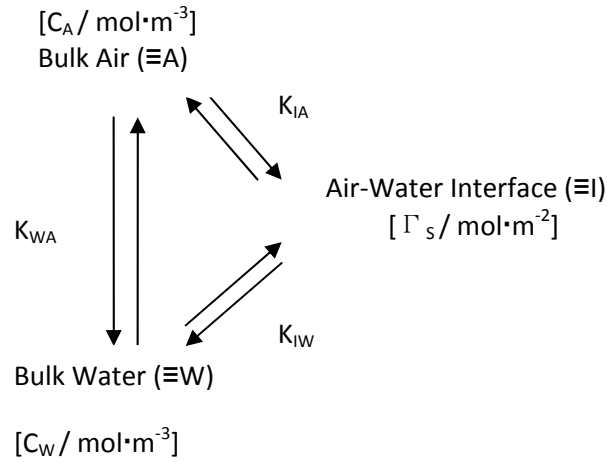


**Figure 3.1.** Equilibrium partition relationships between the interface and the bulk phases [63].

During the adsorption of PAH vapor onto a water film, the concentration change of the PAH in the water phase is given by [24]

$$\frac{dC_w}{dt} = K_c \cdot \frac{A_w}{V_w} \left[ C_A - \left[ \frac{C_w}{\left( K_{WA} + K_{IA} \cdot \frac{A_w}{V_w} \right)} \right] \right] \quad \text{Eqn. 3.2}$$

where  $A_w$  ( $m^2$ ) is the surface area of the water film,  $V_w$  ( $m^3$ ) is the volume of the water and  $K_C$  ( $m \cdot s^{-1}$ ) is the overall mass transfer coefficient. The overall mass transfer rate is affected by three factors: gas phase diffusion, mass accommodation at the interface and liquid phase solubility.

Define  $C_w/C_A$  as  $K_{WA}'$ . Integrating Eqn. 3.2, we get the following equation [24]:

$$K_{WA}' = \frac{C_w}{C_A} = K_{WA} * \left[ 1 - \exp\left(-K_C \cdot \frac{1}{K_{WA} *} \cdot \frac{A_w}{V_w} \cdot \tau\right) \right] \quad \text{Eqn. 3.3}$$

In the above equation  $K_{WA} * = K_{WA} + (A_w/V_w) \cdot K_{IA}$  and  $\tau$  (s) is the time required for equilibrium state to be achieved. For thin water films, the value of  $A_w/V_w$  is large and the term

$$\phi(\tau) = 1 - \exp\left(-K_C \cdot \frac{1}{K_{WA} *} \cdot \frac{A_w}{V_w} \cdot \tau\right)$$

can be approximated as 1. Therefore, in the case of adsorption onto thin water films,  $C_w/C_A = K_{WA}' \approx K_{WA} *$ . As shown in the expression of  $K_{WA} *$  ( $=K_{WA} + (A_w/V_w) \cdot K_{IA}$ ), the term  $(A_w/V_w) \cdot K_{IA}$  shows the deviation in thin water films from conventional Henry's Law partitioning between bulk air and water phases.

### 3.2 Adsorption of Naphthalene on Thin Water Films

Naphthalene is the first in the series of PAHs and provides a simple example of the adsorption and photo-transformation behavior of PAHs in thin water films. Besides, it also has industrial and commercial applications as active ingredients in mothballs, pesticides, crude oils and gasoline. It is a ubiquitous pollutant in the atmosphere. For example, in the Baton Rouge air it has been noted to be the most prevalent PAH molecule [64]. Table 3.1 lists the physico-chemical properties of naphthalene.

**Table 3.1.** Literature values of the physico-chemical properties of naphthalene [65].

Property	Value	Dimension
Molecular weight	128	$\text{g}\cdot\text{mol}^{-1}$
Aqueous solubility at 298K	0.097 - 0.265	$\text{mol}\cdot\text{m}^{-3}$
Vapor pressure (sub-cooled liquid) at 298K	0.01 - 0.03	kPa
Bulk air-water Henry's constant, $K_{WA}$ at 298K	33 - 68	[-]
Octanol-water partition constant, $K_{ow}$ at 298K	$10^{3.29} - 10^{3.59}$	[-]

### 3.2.1 Experimental Section

The experimental apparatus shown in Figure 2.1 was used for the adsorption experiments. Helium was used to generate the saturated naphthalene stream. The carrier gas containing naphthalene vapor was passed through the movable injector and the MS signal was monitored. Thin water films were prepared by coating the bottom surface of the glass trough with a known amount of deionized water (pH=6.3). To easily obtain a uniform water film, the bottom surface of the glass trough was covered with 50 wt% NaOH solution for 1hr and then washed clean with deionized water. The trough coated with a thin film of water was then placed in the cylindrical reactor and allowed to come to equilibrium temperature determined by the coolant inside the cooling tube placed underneath. The gas flow was started and the background MS signal was recorded. Thereupon, the naphthalene stream in air was introduced through the movable injector, which was placed at the entrance of the reactor. Therefore, the entire reactor was used for adsorption. The reduction in MS signal because of adsorption uptake on the water film was monitored.

The experiments were conducted under atmospheric pressure and were repeated for different temperature and water film thickness. All experiments were repeated 3 times to confirm reproducibility. To exclude the effect of naphthalene adsorption onto surfaces other than the

water film in the system, a blank experiment was first conducted using the glass trough without any water film.

### 3.2.2 Results and Discussion

#### 3.2.2.1 Data Analysis

The MS signal intensity is related to the apparent dimensionless partition constant (Henry's constant),  $K_{WA}^*$  for naphthalene between air (gas) and water (film) as follows [66]

$$K_{WA}^* = \frac{I(t)}{S_0} \cdot \frac{Q_g}{V} \quad \text{Eqn. 3.4}$$

where  $I(t)$  is the area (integral) difference between the baseline signal ( $S_0$ ) from the blank experiment and the signal from the water film experiment.  $V$  is the volume of the water film ( $m^3$ ) and  $Q_g$  is the total volumetric flow rate ( $m^3 \cdot \text{min}^{-1}$ ) of the helium stream. Note that  $K_{WA}^*$  is a composite of the bulk water-air partition constant,  $K_{WA}$  (the conventional Henry's constant for absorption) and the air-interface adsorption constant,  $K_{IA}$ . Thus,

$$K_{WA}^* = K_{WA} + \frac{K_{IA}}{\delta} \quad \text{Eqn. 3.5}$$

where  $\delta$  is the film thickness. As  $\delta \rightarrow \infty$  and/or for small values of  $K_{IA}$ , the interfacial adsorption term is not significant and  $K_{WA}^* \rightarrow K_{WA}$ . For small values of  $\delta$ , the interfacial adsorption term cannot be neglected.

Figure 3.2 is a typical naphthalene MS signal at the exit of the reactor for two cases. The first one is the control experiment where the glass boat reactor was empty, i.e., without any water film and the second one is that in which a 166  $\mu\text{m}$  water film was placed in the glass boat. The injected gas is initially exposed to a fresh surface upon which there is rapid uptake immediately following the down-stream of the injection point. This leads to the initial drop in the naphthalene signal at the outlet of the reactor. The maximum value of the concentration corresponds to the

inlet gas concentration up-stream of the reactor and is reached after uptake equilibrium is reached. The slow rise of the signal to that of the inlet stream shows that the film has reached saturation uptake.

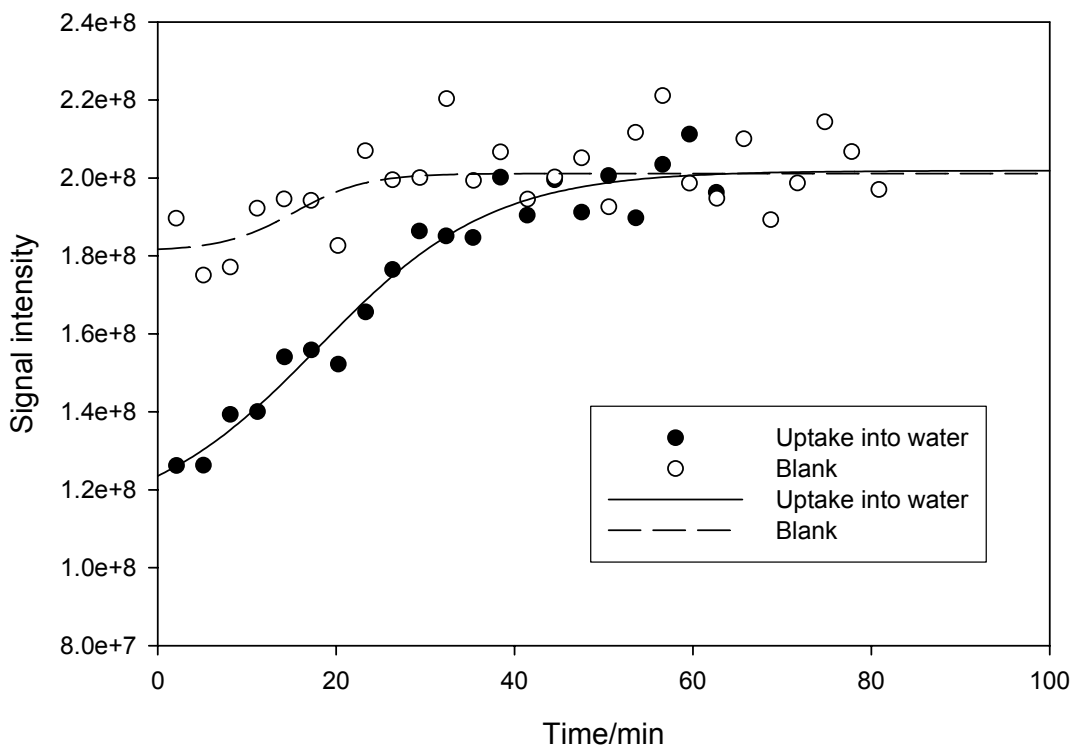


**Figure 3.2.** MS signal of naphthalene for the two cases involving control and water film experiments.

For semi-volatile compounds such as naphthalene, the mass transport from the gas phase to an aqueous phase can be gas-phase diffusion limited [67]. The gas-side mass transfer resistance will be lowered as the gas-flow rate (velocity) increases. Increasing gas flow rate therefore should increase the overall mass transfer coefficient. In order to ascertain the mass transfer regime in the reactor a set of initial experiments was undertaken for a relatively thick film (950  $\mu\text{m}$ ). The measured concentration ratio increased with increasing gas flow rate at a temperature of 293K. We observed that at flow rates larger than  $100 \text{ mL}\cdot\text{min}^{-1}$  there was no discernible change in the partition constant. For the subsequent experiments, the gas flow rate in the reactor was fixed at  $100 \text{ mL}\cdot\text{min}^{-1}$ .

### 3.2.2.2 Effect of Water Film Thickness on Partitioning to the Film

The effect of water film thickness on the overall partition constant,  $K_{WA}^*$  was studied by varying the water film thickness in the reactor from 45 to 950  $\mu\text{m}$  at a constant temperature of 293K and a flow rate of 100  $\text{mL}\cdot\text{min}^{-1}$ . The bottom surface of the glass trough was always fully coated with the water film and its surface area was determined ( $A_w=317 \text{ cm}^2$ ). Varied water film thicknesses were obtained by changing the volume of the water while keeping the surface area of the film constant. The partition constant increased only slightly with increasing surface area per unit volume,  $1/\delta$ . The variation in surface area per unit volume was from 10 to 2,300  $\text{cm}^{-1}$  and the corresponding increase in the partition constant was 18.6. In previous work from our laboratory [4] we used an inverse gas chromatography (IGC) technique to obtain very thin water films ( 0.025 to 0.2  $\mu\text{m}$ ) and corresponding  $K_{WA}^*$  values varying from 200 to 900 for naphthalene. These two sets of data are plotted in Figure 3.3. A trend line (linear fit from Microsoft Excel) can be drawn such that as  $\delta \rightarrow \infty$  (i.e.,  $1/\delta \rightarrow 0$ ), the intercept  $K_{WA}^* \rightarrow K_{WA} = 86 \pm 23$ . The slope of the line when  $1/\delta$  is large gives the air-water interface partition constant,  $K_{IA} = 21 \pm 1 \mu\text{m}$ . The correlation coefficient for the linear trend line fit ( $r^2 = 0.97$ ) is acceptable. The experimental values at 293K are compared to available literature values in Table 3.2. The effect of the interface thickness on the overall partition ratio for naphthalene becomes evident only at  $\delta < 1 \mu\text{m}$ . Obtaining the precise thickness of the water film for small  $\delta$  is precluded by the difficulty in creating a uniform thin water film.

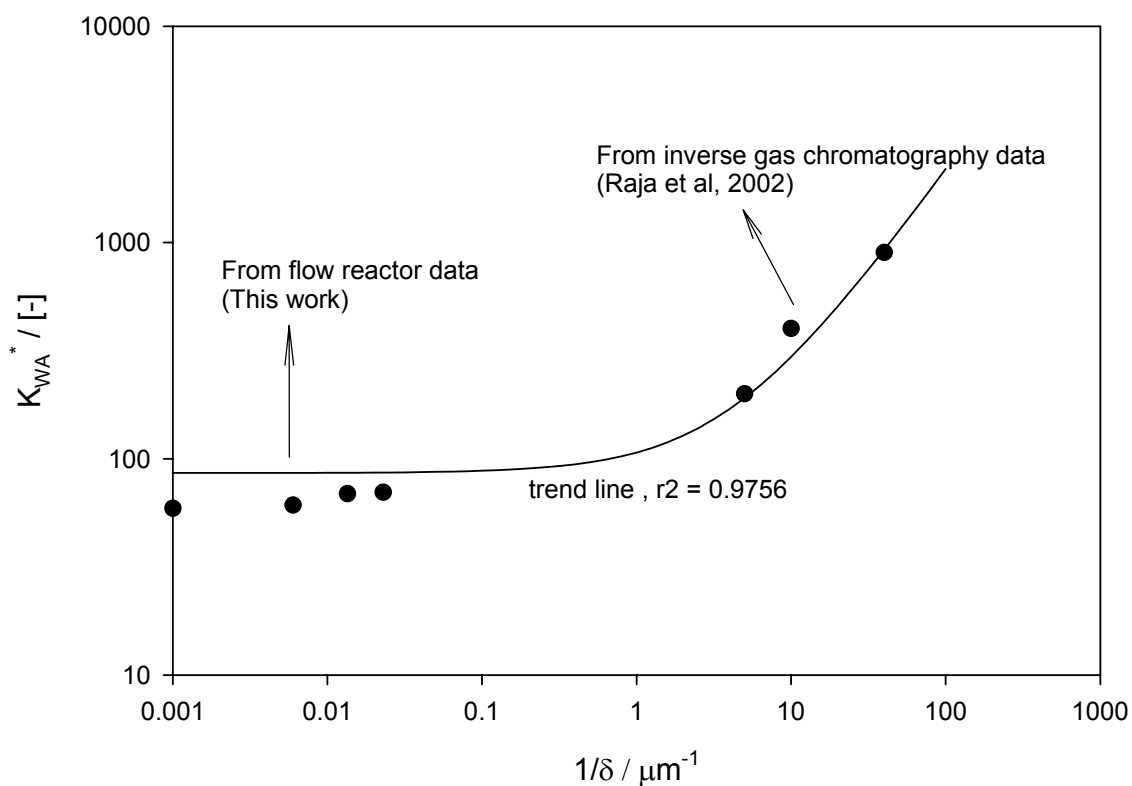


**Figure 3.3.** The effect of water film thickness on the partition constant for naphthalene.

**Table 3.2.** Experimental and literature values of air-water partition constants for naphthalene at 293K.

<i>Parameter</i>	<i>Data</i>	<i>Reference</i>
Air-water bulk phase partition constant, $K_{WA} / [-]$	86±23	This work
	64	Extrapolated from NIST handbook [68]
	72	Alaee et al [69]
Air-water interface partition constant, $K_{IA} / [\mu\text{m}]$	21±1	This work
	27±2	Raja et al [4]

### 3.2.2.3 Effect of Temperature on Uptake into the Film

The temperature dependence is described by the van't Hoff equation

$$\ln(K_{WA}^*) = -\frac{\Delta_{g \rightarrow w}H}{R} \frac{1}{T} + \frac{\Delta_{g \rightarrow w}S}{R} \quad \text{Eqn. 3.6}$$

Experiments were conducted on a 150  $\mu\text{m}$  water film within a temperature range of 278 – 303K. At this film thickness, absorption into the bulk phase of the thin film is dominant over the surface adsorption term. At the lowest temperature uptake occurs on a water film only 5K above the freezing temperature. Figure 3.4 is a plot of  $\ln K_{WA}^*$  versus  $1/T$  which gives an enthalpy of solvation,  $\Delta_{g \rightarrow w}H$  of  $-22 \pm 6 \text{ kJ} \cdot \text{mol}^{-1}$  and an entropy of solvation,  $\Delta_{g \rightarrow w}S$  of  $-41 \pm 20 \text{ J} \cdot \text{mol}^{-1} \cdot \text{K}^{-1}$ . The straight-line plot has a correlation coefficient of 0.882 indicating that over the temperature range the fit is satisfactory. In the literature, data exist on the enthalpy of partitioning of naphthalene between the air and water bulk phases. For example, values of  $-28 \text{ kJ} \cdot \text{mol}^{-1}$  and  $-45 \text{ kJ} \cdot \text{mol}^{-1}$  have been reported [68, 69]. The enthalpy of solvation is considerably smaller than the enthalpy of adsorption at the air-water interface,  $\Delta_{g \rightarrow \sigma}H$ , which is reported from our laboratory to be  $-67 \pm 17 \text{ kJ} \cdot \text{mol}^{-1}$  [4]. Similarly the entropy of solvation is twice as small as the entropy of adsorption,  $\Delta_{g \rightarrow \sigma}S = -95 \pm 5 \text{ J} \cdot \text{mol}^{-1} \cdot \text{K}^{-1}$ . According to the free energy of adsorption and solvation, we conclude that adsorption (partial solvation) at the air-water interface is a favorable process, but solvation (transport into the bulk aqueous film) involves considerable energy input into the hydration process.

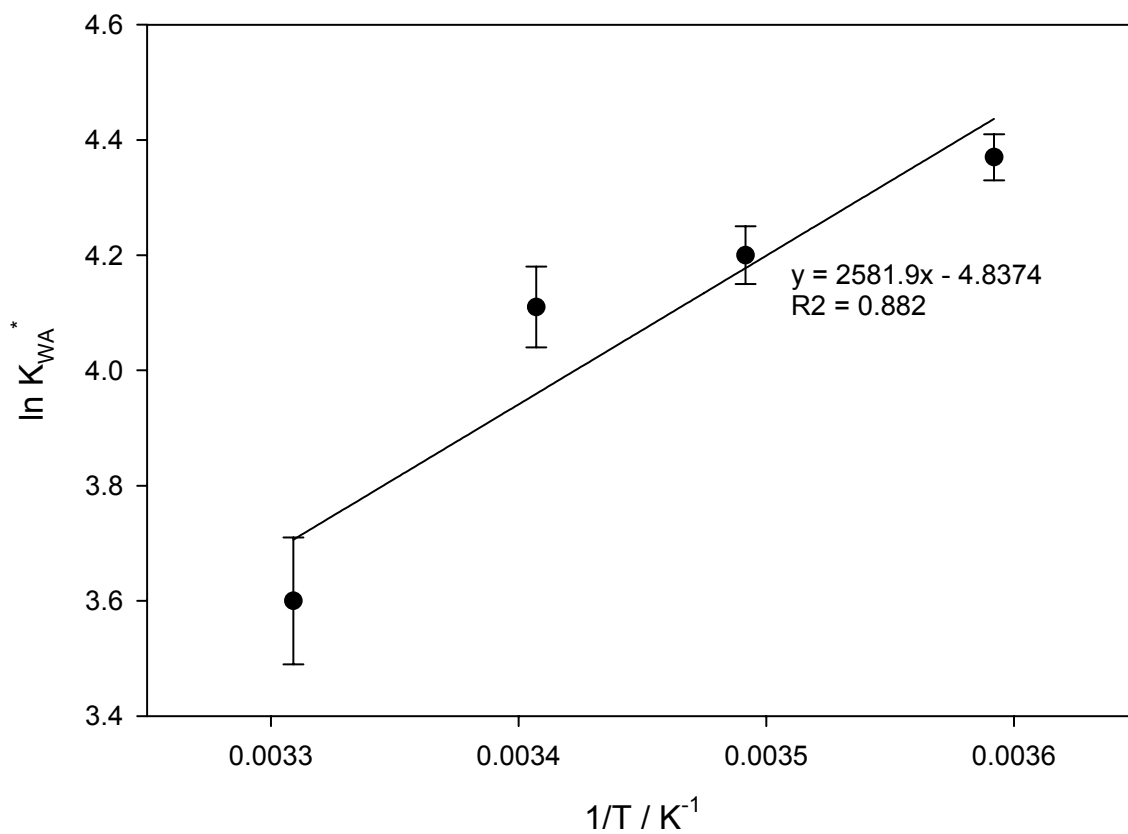


**Figure 3.4.** The effect of temperature on naphthalene partitioning to the thin water film. The thickness of the water film was 150  $\mu\text{m}$ .

### 3.3 Adsorption of Phenanthrene on Thin Water Films

Phenanthrene is a 3-ring PAH often detected in the ambient atmosphere. Phenanthrene is a persistent organic pollutant (POP) and is among the species monitored in the polar contaminant study [70]. The behavior of phenanthrene is expected to be markedly different from naphthalene, since they differ in vapor pressure, aqueous solubility and hydrophobicity. Table 3.3 lists the physico-chemical properties of phenanthrene.

**Table 3.3.** Literature values of the physico-chemical properties of phenanthrene [65].

Property	Value	Dimension
Molecular weight	178	$\text{g}\cdot\text{mol}^{-1}$
Aqueous solubility at 298K	0.004 - 0.009	$\text{mol}\cdot\text{m}^{-3}$
Vapor pressure (sub-cooled liquid) at 298K	$9\times 10^{-5}$	kPa
Bulk air-water Henry's constant, $K_{WA}$ at 298K	955	[-]
Octanol-water partition constant, $K_{ow}$ at 298K	$10^{4.16} - 10^{4.57}$	[-]

#### 3.3.1 Experimental Section

##### 3.3.1.1 Interfacial Partitioning at the Air-Water Interface

The experimental apparatus shown in Figure 2.1 was used for the adsorption experiments. The experimental procedure was similar to that of the naphthalene adsorption experiments. However, the online GC-MS was not used to analyze the gas-phase phenanthrene due to its low vapor pressure. Instead, the liquid phase phenanthrene was directly analyzed using HPLC. Phenanthrene vapor was generated by passing air through a PAH saturator and was then introduced to the flow tube photoreactor in which gas phase phenanthrene adsorbed onto a thin aqueous film coated on the glass trough. The flow rate of air to the saturator columns was set at  $75 \text{ mL}\cdot\text{min}^{-1}$  to obtain reproducible carrier gas flow rate in the PAH saturator. The gas phase concentration of phenanthrene obtained in this manner ranged from  $0.4$  to  $0.7 \mu\text{g}\cdot\text{L}^{-1}$  at room

temperature (23°C), while the reported value of the saturated gas phase concentration of phenanthrene ranges from 2.0 to 6.5  $\mu\text{g}\cdot\text{L}^{-1}$  [65].

Uptake of phenanthrene onto thin aqueous films was investigated to study the interfacial behavior of phenanthrene at the air-water interface. The phenanthrene vapor/air mixture was introduced to the flow tube photoreactor through the moveable injector and adsorption of phenanthrene occurred on the aqueous film coated on the glass trough. The temperature of the film was maintained at 296 K by the cooling bath. The aqueous sample was collected and the concentration of phenanthrene was quantified using a high performance liquid chromatograph (HPLC) after partition equilibrium was achieved between the gas and liquid phases and the aqueous concentration of phenanthrene ceased increasing. The time it took to reach equilibrium varied with the thickness of the aqueous film. To maintain consistency of our experiments, the adsorption duration was set as 10 hours, which is the time required to reach equilibrium on the thickest film (1714  $\mu\text{m}$ ) employed in our experiments. The experiments were conducted under atmospheric pressure and were repeated for different water film thickness. The thickness of the water film ranged from 22 to 515  $\mu\text{m}$ . As has been mentioned above, the gas phase concentration of phenanthrene generated by the PAH saturator varied from day to day between 0.4 and 0.7  $\mu\text{g}\cdot\text{L}^{-1}$ . In order to correct for the aqueous concentration variation brought about by the gas phase concentration change of phenanthrene, a pure water film of fixed thickness (1714  $\mu\text{m}$ ) was coated on a 3.5  $\times$  5 cm glass trough and placed next to the target film, serving as the control for the adsorption experiments. The equilibrium concentration of phenanthrene in the target film was normalized to the equilibrium concentration in the control film for data analysis.

### **3.3.1.2 Measurement of Henry's Law Constant**

The Henry's constant for phenanthrene was obtained by measuring the concentrations of phenanthrene in the bulk water and vapor phases in contact after equilibrium. A mini-bubbler (10

mL in capacity) filled with 5 mL deionized water was connected to the PAH saturator and the phenanthrene vapor/air mixture was bubbled through the bubbler at  $75 \text{ ml}\cdot\text{min}^{-1}$ . After equilibrium was achieved between the water and vapor phases, a polymer trap was connected downstream to the bubbler to trap the vapor phase phenanthrene over a period of several hours. Water samples were withdrawn from the top of the bubbler both before and after collection of the vapor and analyzed using HPLC. The adsorbed phenanthrene was extracted into acetonitrile and also analyzed in HPLC. The vapor phase concentration of phenanthrene was estimated based on the gas flow rate, the vapor collection time, and the volume of acetonitrile used for extraction. Henry's constant was obtained by the direct ratio of the average aqueous concentration over the vapor collection period and the measured vapor phase concentration.

### **3.3.1.3 Sample Analysis in HPLC**

Quantification of phenanthrene was done using HPLC. The HPLC instrument consisted of an Agilent Technologies HPLC 1100 series with online degasser (G1322A), quaternary pump (G1311A), autosampler (G1313A), column thermostat (G1316A), and diode array detector (G1315A). An EnviroSep-PP column of 125 mm x 3.20 mm with 5  $\mu\text{m}$  particle size (Phenomenex Corp, USA) was used. The injection volume was 25  $\mu\text{L}$  and the column thermostat was set to 40  $^{\circ}\text{C}$ . The mobile phase started with a 20/80 acetonitrile/water mixture and ramped to 80/20 acetonitrile/water within 12 min, then held at this concentration for 3 min, and finally returned to 20/80 acetonitrile/water in 3 min at a constant flow rate of 0.5 ml/min. The detection wavelength was set to 250 nm with 100 nm bandwidth and 4 nm slit.

## **3.3.2 Results and Discussion**

### **3.3.2.1 Equilibrium Uptake of Gas-Phase Phenanthrene on Water Films**

Let us consider a film of water of thickness  $\delta$  in the flow reactor that is exposed to a gaseous stream of phenanthrene at a constant concentration. The overall equilibrium uptake of

phenanthrene in the water film is due to two processes, viz., adsorption at the air-water interface and dissolution within the bulk liquid. Thus, the overall equilibrium concentration of phenanthrene in the water film,  $C_w^T$  is given by

$$C_w^T = C_{w0} + \frac{C_{w0}}{K_{WA}} \frac{K_{IA}}{\delta} \quad \text{Eqn. 3.7}$$

where  $K_{WA}$  is the dimensionless bulk water-air equilibrium partition constant (Henry's constant) for phenanthrene.  $K_{IA}$  ( $\mu\text{m}$ ) is the partition constant between the air and the air-water interface.  $C_{w0}$  is the concentration in the bulk water phase for which the surface area is negligible in comparison to the bulk volume. The above equation clearly demonstrates that as the film thickness,  $\delta$  is small, and the surface partition constant,  $K_{IA}$  is large, the contribution from the surface adsorption becomes larger.

### 3.3.2.2 Effect of Water Film Thickness on Partitioning to the Film

Figure 3.5 shows the variation in the total aqueous concentration of phenanthrene in the film as a function of the inverse of the water film thickness. A linear relationship was observed indicating the validity of the assumption that with decreasing film thickness (increasing  $1/\delta$ ) the surface adsorption becomes the predominant uptake mechanism. The y-intercept and the slope of the plot give the values of the bulk phase uptake ( $C_{w0}$ ) and  $(C_{w0}/K_{WA}) \cdot K_{IA}$ . The bulk water-air equilibrium partition constant ( $K_{WA}$ ) was determined separately by passing the phenanthrene vapor/air mixture through a bubbler and measuring the equilibrium concentrations of phenanthrene in the liquid and gas phases. The value determined is  $K_{WA} = 1019$ , which agrees with the value reported in other literature (Table 3.4). From the y-intercept and the slope of Figure 3.5, one can, therefore calculate the value of the interface partition (adsorption) constant,  $K_{IA}$ . The value of  $K_{IA}$  obtained was  $3.3 \times 10^4 \mu\text{m}$  and compares well with the estimate from correlation as shown in Table 3.4. Using this value one estimates that at equilibrium 60% of

phenanthrene will be present on the surface of an aqueous film 22  $\mu\text{m}$  thick, whereas for a 515  $\mu\text{m}$  film only 6% of the total mass of phenanthrene will be on the surface.

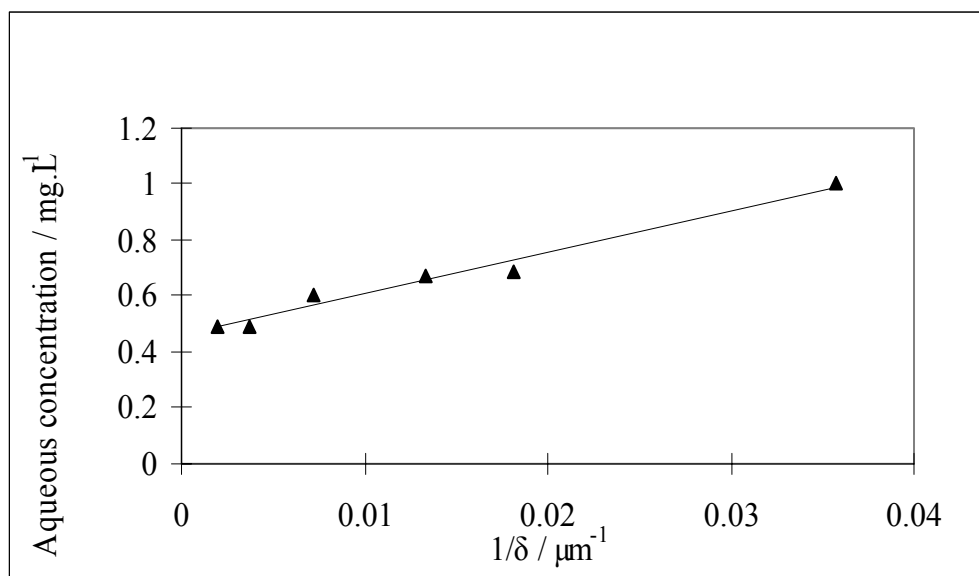


**Figure 3.5.** Uptake of phenanthrene from the gas phase on aqueous films with varying thicknesses.

**Table 3.4.** Experimental and literature values of air-water partition constants for phenanthrene at 296K.

<i>Parameter</i>	<i>Data</i>	<i>Reference</i>
Air-water bulk phase partition constant, $K_{WA} / [-]$	1019	This work
	955	Groundwater Chemicals: Desk Reference [65]
Air-water interface partition constant, $K_{IA} / [\mu\text{m}]$	$3.3 \times 10^4$	This work
	$3.5 \times 10^4$	Data obtained from correlation <sup>(a)</sup> [63]

a. Data obtained from correlation:  $\log (K_{IA}/m) = +0.940 \log (K_{OA}/[-]) - 8.607$ ;  $r^2 = 0.987$  [63].  $K_{OA}$  is the octanol-air partition constant for the compound.  $\log K_{OA} = 7.602$  for phenanthrene at 298 K [71].

### 3.4 Molecular Dynamics Simulation

Although the adsorptive behavior of PAHs at the air-water interface has been experimentally presented in our work, there has been no molecular scale discussion presented on the behavior of PAH molecules at the air-water interface until recently. In 2006, a computational research group directed by Prof. Jungwirth of the Academy of Sciences of the Czech Republic

conducted molecular dynamics (MD) simulations of the aqueous solvation of four typical aromatic compounds. They began with the monocyclic aromatic hydrocarbon (benzene) and then moved towards three PAH molecules (naphthalene, anthracene, and phenanthrene). For each species, they obtained the free energy profile for moving the molecule from the gas phase to the aqueous phase through the air-water interface. In a collaborative research paper co-authored by Prof. Jungwirth's group and our group, the results of the MD simulations were presented and compared to the experimental results we obtained.

### 3.4.1 Systems and Computational Method

Classical molecular dynamics (MD) simulations for investigation of the aqueous hydration and surface propensity of PAHs were used. In particular, the program package Gromacs 3.15 were employed to evaluate the potential of mean force (PMF), i.e., the free energy profile  $\Delta G$  associated with moving the molecule from the gas phase across the aqueous interface to the liquid bulk and back into the gas phase. From the free energy difference between the two points in the path (e.g., in the liquid, at the surface, or in the gas phase) one can evaluate the molecular concentration ratio of the studied species:

$$\frac{c_1}{c_2} = e^{-\frac{\Delta G_{12}}{RT}}$$

The hydration free energy is related to the Henry's constant by the state equation of an ideal gas and the above equation. The values of Henry's law constant were taken from a compilation by Sander [72] and were used to verify the quality of employed force-fields. Note that hydration free energy depends on the choice of a standard state, which in this case is that corresponding to infinite dilution. The solvation free energies at ambient conditions (i.e.,  $p_0 = 1$  atm gas pressure and  $c_0 = 1$  M concentration) differ from those corresponding to a single gas molecule (pertinent to the present simulations) by a factor  $RT \ln(RTc_0/p_0) = 7.9 \text{ kJ}\cdot\text{mol}^{-1}$  [73].

The system investigated consisted of 215 - 430 water molecules and one molecule from the following list: benzene, naphthalene, anthracene, and phenanthrene. This system was placed in a prismatic unit cell of dimensions 18.6 x 18.6 x 388 Å (215 water molecules and benzene or naphthalene) or 23.5 x 23.5 x 200 Å (430 water molecules and naphthalene, anthracene, or phenanthrene) and 3D periodic boundary conditions were applied. This results in an extended slab with an aqueous bulk between two air-water interfaces.[74]

Detailed description of the computational method used in the MD simulations can be found in our paper [2].

### 3.4.2 Computational Results

Figures 3.6-3.9 show for each of the investigated systems the corresponding potential of mean force (PMF), which is the free energy profile of moving the PAH molecule through the aqueous slab, i.e., from the gas phase across the air-water interface into the aqueous bulk and across the second interface back into the air. Ideally, the PMF curves should be perfectly symmetric with respect to the center of the slab, and indeed very good left-right symmetry is shown in Figures 3.6-3.9, indicating convergence of the free energy profiles.

All the aromatic molecules under study – benzene, naphthalene, anthracene, and phenanthrene, are volatile species, with their volatility gradually decreasing with molecular size. Note that in all these cases, the hydration free energy is negative, meaning that the concentration of the molecule is lower in gas phase than in the aqueous bulk. Experimental hydration free energies evaluated from Henry's constants [72] were very well reproduced for all studied molecules (Figures 3.6-3.9). Note that with the increasing number of aromatic rings of the molecules the hydration free energy increased from less than  $-1 \text{ kcal}\cdot\text{mol}^{-1}$  for benzene to more than  $-4 \text{ kcal}\cdot\text{mol}^{-1}$  for phenanthrene.

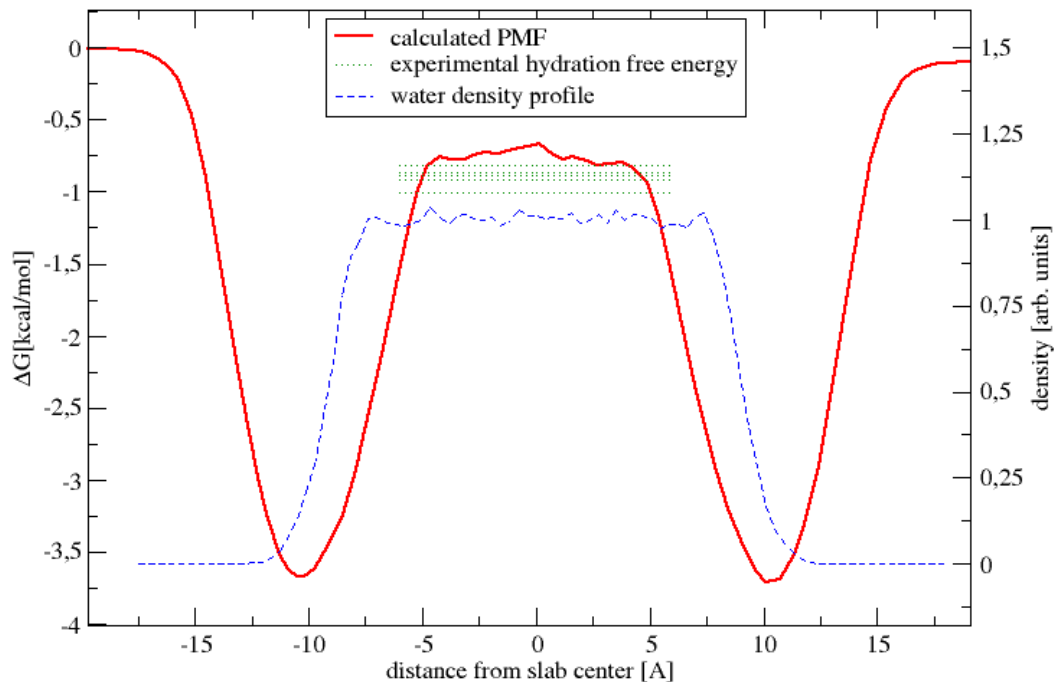


**Figure 3.6.** Potential of mean force for moving benzene through an aqueous slab defined via the water density profile. The experimental hydration energies obtained from the Henry's law constants in several measurements are displayed as horizontal lines [72].

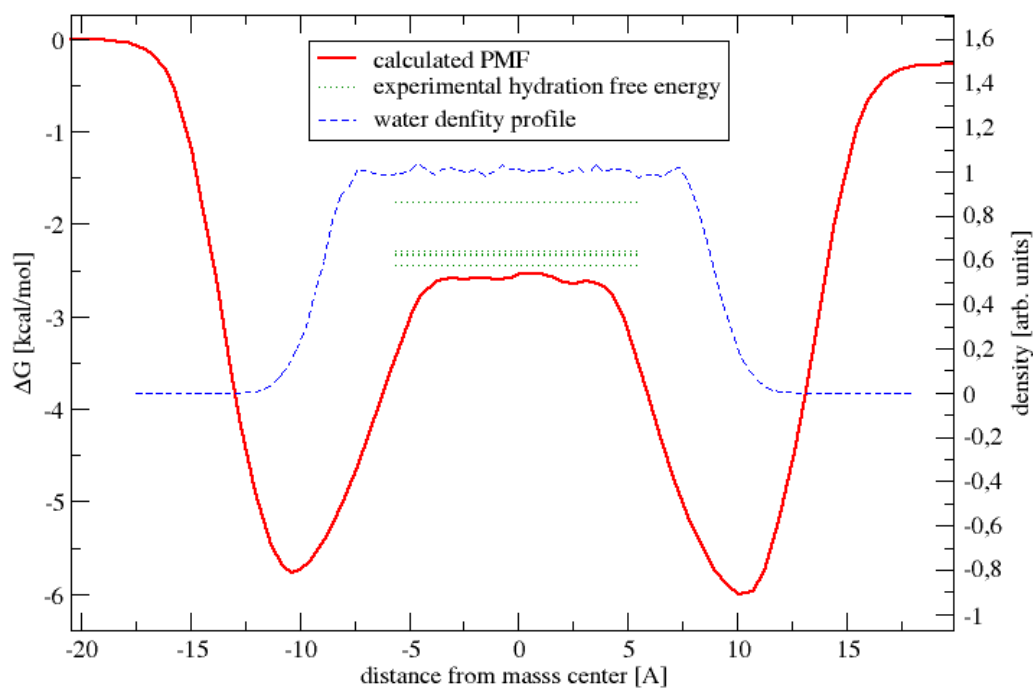


**Figure 3.7.** Potential of mean force for moving naphthalene through an aqueous slab defined via the water density profile. The experimental hydration energies obtained from the Henry's law constants in several measurements are displayed as horizontal lines [72].

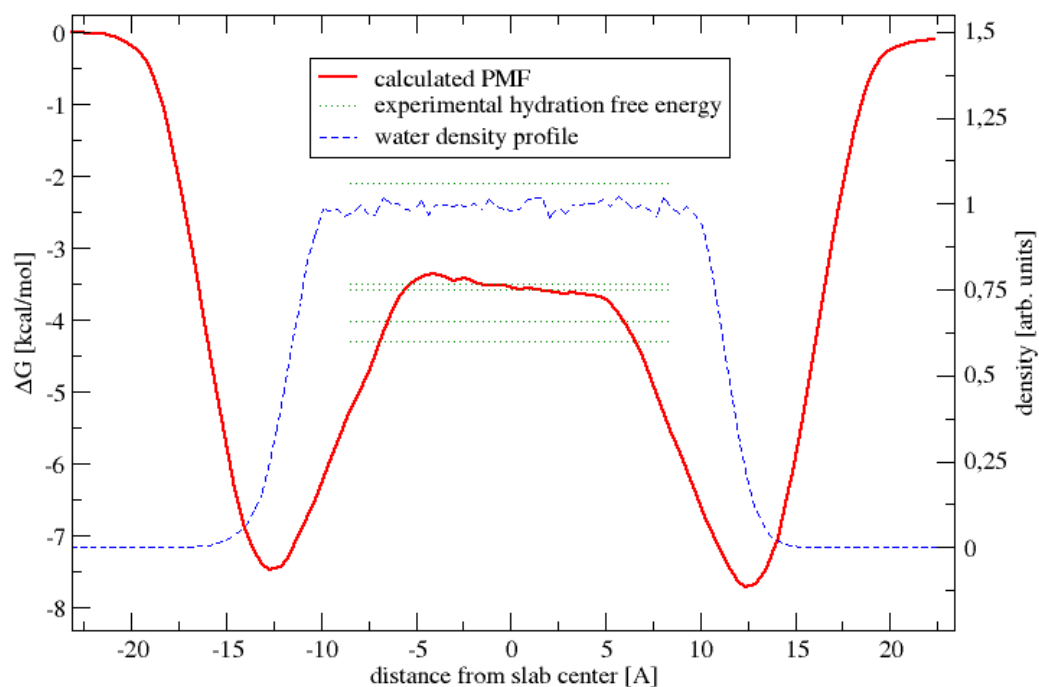


**Figure 3.8.** Potential of mean force for moving anthracene through an aqueous slab defined via the water density profile. The experimental hydration energies obtained from the Henry's law constants in several measurements are displayed as horizontal lines [72].

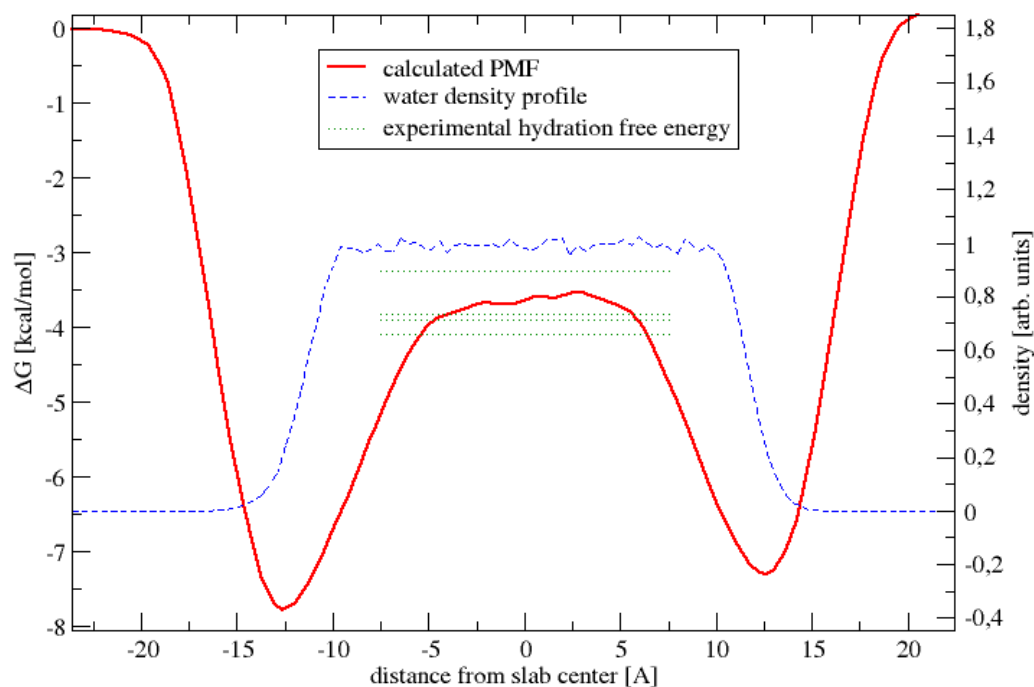


**Figure 3.9.** Potential of mean force for moving phenanthrene through an aqueous slab defined via the water density profile. The experimental hydration energies obtained from the Henry's law constants in several measurements are displayed as horizontal lines [72].

One significant result of the present calculations is the deep surface minimum at the PMF of benzene and, even more prominently, for the investigated PAHs. Occurrence of such a pronounced minimum is directly reflected in a large surface enhancement of the studied aromatic molecules. This huge surface enhancement, which is clearly a generic feature of benzene and PAHs, is quantified in Table 3.5. Compared to the gas phase, there is more than two orders of magnitude surface enhancement for benzene, while for phenanthrene it is almost six orders of magnitude. Interestingly, the mean enhancement at the surface with respect to the aqueous bulk is much less system dependent and amounts to roughly a factor of one hundred for all investigated molecules. Finally, note that a non-polarizable force-field was employed in the MD simulation, which was likely to lead to underestimation of the surface effect. The present results can, therefore, be viewed as a lower estimate to the concentration enhancement of benzene and PAHs at the aqueous surface.

**Table 3.5.** Aqueous bulk concentrations and the highest and averaged values in the interfacial region, compared to the gas phase value (normalized to 1.0).

Molecule	Gas Phase	Aqueous bulk	Aqueous surface highest value	Aqueous surface averaged value
Benzene	1.0	3.3	480	250
Naphthalene	1.0	90	16000	7100
Anthracene	1.0	350	285000	120000
Phenanthrene	1.0	550	500000	170000

### 3.4.3 Comparison of Computational Results and Experimental Observations

As shown in Eqn. 3.1, the air-water interfacial partition constant,  $K_{IA}$  at any given temperature is related to the overall free energy of adsorption

$$\Delta_A^I G^0 = -RT \ln \left( \frac{K_{IA}}{\delta_0} \right) \quad \text{Eqn. 3.1}$$

where  $\delta_0$  is a standard surface thickness ( $= 6 \times 10^{-10}$  m), which is the ratio of the standard state pressure for the gas phase ( $= 101.325$  kPa) and the standard state Kemball-Rideal surface pressure ( $= 0.06084$  mN.m<sup>-1</sup>). The Kemball-Rideal standard state for the surface is the exact equivalent of the 1 atm pressure standard state for the bulk gas phase. Using the  $K_{IA}$  values obtained for naphthalene and phenanthrene, the overall free energy of adsorption can be calculated. The calculated values are  $-25.5$  kJ.mol<sup>-1</sup> for naphthalene and  $-43.9$  kJ.mol<sup>-1</sup> for phenanthrene at room temperature. As shown in Figure 3.10, the free energy obtained experimentally was compared to the value predicted from MD simulation. The experimental data of the free energy of benzene was obtained from Raja et al [4]. Figure 3.10 is a parity plot where the 1:1 correspondence is shown as the solid line. Note that the computational and experimental values for naphthalene and benzene are in very good agreement, while the free energy of phenanthrene shows a relatively large difference between the experimental and the computational values.

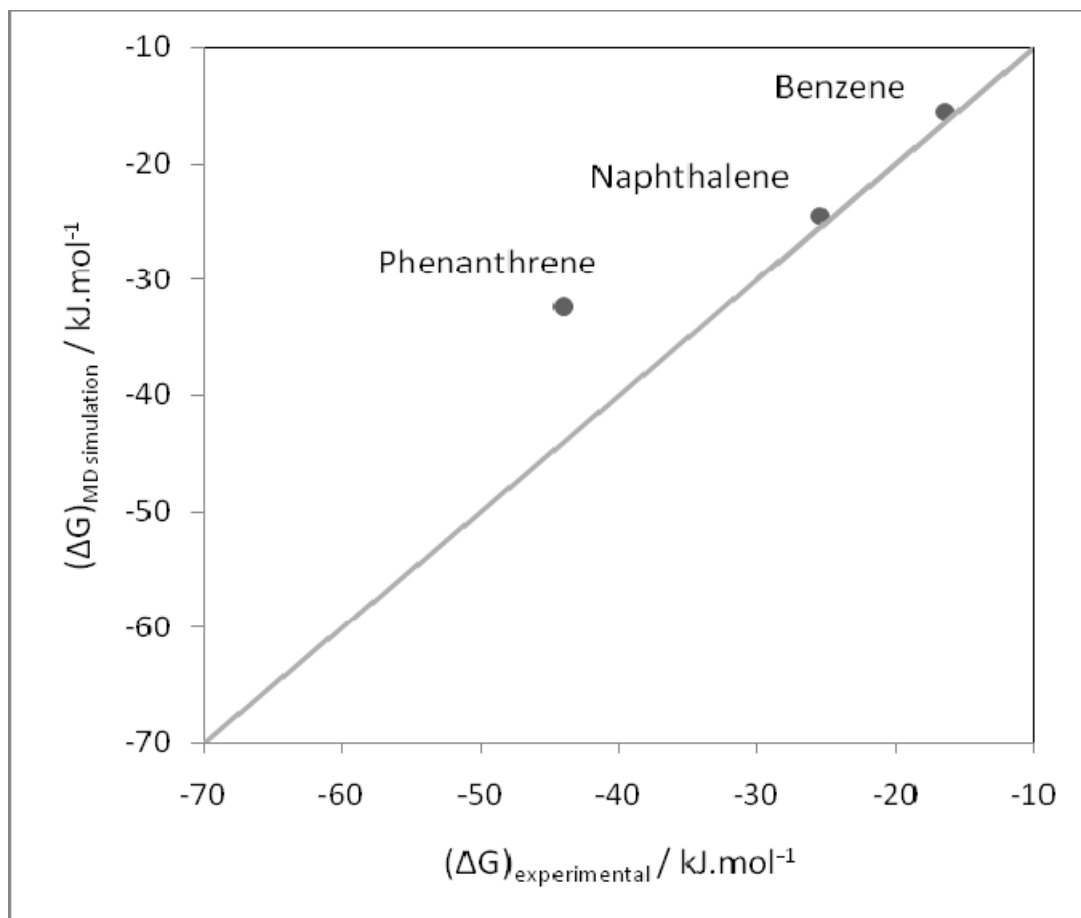


**Figure 3.10.** Comparison of the experimental and MD-simulated free energy of adsorption from the gas phase for benzene, naphthalene and phenanthrene. Experimental data of benzene obtained from Raja et al [4].

## CHAPTER 4

# EFFECTS OF DISSOLVED SURFACTANTS ON PAH ADSORPTION AT THE AIR-WATER INTERFACE\*

### 4.1 Introduction

Atmospheric aerosols typically contain several inorganic salts and 10 – 70% of organic compounds. Single particle laser mass spectrometry measurements indicate that much of the organic material in atmospheric aerosols resides at their surface [75]. The current picture of aerosols is that of a solid core coated with a thin film of water that contains surface-active organic compounds [76, 77]. Thin atmospheric water films on aerosols, fogs and ice surfaces play an important role in atmospheric chemistry, and their interfacial properties are affected to a great extent by the surface-active substances present. The types and concentrations of surface-active substances in atmospheric water films are variable [78]. They involve a variety of organic compounds such as n-alkanoic acids (fatty acids) and humic-like substances (HULIS) [79, 80]. Surface-active substances influence the state of gas-liquid interface of atmospheric aerosols by lowering their surface tension and consequently affect aerosol nucleation and growth. They also act as adsorptive surfaces for the uptake of gaseous molecules and participate in heterogeneous reactions with atmospheric radicals [81]. Extensive studies have shown that long-chain fatty acid monolayers inhibit reactive uptake of  $N_2O_5$  and anthracene on water surfaces [43, 82-84]. Understanding the effects of surface-active substances in atmospheric water

---

\* Reproduced in part with permission from Journal of Physical Chemistry A, 2007, Volume 111, Pages 4289-4296, J. Chen and K. T. Valsaraj, *Uptake and UV-Photooxidation of Gas-Phase Polyaromatic Hydrocarbons on the Surface of Atmospheric Water Films. 2. Effects of Dissolved Surfactants on Naphthalene Photooxidation*. Copyright 2007 American Chemical Society.

films is important for elucidating the processing of organic compounds by aerosols and fogs in the atmosphere [85].

The predominant fraction of water-soluble organic compounds present in fog waters is acidic and comprises both mono- and di-carboxylic acids and polycarboxylic acids. Polycarboxylic acids, which are the most surface-active species in fog droplets, have been found to be chemically similar to naturally occurring humic (or fulvic) acids and are referred to in the literature as HULIS. It has been shown via molecular characterization that Suwannee River fulvic acid (SRFA) is a good surrogate model to represent polycarboxylic acids in fog waters [79]. In this work, we chose SRFA to study the effect of dissolved surfactants on PAH adsorption at the air-water interface. In order to compare the result with conventional surfactants, we also conducted separate experiments using sodium dodecyl sulfate (SDS) as the water-soluble surfactant.

## **4.2 Experimental Section**

### **4.2.1 Materials**

Naphthalene ( $\geq 99\%$ ) and phenanthrene ( $>96\%$ ) were obtained from Aldrich. SRFA was obtained from the International Humic Substances Society (Cat. No. 1S101F). SDS ( $\geq 99.5\%$ ) was obtained from Gibco BRL (Grand Island, NY). All chemicals were used as received. Table 4.1 lists the physicochemical properties of SRFA and SDS.

### **4.2.2 Adsorption of PAHs on Thin Water Films Containing Surfactants**

The experimental procedure for the adsorption of PAHs on aqueous surfactant films was similar to that on pure water films as described in Section 3.3.1.1. After partition equilibrium was achieved between the gas and liquid phases and the aqueous PAH concentration ceased increasing, the aqueous sample was collected and the PAH concentration was quantified using the HPLC described in Chapter 3. For the adsorption of naphthalene, the film thickness was

fixed at 450  $\mu\text{m}$  and the concentration of SRFA solution used to make the film ranged between 0 and 489  $\text{mg}\cdot\text{L}^{-1}$ . Separate experiments using SDS as the water-soluble surfactant were also conducted. Concentrations of the SDS solutions used to make the SDS film ranged between 0 and 4100  $\text{mg}\cdot\text{L}^{-1}$ . For the adsorption of phenanthrene, the thickness of the aqueous surfactant film ranged from 22 to 515  $\mu\text{m}$  for each surfactant solution of fixed concentration. Effects of two different levels of SRFA in the aqueous phase, 51.5 and 280  $\text{mg}\cdot\text{L}^{-1}$ , and SDS solution with a fixed concentration, 207  $\text{mg}\cdot\text{L}^{-1}$ , were investigated.

### 4.2.3 Surface Tension of SRFA Solutions

To obtain the surface excess of SRFA, surface tensions of SRFA solutions were measured by the Wilhelmy plate method using a Krüss Process Tensiometer Model K-14. Surface tensions were measured at room temperature (23°C) over a wide range of SRFA concentration (0-20  $\text{g}\cdot\text{L}^{-1}$ ). Deionized water was used in the preparation of all SRFA solutions.

**Table 4.1.** Physicochemical properties of SRFA and SDS

<b>SDS</b>					
Molecular weight				288.38 g/mol	
Critical micelle concentration at 298 K [86]				8 mmol/l	
<b>SRFA</b>					
Average molecular weight [87]				800 g/mol	
<i>Elemental composition<sup>(a)</sup> %</i>					
Carbon	Hydrogen	Oxygen	Nitrogen	Sulfur	Phosphorous
52.44	4.31	42.20	0.72	0.44	<0.01
<i>Solution state <sup>13</sup>C NMR estimate of carbon distribution [88] %</i>					
Carbonyl 220-190 ppm	Carboxyl 190-165 ppm	Aromatic 165-110 ppm	Acetal 110-90 ppm	Heteroaliphatic 90-60 ppm	Aliphatic 60-0 ppm
7	20	24	5	11	33

a. From product information provided by IHSS.

## 4.3 Results and Discussion

### 4.3.1 Surface Excess of SRFA

Figure 4.1 shows the adsorption of SRFA on the water surface and the decrease in the air-water interfacial tension. The surface tension of SRFA solution decreased monotonically with increase in the aqueous concentration of SRFA indicating that the fulvic acid is surface active. The surface tension decreased sharply at low aqueous concentrations whereas the rate of decrease was slower at high concentrations. Previous report [89] on the surface tension of a sediment-derived fulvic acid showed that the surface tension decrease showed a distinct break at what was termed an aggregation concentration of  $12.3 \text{ g}\cdot\text{L}^{-1}$  ( $1.5 \times 10^{-2} \text{ mol}\cdot\text{L}^{-1}$ ). However, no such distinct aggregation concentration was observed in the present case. From the surface tension change, the surface excess of SRFA was obtained using the Gibbs adsorption equation

$$\Gamma_s = -\left(\frac{a_s}{RT}\right) \frac{d\sigma}{da_s} \quad \text{Eqn. 4.1}$$

where  $\Gamma_s$  is the surface excess of SRFA ( $\text{mol}\cdot\text{cm}^{-2}$ ),  $\sigma$  is the aqueous surface tension ( $\text{mN}\cdot\text{m}^{-1}$ ), and  $a_s$  is the activity of SRFA in the bulk solution ( $\text{mol}\cdot\text{L}^{-1}$ ). For dilute solutions activity is the same as concentration,  $C_s$ , of SRFA in the aqueous phase ( $\text{mol}\cdot\text{L}^{-1}$ ). The surface excess data was fitted to a Langmuir equation of the form

$$\Gamma_s = \frac{\Gamma_{\max} C_s}{C_{1/2} + C_s} \quad \text{Eqn. 4.2}$$

As shown in Figure 4.1, we obtained values of  $\Gamma_{\max} = 2.3 \times 10^{-10} \text{ mol}\cdot\text{cm}^{-2}$  and  $C_{1/2} = 3.5 \times 10^{-4} \text{ mol}\cdot\text{L}^{-1}$  by fitting the surface excess data to the above equation. The maximum monolayer adsorption capacity,  $\Gamma_{\max}$ , was used to obtain the surface area occupied by an SRFA molecule, which was  $0.72 \text{ nm}^2$ . Reported literature values [89] are in the range  $0.3 - 0.72 \text{ nm}^2$ .

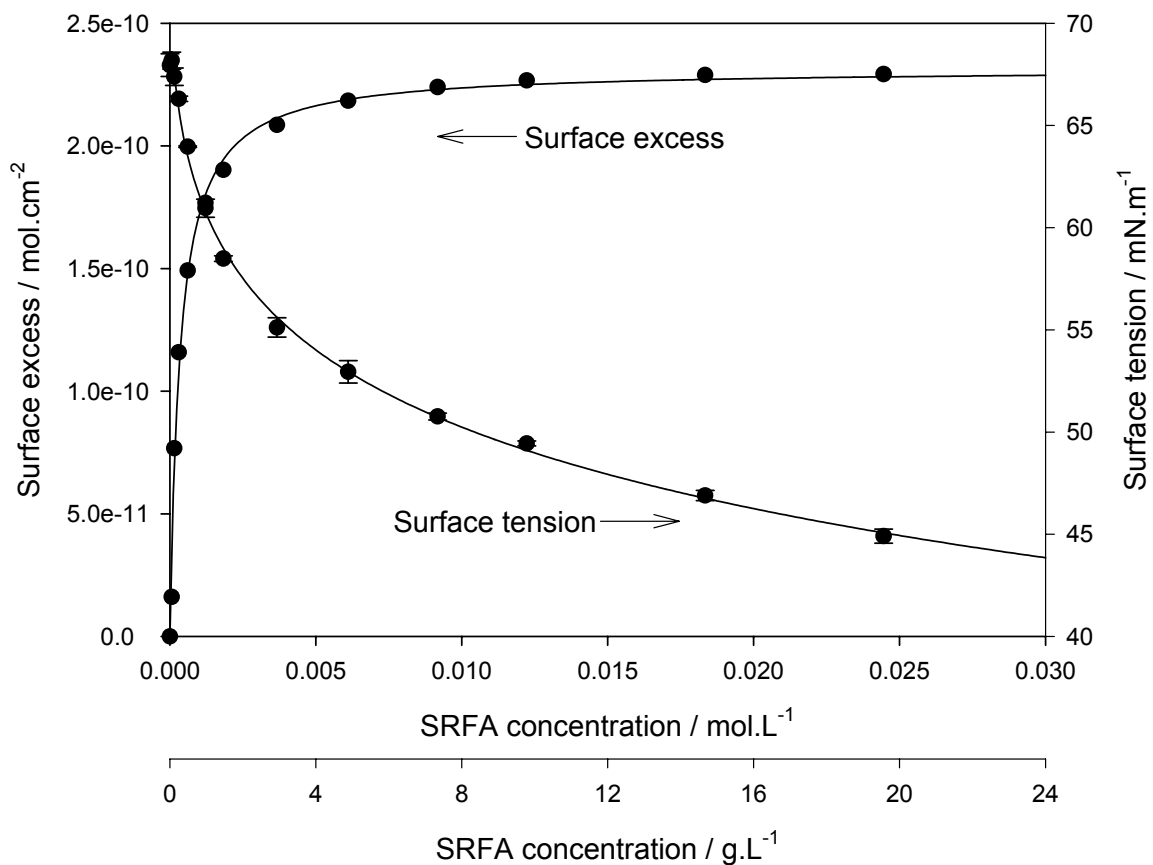


**Figure 4.1.** Surface tension change of the aqueous solution of SRFA. Also shown is the surface excess of SRFA at the air-water interface fitted to a Langmuir isotherm.

### 4.3.2 Uptake of Naphthalene into Surfactant Films

The uptake of naphthalene from the gas phase by a 450  $\mu\text{m}$  aqueous film as a function of the aqueous phase surfactant (SRFA and SDS) concentration is shown in Figure 4.2. In all these cases, a constant gas-phase naphthalene concentration was maintained in the flow reactor. The uptake of naphthalene into the film is gas-phase diffusion controlled at very low gas flow rates. Previous work from our laboratory had determined that for uptake into pure water a gas flow rate  $> 100 \text{ cm}^3 \cdot \text{min}^{-1}$  in the reactor was enough to eliminate the gas-phase diffusion resistance to mass transfer of naphthalene [90]. The aqueous naphthalene concentration was determined after equilibrium between the aqueous and gas phases in the flow reactor had been achieved. As has been demonstrated in Chapter 3, the effect of the interface thickness on the overall partition ratio for naphthalene becomes evident only at  $\delta < 1 \mu\text{m}$ . Therefore, the uptake of naphthalene from the gas phase by the 450  $\mu\text{m}$  aqueous film can be seen as bulk phase behavior. For most conventional surfactants such as SDS the expected trend is a minimal increase in naphthalene uptake (solubility) until the critical micelle concentration (CMC) of the surfactant is reached. Above the CMC, the micellar pseudo-phase in the aqueous solution greatly increases the uptake and a sharp linear increase in solubility is to be expected [91]. Indeed such behavior was noted for naphthalene uptake in the presence of SDS. However, we observed that the aqueous naphthalene concentration only slightly increased at small SRFA concentrations. Only at high SRFA concentrations did the naphthalene solubility in the aqueous phase exceed the pure water solubility. No sharp increase in naphthalene uptake was noted in the case of SRFA. This is due to the lack of a critical aggregation concentration for SRFA at which a micelle-like structure is formed in the aqueous phase. The observed small increase in naphthalene uptake results from the “partition-like” hydrophobic interaction between naphthalene and SRFA.

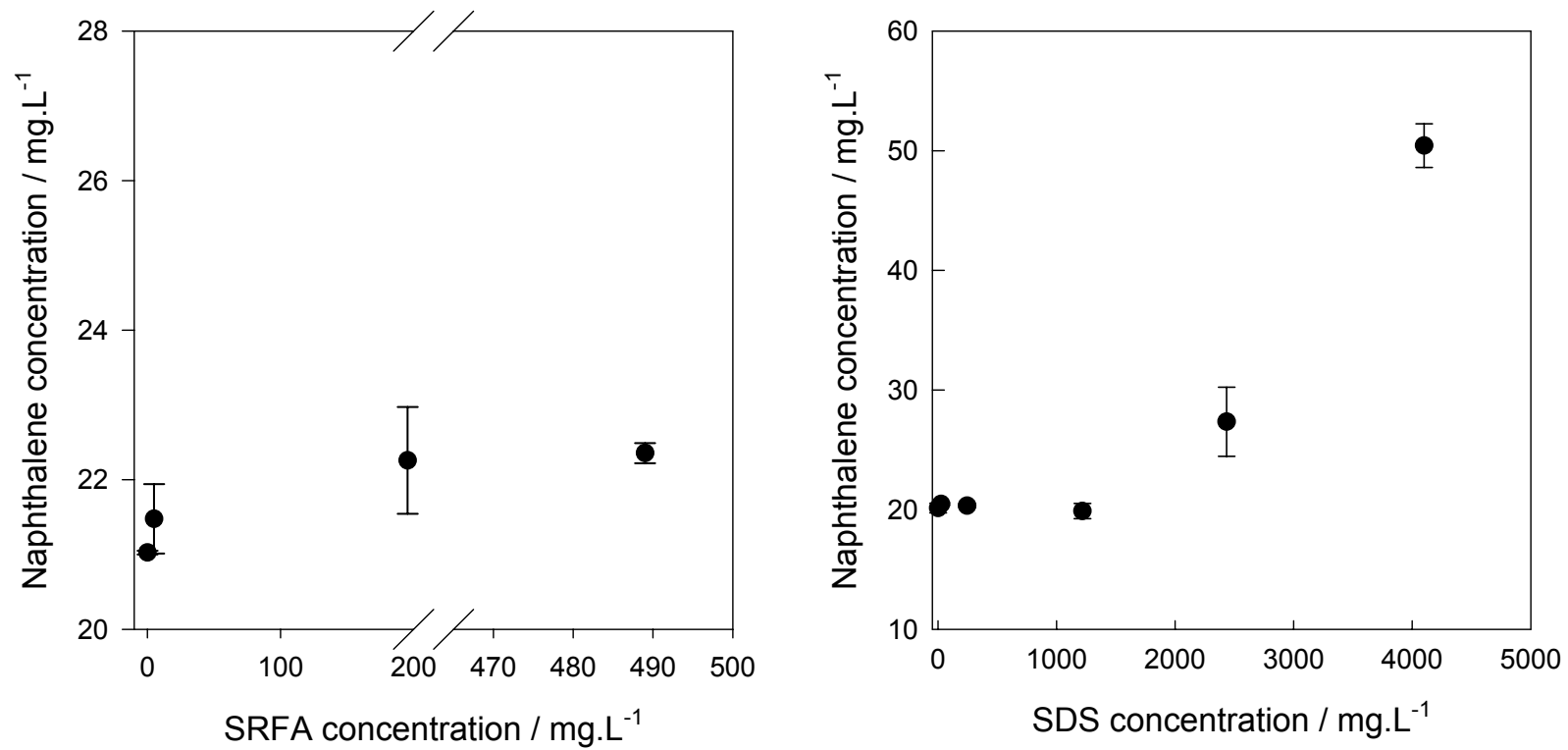


**Figure 4.2.** Uptake of naphthalene from the gas phase on an aqueous film (450  $\mu\text{m}$ ) with different surfactant (SRFA and SDS) concentrations.

### 4.3.3 Adsorption of Phenanthrene on Surfactant Films

Figure 4.3 shows the variation in the total aqueous concentration of phenanthrene in surfactant aqueous films and pure water films as a function of the inverse of the film thickness. A linear relationship was observed indicating the validity of the assumption that with decreasing film thickness (increasing  $1/\delta$ ) the surface adsorption becomes the predominant uptake mechanism. According to Eqn. 3.7, we can calculate the value of the bulk partition constant,  $K_{WA}$ , from the y-intercept of Figure 4.3 and the value of the interface partition (adsorption) constant,  $K_{IA}$ , from the y-intercept and the slope of Figure 4.3. Values of  $K_{IA}$  and  $K_{WA}$  for each solution film are shown in Table 4.2. In pure water, the  $K_{IA}$  and  $K_{WA}$  values obtained were  $3.3 \times 10^4 \mu\text{m}$  and 1019 respectively. For an aqueous film that contains  $207 \text{ mg}\cdot\text{L}^{-1}$  of SDS in the aqueous phase, which is equivalent to a monolayer of SDS, the partition constant,  $K_{IA}$  increased to  $1.2 \times 10^5 \mu\text{m}$ . The corresponding bulk water-air partition constant with aqueous phase SDS was 1019 showing no variation in the bulk phase equilibrium. Also, for two different levels of SRFA in the aqueous phase, 51.5 and  $280 \text{ mg}\cdot\text{L}^{-1}$ , which correspond to 15% and 50% surface coverage of SRFA, the values of  $K_{IA}$  obtained were  $3.1 \times 10^4$  and  $8.1 \times 10^4 \mu\text{m}$  respectively. The corresponding  $K_{WA}$  values for the two aqueous concentrations of SRFA were 1019 and 1175 respectively indicating little variation in the bulk phase equilibrium. Thus, it is clear that the presence of surface active materials in the aqueous phase at substantial concentrations effectively increase the overall equilibrium partitioning to the air-water interface and uptake by the water film. The degree of increase in the equilibrium partitioning was determined by the surface coverage of the surfactants and the hydrophobic interactions between the surfactants and phenanthrene.

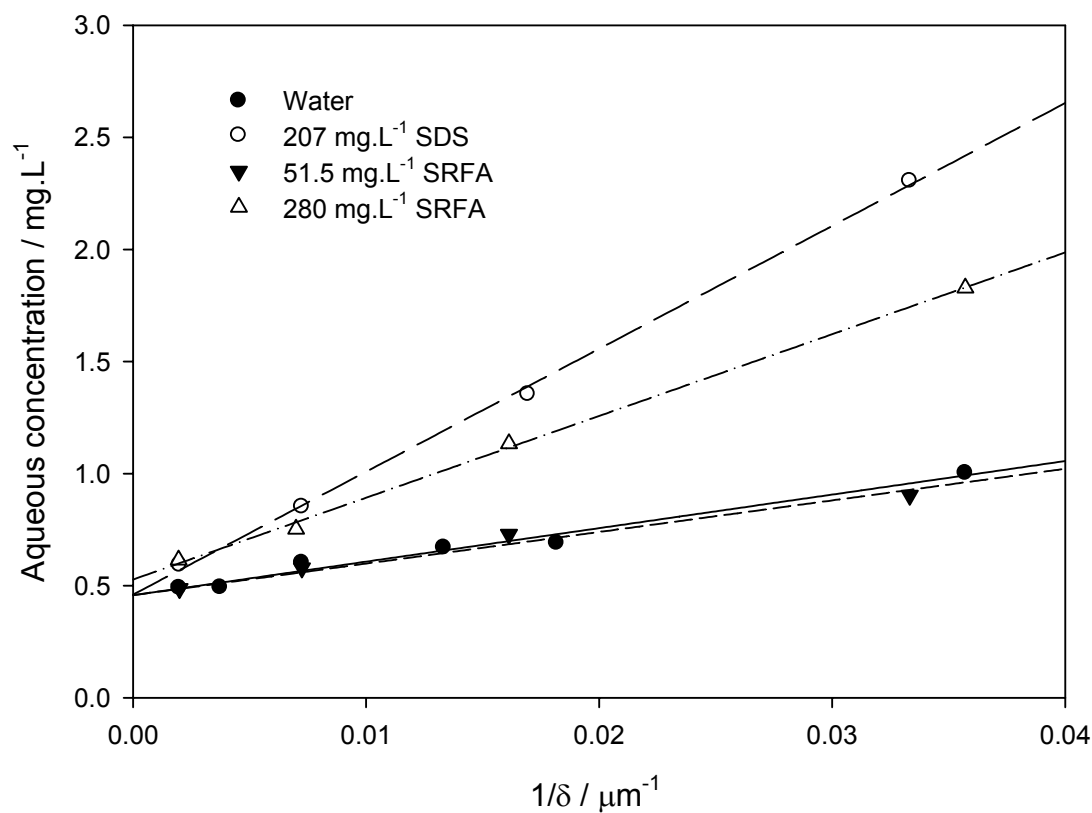


**Figure 4.3.** Uptake of phenanthrene from the gas phase on aqueous films with varying thicknesses.

**Table 4.2.** Bulk and Interface Air-water Partition Constants of Phenanthrene (T=296 K)

<i>Partition constant</i>	<i>Water</i>		<i>SDS</i>	<i>SRFA</i>	<i>SRFA</i>
	<i>This work</i>	<i>Reference</i>	<i>207 mg.L<sup>-1</sup></i>	<i>51.5 mg.L<sup>-1</sup></i>	<i>280 mg.L<sup>-1</sup></i>
$K_{WA} / [-]$	1019	955 <sup>a</sup>	1019	1019	1175
$K_{IA} / [\mu\text{m}]$	$3.3 \times 10^4$	$3.5 \times 10^4$ <sup>b</sup>	$1.2 \times 10^5$	$3.1 \times 10^4$	$8.1 \times 10^4$

*a.* Data obtained from “Groundwater Chemicals: Desk Reference” [65].

*b.* Data obtained from correlation:  $\log(K_{IA}/m) = +0.940 \log(K_{OA}/[-]) - 8.607$ ;  $r^2 = 0.987$  [63].  $K_{OA}$  is the octanol-air partition constant for the compound.  $\log K_{OA} = 7.602$  for phenanthrene at 298K [71].

## CHAPTER 5

# UV PHOTO-OXIDATION OF GAS-PHASE NAPHTHALENE ON ATMOSPHERIC WATER FILMS\*

### 5.1 Introduction

Atmospheric PAHs are subjected to a number of fate and transport processes through which their removal, distribution and transformations could occur. These processes can include physical removal by dry and wet deposition (rain, fog, snow), chemical and photochemical reactions in the gas phase and aerosol phase, and dispersion by convection. PAHs in the atmosphere can be converted through oxidation and photooxidation reactions. Photooxidation reactions play an important part in converting PAHs because of their strong absorption of UV light in the range of 300-420nm, which is a part of the solar light spectrum.

There have been numerous reports of the homogeneous reactions of gas-phase PAHs with atmospheric oxidants [45]. Similarly, there have been some reports of the heterogeneous reactions of adsorbed PAHs with ozone, hydroxyl and nitrate radicals on solid particulate surfaces (soot, and aerosols) in the atmosphere [92-94]. In general PAHs adsorbed to natural particles such as soot or fly-ash are more stable than in the pure form or adsorbed on silica gel, alumina or glass surfaces. Most of these reports are for dry particles in the atmosphere.

---

\* Reproduced in part with permission from Journal of Physical Chemistry A, 2006, Volume 110, Pages 9161-9168, J. Chen, F. S. Ehrenhauser, K. T. Valsaraj, M. J. Wornat, *Uptake and UV-photooxidation of Gas-phase PAHs on the Surface of Atmospheric Water Films. 1. Naphthalene*. Copyright 2006 American Chemical Society. Reproduced in part with permission from Journal of Physical Chemistry A, 2007, Volume 111, Pages 4289-4296, J. Chen and K. T. Valsaraj, *Uptake and UV-Photooxidation of Gas-Phase Polyaromatic Hydrocarbons on the Surface of Atmospheric Water Films. 2. Effects of Dissolved Surfactants on Naphthalene Photooxidation*. Copyright 2007 American Chemical Society.

Air-water interface presents the largest environmental interface. This can be in the form of bulk phases in contact (air-sea), dispersed phases (air bubbles or water droplets) or thin films of water (aerosols). Apart from the equilibrium distribution of a chemical between bulk phases (water and air), very little information is available on the behavior at the air-water interface. When the surface area presented by water is much larger than the bulk volume, heterogeneous chemistry becomes more important than homogenous reactions in either the bulk air or water phases.

In this work, photochemical transformations of gas-phase naphthalene were studied in the flow-tube reactor with a view to understanding the photochemical reactions occurring in thin water films such as those of aerosols and fogs. Naphthalene was first selected for this study because of its relatively high vapor pressure under room temperature compared to other PAHs. Suwannee River fulvic acid (SRFA) was chosen as a surrogate for the surface active humic-like substances present in atmospheric water films. To compare with SRFA, the effect of a conventional surfactant, sodium dodecyl sulfate, on photochemical transformations of naphthalene was also studied.

## **5.2 Photooxidation of Naphthalene on Pure Water Films**

### **5.2.1 Experimental Section**

The system used for the photooxidation reactions of naphthalene on water films was identical to that used for adsorption experiments [90]. Naphthalene vapor/air mixture was introduced to the horizontal flow-tube reactor at a total flow rate of  $100 \text{ cm}^3 \cdot \text{min}^{-1}$  and naphthalene adsorbed onto the water film coated on the glass trough inside of the flow-tube reactor. After the aqueous concentration of naphthalene ceased increasing indicating that partition equilibrium was achieved between the gas and liquid phases, two UV lamps on top of the flow-tube reactor were switched on, delivering UV light with wavelengths that ranged

between 280 and 315 nm and peaked at 302 nm. The UV light intensity on the surface of the film was  $1.85 \text{ W.m}^{-2}$ . Photoreaction of naphthalene was allowed to occur for a given duration of time before samples were taken for analysis. During the photooxidation experiments, the gas phase concentration of naphthalene was assumed constant and the reactor temperature was maintained at 296 K by the cooling bath. Naphthalene vapor was continuously introduced into the reactor to compensate for loss of naphthalene during the reaction and thus naphthalene concentration in the liquid phase remained constant. The ratio of the volume to the surface area of the film was determined to be the film thickness. Films with two different levels of thickness, 22  $\mu\text{m}$  and 450  $\mu\text{m}$ , were employed for photoreaction.

To compare the reactions in water films with that in bulk water, we also conducted experiments in the same reactor but with several small (i.d. 0.0254 m) vials containing 6 mL solution of naphthalene. To keep the conditions similar to the thin film case (constant naphthalene concentration in the liquid phase) we placed pure crystals of naphthalene in the vials during the reaction as was done by McConkey et al [40].

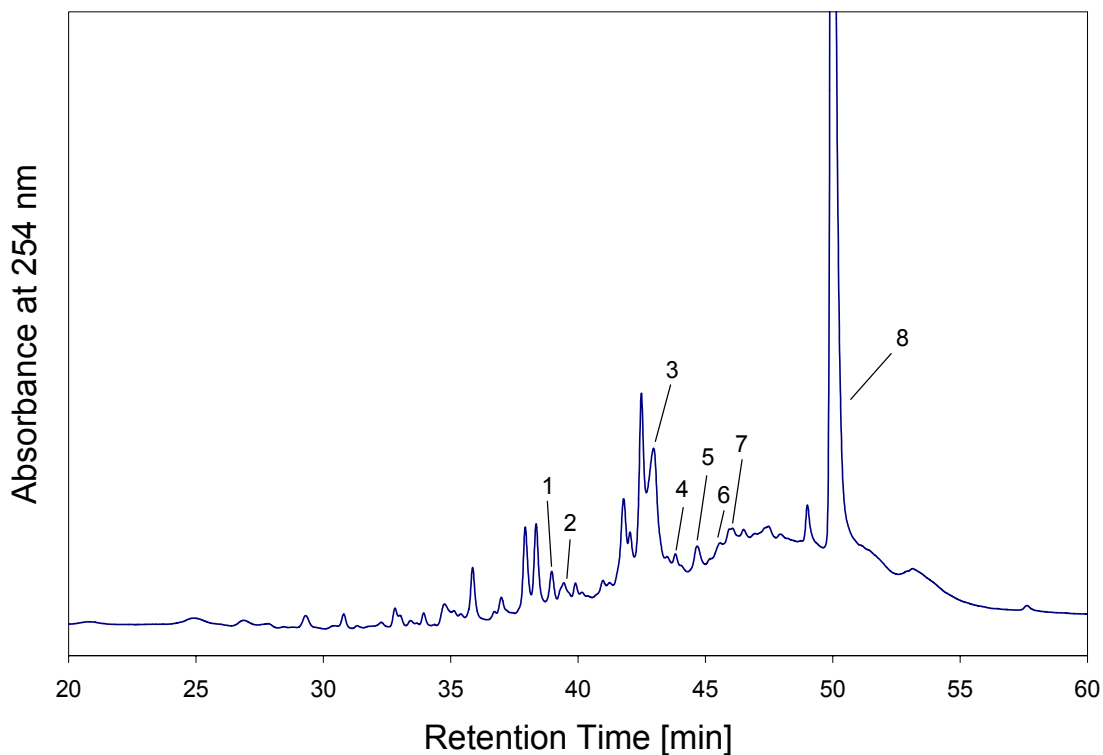
Quantification of naphthalene and products in the aqueous samples was done using liquid chromatography. Identification of compounds was achieved by matching retention times of standard solutions within  $\pm 0.1$  min and by matching the UV spectrum of the standards and the sample. The instrument consisted of an Agilent Technologies HPLC 1100 series with online degasser (G1379A), quaternary pump (G1311A), autosampler (G1313A), column thermostat (G1316A), diode array UV detector (G1315B) and mass spectrometer (G1956B) with atmospheric pressure photo ionization (APPI) interface. An Ultra Aqueous C18<sup>®</sup> column of 0.25 m x 0.0021 m with 5  $\mu\text{m}$  particle size (Restek Corp, USA) was used. The injection volume was 100  $\mu\text{l}$  and the column thermostat was set to 30  $^{\circ}\text{C}$ . The mobile phase started at 100 % ammonia formate buffer pH 3.0; 5 M ammonia formate solution and held for 10 min, then ramped up to

100 % Methanol within 60 min and held for 15 minutes at a constant flow rate of  $2 \times 10^{-7}$  m<sup>3</sup>/min. The detection wavelength was set to 254 nm with 4 nm bandwidth and 4 nm slit.

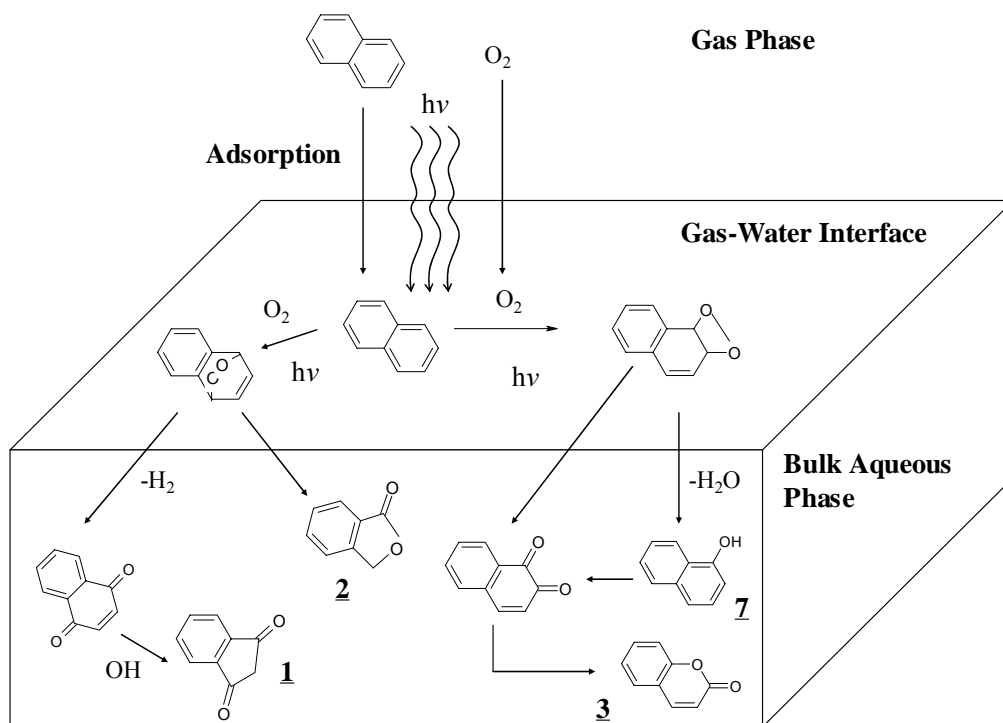
### 5.2.2 Results and Discussion

Figure 5.1 shows a typical HPLC chromatogram of a sample of thin water film (450  $\mu$ m) with adsorbed naphthalene exposed to UV irradiation for 16 hours. There are several peaks in the chromatogram, eight of which have been unequivocally identified by matching the UV spectra and retention times with those of authentic reference standards. Our analyses demonstrated that the major photooxidation products of naphthalene on thin films were several oxygenated products. We focused on four major products that were always observed in the aqueous samples; these are peaks 1, 2, 3 and 7, identified respectively as 1,3-Indandione, 1(3H)-Isobenzofuranone (Phthalide), 2H-1-benzopyran-2-one (Coumarin), and 1-Naphthol. Quantification of compounds was also done on the HPLC.

The mechanisms of photooxidation of PAHs are well established in the literature [40, 95]. The possible route for the formation of these compounds is by the addition of oxygen to the naphthalene ring by either [2 + 2] or [2 + 4] photocycloaddition mechanism [40] and shown schematically in Figure 5.2. The two types of endoperoxides so formed undergo further transformations. Although most oxidizing reactions produced dimerized or larger ring products, none was observed in this work. 1-Naphthol is a major compound obtained from one of the endoperoxides, which has been shown to easily lead to 1,2-naphthoquinone [96]. The endoperoxide can also lead directly to 1,2-naphthoquinone by elimination of a molecule of H<sub>2</sub>. Naphthoquinone was observed in some of our samples. However, it was quickly subjected to further chemical reactions, and did not accumulate in sufficient concentration to be detected in our analytical system under all conditions. 1,2-naphthoquinone is known to lead to the formation



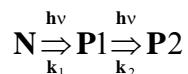
**Figure 5.1.** Detailed HPLC trace of the aqueous film sample after 16 h exposure to UV light. The compounds identified are: 1,3-Indandione (1), Phthalide (2), Coumarin (3), 1-Indanone (4), 1,4-Naphthoquinone (5), 2-Naphthol (6), 1-Naphthol (7), Naphthalene (8).



**Figure 5.2.** Mechanisms for the formation of main products identified in the HPLC trace of the aqueous film samples.

of coumarin. Although coumarin is known to form dimers under certain conditions [97], no such dimers were detected in our system. The [2 + 4] cycloaddition endoperoxide is known to form 1(3H)-Isobenzofuranone (Phthalide) upon photolysis by elimination of an acetylene molecule, which is known to be a stable compound. The [2 + 4] cycloaddition product also is known to produce 1,4-naphthaquinone which easily undergoes hydroxylation and a carbon atom loss leading to 1,3-indandione [98]. Thus, in the UV photodegradation of naphthalene some products are unstable intermediates while others are stable products.

As stated in Chapter 3, there is a substantial free energy minimum (-24 kJ/mol) for naphthalene adsorption at the air/water interface from the gas phase. This is equivalent to a 16,000 times enrichment at the interface over the gas phase. It has been reported by Vacha et al that molecular dynamics simulations showed that oxygen also has a free energy minimum of -0.5 kJ/mol for adsorption at 300 K which translates to a 240% enhancement of O<sub>2</sub> at the interface compared to the gas phase [99]. Thus, it can be hypothesized that the reaction starts by adsorption of naphthalene and reaction with oxygen at the air-water interface to form either a [2+2] or a [2+4] adduct molecule as shown in Figure 5.2. The adduct molecule further reacts and converts to products that are water-soluble and have very low volatility (Figure 5.2). The reactor data can be explained based on the following “global” mechanism:



where N is the adsorbed naphthalene, P1, and P2 are products of photoreaction. Note that both  $k_1$  and  $k_2$  in the above scheme are overall rate constants that include the photochemistry in the bulk phase and surface reactions [100]. For the special case where N is constant the overall rate of product formation is given by [101]

$$C_{P1}(t) = \frac{k_1}{k_2} \cdot C_{N0} [1 - e^{-k_1 t}] \quad \text{Eqn. 5.1}$$

Thus, for this general case, the product concentration exponentially reaches a constant value given by  $(k_1/k_2)C_{N0}$ . If P1 is a stable product, further degradation can be neglected. In this case, one obtains

$$C_{P1}(t) = k_1 C_{N0} t \quad \text{Eqn. 5.2}$$

Thus for the special case where P1 is a stable product, a linear increase in product concentration with time will be noted. Fitting the data to Eqn. 5.1 will give  $k_1$  and  $k_2$  for a specific product.

Figures 5.3 and 5.4 show the change in the concentration of various products and naphthalene in the liquid phase as a function of time for reactions respectively in a thick film (450  $\mu\text{m}$ ) and a thin film (22  $\mu\text{m}$ ). In each case, the average of five replicate experiments is shown. The concentration of three products (coumarin, 1,3-indandione and 1-naphthol) reached a maximum whereas that of phthalide continued to increase. The rate constants of formation of products ( $k_1$ ) and their dissipation ( $k_2$ ) obtained by fitting data to Eqn. 5.1 are given in Table 5.1. The fit to the non-linear equation was good in all cases. The rate constant for the formation of the product from naphthalene,  $k_1$ , was in all cases larger for the thin film than for the thick film case. In other words,  $k_1$  was larger when the surface area per unit volume of the water film ( $1/\delta$ ) increased, indicating contribution from heterogeneous reactions. Moreover, for the bulk reaction, we observed that the rate constants were very similar to those for the thick film reaction. Increases of 30% (coumarin), 192% (phthalide), 31% (indandione) and 80% (1-naphthol) were observed as the surface area per unit volume increased 568-fold.

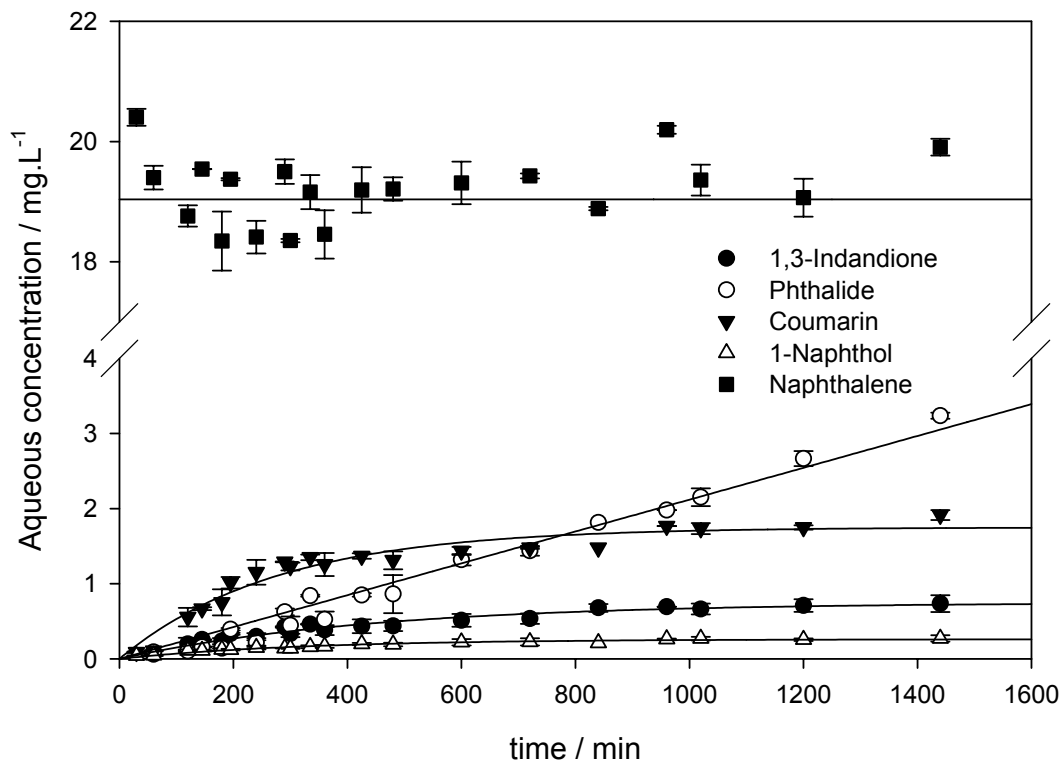


**Figure 5.3.** Photooxidation of naphthalene vapor on a 450  $\mu\text{m}$  water film.

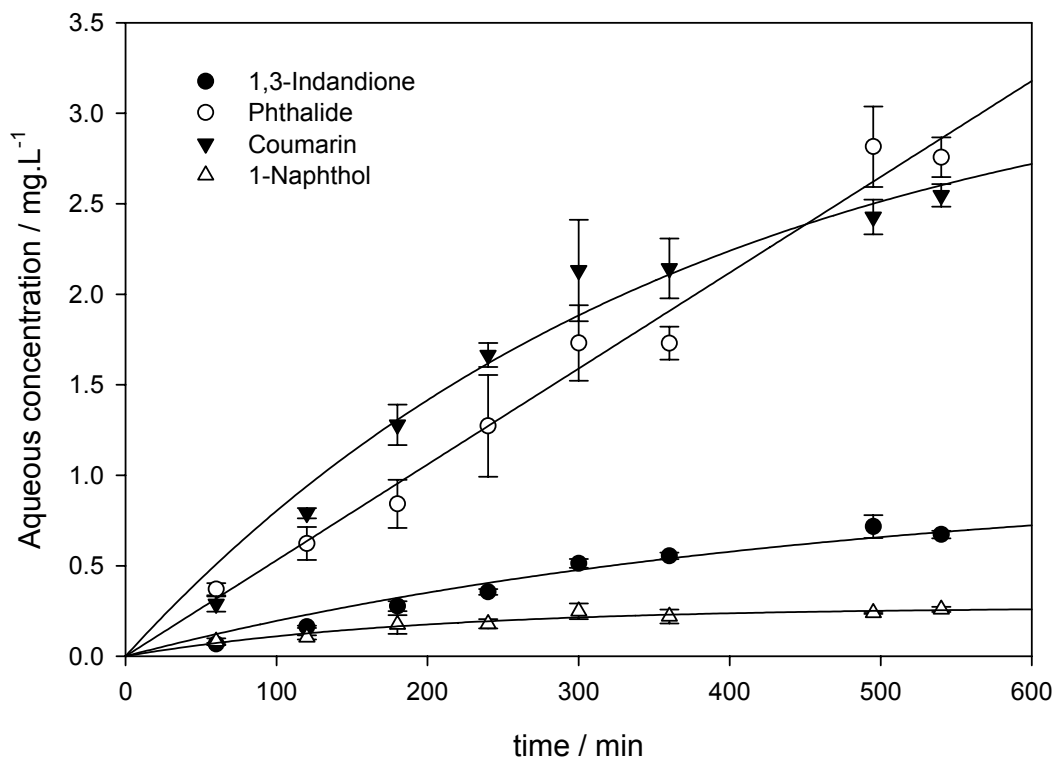


**Figure 5.4.** Photooxidation of naphthalene vapor on a 22  $\mu\text{m}$  water film.

**Table 5.1.** Kinetic rate constants for product formation in water films in the reactor <sup>a</sup>

<i>Compound</i>	<i>Thin film (22 μm) reaction (1/δ = 454 cm<sup>-1</sup>)</i>			<i>Thick film(450 μm) reaction (1/δ = 25 cm<sup>-1</sup>)</i>			<i>Bulk Liquid reaction (1/δ = 0.8 cm<sup>-1</sup>)</i>		
	<i>k<sub>1</sub> / min<sup>-1</sup></i>	<i>k<sub>2</sub> / min<sup>-1</sup></i>	<i>R<sup>2</sup></i>	<i>k<sub>1</sub> / min<sup>-1</sup></i>	<i>k<sub>2</sub> / min<sup>-1</sup></i>	<i>R<sup>2</sup></i>	<i>k<sub>1</sub> / min<sup>-1</sup></i>	<i>k<sub>2</sub> / min<sup>-1</sup></i>	<i>R<sup>2</sup></i>
Coumarin	4.8 x 10 <sup>-4</sup>	2.7 x 10 <sup>-3</sup>	0.969	3.3 x 10 <sup>-4</sup>	3.6 x 10 <sup>-3</sup>	0.945	3.7 x 10 <sup>-4</sup>	4.0 x 10 <sup>-3</sup>	0.982
Phthalide	2.8 x 10 <sup>-4</sup>	--	0.981	1.1 x 10 <sup>-4</sup>	--	0.976	9.6 x 10 <sup>-5</sup>	--	0.991
1,3-Indandione	1.1 x 10 <sup>-4</sup>	2.2 x 10 <sup>-3</sup>	0.956	9.7 x 10 <sup>-5</sup>	2.2 x 10 <sup>-3</sup>	0.950	8.4 x 10 <sup>-5</sup>	2.3 x 10 <sup>-3</sup>	0.972
1-Naphthol	7.4 x 10 <sup>-5</sup>	5.2 x 10 <sup>-3</sup>	0.927	4.3 x 10 <sup>-5</sup>	3.1 x 10 <sup>-3</sup>	0.952	4.1 x 10 <sup>-5</sup>	3.4 x 10 <sup>-3</sup>	0.903

a. R<sup>2</sup> is the correlation coefficient for the data fit to Eqn. 5.1.

The measured *initial* rate of product formation in the flow reactor is given by

$$+r_{P0} = k_{\text{homo}} C_{N0} + k_{\text{hetero}} \frac{\Gamma_{N0}}{\delta} \quad \text{Eqn. 5.3}$$

where  $\Gamma_{N0}$  (mol.m<sup>-2</sup>) is the surface concentration of naphthalene,  $\delta$  is the film thickness (m), and  $C_{N0}$  is the bulk aqueous phase concentration of naphthalene (mol.m<sup>-3</sup>).  $k_{\text{homo}}$  (min<sup>-1</sup>) is the homogenous (bulk liquid phase) reaction rate constant and  $k_{\text{hetero}}$  (min<sup>-1</sup>) is the heterogeneous (surface) reaction rate constant. Since,  $\Gamma_{N0}=(K_{IA}/K_{WA})C_{N0}$ , we can rewrite the above equation as

$$+r_{P0} = \left( k_{\text{homo}} + \frac{k_{\text{hetero}}}{\delta} \cdot \frac{K_{IA}}{K_{WA}} \right) C_{N0} \quad \text{Eqn. 5.4}$$

We established earlier that surface effects are negligible for bulk (or thick film) reactions, which therefore, give us directly the value of  $k_{\text{homo}}=k_{1,\text{bulk}}$ . Using Eqn. 5.4 the value of  $k_{\text{hetero}}$  can be calculated from the overall  $k_1$  obtained for the thin film reaction. The values of  $k_{\text{hetero}}$  (min<sup>-1</sup>) obtained were  $9.9 \times 10^{-3}$  (coumarin),  $1.66 \times 10^{-2}$  (phthalide),  $2.3 \times 10^{-3}$  (indandione) and  $3.0 \times 10^{-3}$  (1-naphthol).

The reasons for higher reaction rates at the air-water interface compared to the case in the bulk water phase are probably twofold. First, the interfacial concentrations of reactive species are enhanced due to their free energy minimum at the interface. Second, the quantum yield for photolysis is larger at the interface than in the case in the bulk water phase due to the decreased solvent-cage effect at the interface. Solvents in bulk-liquids tend to encapsulate photo-fragments, which leads to higher probability of recombination and a correspondingly lower quantum yield for decomposition. This is termed as the solvent-cage effect [102]. Half of the solvent-cage is absent on the surface, therefore, the solvent-cage effect is decreased. As a result, the photolysis quantum yield is enhanced on the surface, leading to enhanced production of free radicals and other reactive species.

### 5.2.3 Atmospheric Implications

In films of water that comprise aerosols and fog, reactions can be expected to occur similar to those observed in thin water films. The rates of product formation in water films can rival or exceed those observed in bulk water reactions. In the atmosphere, the loss of naphthalene via photooxidation in thin water films on particles and dispersoids should be weighed against other dominant reaction loss processes. The competing reactions include (i) the homogeneous gas-phase oxidation of naphthalene by photochemically generated hydroxyl radical, and (ii) the heterogeneous oxidation of adsorbed naphthalene on solid particles by photochemically generated gas-phase hydroxyl radical. Let us consider 1 m<sup>3</sup> of air containing 1 ppm<sub>v</sub> of gas-phase naphthalene and estimate the reaction life time in the atmosphere due to the three processes considered above.

The lifetime due to homogeneous oxidation in air by hydroxyl radical is given by

$$\tau_1 = \frac{1}{k_{OH}[OH^*]} \quad \text{Eqn. 5.5}$$

where  $k_{OH}$  is the second order reaction rate constant of naphthalene with  $OH^*$  ( $= 2.2 \times 10^{-17} \text{ m}^3 \cdot \text{molecule}^{-1} \cdot \text{s}^{-1}$ ). Adopting a typical atmospheric  $[OH^*]$  of  $1.4 \times 10^{12} \text{ molecules} \cdot \text{m}^{-3}$ , we derive  $\tau_1 = 9$  hours.

The lifetime due to heterogeneous oxidation of naphthalene adsorbed on solid particles by photochemically generated OH radicals in air is given by [103]

$$\tau_2 = \frac{C_g}{-r_{het,s}} = \frac{C_g}{\omega \frac{\gamma}{4} A_N [OH^*]} \quad \text{Eqn. 5.6}$$

where  $\omega$  is the thermal velocity of the hydroxyl radical ( $= 661 \text{ m} \cdot \text{s}^{-1}$ ).  $\gamma$  is the reaction probability of  $OH^*$  with adsorbed naphthalene molecule which is taken to be 0.5 consistent with experimental data for PAHs [104]. Assuming a molecular cross section of  $0.5 \text{ nm}^2$  for a

naphthalene molecule, the surface area concentration of naphthalene,  $A_N$  was estimated to be  $12 \text{ m}^2 \cdot \text{m}^{-3}$ . This gives a value of  $\tau_2 = 4.8$  hours.

The lifetime due to UV photochemical reaction of naphthalene adsorbed on a water film is given by the following equation

$$\tau_3 = \frac{C_g}{r_P^0} = \frac{1}{\left( k_{\text{homo}} + \frac{k_{\text{hetero}}}{\delta} \cdot \frac{K_{\text{IA}}}{K_{\text{WA}}} \right) \cdot K_{\text{WA}}} \quad \text{Eqn. 5.7}$$

Consider, for example, the experimental values of the initial rate constants for the formation of coumarin from naphthalene described in Table 5.1. Using the values of  $K_{\text{IA}}$  ( $=21 \text{ } \mu\text{m}$ ) and  $K_{\text{WA}}$  ( $=86$ ) obtained earlier, and values of  $k_{\text{homo}}$  ( $=3.7 \times 10^{-4} \text{ min}^{-1}$ ) and  $k_{\text{hetero}}$  ( $=9.9 \times 10^{-3} \text{ min}^{-1}$ ) for a  $\delta$  of  $15 \text{ } \mu\text{m}$  gives  $\tau_3 = 22 \text{ min}$ .

It is evident from the above calculation that UV-initiated photochemical reactions in water films can compete with other reaction losses and may be of significance on atmospheric particles and dispersions (fog, mist). However, one should caution that these estimates are only preliminary. It is well known that dissolved organic compounds (DOCs) such as humic and fulvic acids in natural water can affect the photochemical reactions [81]. Therefore, to what extent the reaction lifetime of a PAH such as naphthalene will be affected because of DOC should be investigated before extrapolating our results to the natural environment.

### 5.3 Photooxidation of Naphthalene on Surfactant Aqueous Films

Interfacial properties of thin atmospheric water films on aerosols, fogs and ice surfaces are affected to a great extent by the surface-active substances present. Understanding the effects of surface-active substances in atmospheric water films is important for elucidating the processing of organic compounds by aerosols and fogs in the atmosphere [85]. One would expect from a review of the literature that surfactants exert several effects on the heterogeneous chemistry of

gaseous species at the air-water interface. The presence of surfactants can increase the uptake rate of gaseous species; this can occur either through a micellar trapping mechanism at the surface that results in an enhanced aqueous solubility of gas species or via direct hydrogen bonding or covalent bonding between gaseous species and surface molecules. On the other hand, long chain alcohols and acids ( $C_{12}$  or larger) can decrease the permeability of gaseous species through monolayers on the aqueous surface [105]. Surfactant molecules may be involved in surface reactions with adsorbed molecules from the gas phase. Furthermore, the oxidation of the surfactant in the surface layer may present a hydrophilic surface to which uptake may not be favorable. Previous work has shown that these effects can vary with the type of surfactants forming the monomolecular films at the surface [106].

It has been shown via molecular characterization that Suwannee River fulvic acid (SRFA) is a good surrogate model to represent polycarboxylic acids in fog waters [79]. Some studies on the effect of SRFA on PAH photodegradation in bulk water have been carried out but the results appear conflicting. Fasnacht and Blough [107] reported that photoreactivities of PAHs in bulk water solutions were not affected by SRFA. However, other reports showed that whereas the photodegradation of benzo[a]pyrene and benzo[a]anthracene were slowed by HULIS in water, that of naphthalene increased [108]. In this work, we chose SRFA to study the effect of dissolved surfactants on PAH photooxidation in thin water films. In order to compare the result with conventional surfactants, we also conducted separate experiments using sodium dodecyl sulfate (SDS) as the water-soluble surfactant. As we saw in our earlier work on pure water films [90], the air-water interface and the bulk phase reactions occur at different rates and reactions on thin films are predominantly surface reaction limited. SRFA shows multiple effects on naphthalene photooxidation and its presence results in a different photooxidation rate compared to that in pure water films.

### 5.3.1 Experimental Section

#### 5.3.1.1 Photooxidation of Naphthalene

The experimental procedure for the photooxidation reactions of naphthalene on surfactant aqueous films was identical to that on pure water films described in Section 5.2.1. SRFA solutions with varying concentrations (0-949 mg.L<sup>-1</sup>) were used to make the film. The ratio of the volume to the surface area of the film was determined to be the film thickness. Films with two different levels of thickness, 22 μm and 450 μm, were employed for photoreaction. Separate experiments using SDS as the water-soluble surfactant were also conducted. Concentrations of the SDS solutions used to make the SDS film ranged between 0 and 4100 mg.L<sup>-1</sup>.

Quantification of naphthalene and photoreaction products in the aqueous samples was done using a high performance liquid chromatography (HPLC). Identification of compounds was achieved by matching retention times of standard solutions within +/- 0.1 min and by matching the UV spectrum of the standards and the sample. The HPLC instrument consisted of an Agilent Technologies HPLC 1100 series with online degasser (G1322A), quaternary pump (G1311A), autosampler (G1313A), column thermostat (G1316A), and diode array detector (G1315A). An EnviroSep-PP column of 125 mm x 3.20 mm with 5 μm particle size (Phenomenex Corp, USA) was used. The injection volume was 25 μl and the column thermostat was set to 40 °C. The mobile phase started at 100% water (HPLC grade, EMD Chemicals Inc., USA) and held for 3 min, then ramped to 80% acetonitrile (HPLC grade, EMD Chemicals Inc., USA) and 20% water within 6 min and held at this concentration for 5 min, and finally returned to 100% water in 2 min and held for 1 min at a constant flow rate of 0.5 ml/min. The detection wavelength was set to 250 nm with 100 nm bandwidth and 4 nm slit.

### **5.3.1.2 Light Absorption by SRFA**

SRFA solutions exhibit a significant absorption of UV-visible light, especially at high concentrations. To be able to compare the photochemical reaction rates of naphthalene in SRFA solutions to that in pure water, absorbance of SRFA solutions was measured on a Spectronic Genesys 5 UV/Vis spectrophotometer at 302 nm, which is the peak wavelength of the UV light employed in the photooxidation experiments.

### **5.3.1.3 Fluorescence Measurements**

The binding affinity of naphthalene to SRFA was investigated by fluorescence quenching. Fluorescence measurements were conducted on an OLIS DM 45 Spectrofluorimeter. Aqueous naphthalene solution was prepared by adding excessive solid naphthalene to deionized water and shaking the solution in a Blue M shaking bath overnight for equilibration. The solution was filtered and stored in the dark for future use. Naphthalene concentration of the stock solution was determined to be 23 mg.L<sup>-1</sup> by HPLC. For fluorescence measurements, 1 ml of the stock solution and 0.1 ml of SRFA solution with varying SRFA concentration were added and thoroughly mixed in a 1.25 × 1.25 × 4.5 cm PMMA cuvette and fluorescence of the mixed solution was measured at room temperature after 15 min. To serve as the background, fluorescence of solutions containing SRFA only was also measured with the same SRFA concentrations and instrumental conditions. The excitation wavelength of the fluorescence measurements was set at 286.5 nm where the maximum naphthalene fluorescence intensity was obtained. The emission wavelength ranged between 290 and 460 nm at 1-nm increments and the peak emission wavelength was detected to be 332 nm for naphthalene and 432 nm for SRFA.

To correct for inner filter effects, absorbance measurements were taken at 286.5 nm and 332 nm for the same solutions used in the fluorescence measurements. The fluorescence of naphthalene was corrected for both the background fluorescence and the inner filter effect.

## 5.3.2 Results and Discussion

### 5.3.2.1 Photochemical Reactions of Naphthalene in SRFA Aqueous Films

Photochemical reaction kinetics of naphthalene was investigated in 450  $\mu\text{m}$  and 22  $\mu\text{m}$  water films containing SRFA. HPLC chromatograms of the reaction samples showed similar peaks to those of the pure water reaction samples. No extra peaks were observed except for the signals due to SRFA. As for the reaction in pure water, 1,3-indandione, phthalide, coumarin and 1-naphthol were identified to be the four major photooxidation products of naphthalene in SRFA solutions. Quantification of these compounds was done on HPLC, and the reaction rate constants were obtained by fitting the kinetic data to the equation

$$C_{\text{P1}}(t) = \frac{k_1}{k_2} \cdot C_{\text{N0}} (1 - e^{-k_2 t}) \quad \text{Eqn. 5.8}$$

where  $k_1$  is the product formation rate constant,  $k_2$  is the product reaction rate constant,  $C_{\text{P1}}$  is the concentration of the product, and  $C_{\text{N0}}$  is the concentration of naphthalene. The reaction scheme was  $\text{N} \xrightarrow{k_1} \text{P1} \xrightarrow{k_2} \text{P2}$ . A detailed deduction of Eqn. 5.8 was given in Section 5.2.2. SRFA is known to strongly absorb UV-visible light. To compare the reaction rates in SRFA films and pure water films, the measured kinetic rate constants were divided by the light screening factor,  $S_\lambda$ , to correct for internal light filtering by SRFA [109].  $S_\lambda$  is given by

$$S_\lambda = (1 - 10^{-\epsilon_\lambda l C_s}) / 2.303 \epsilon_\lambda l C_s \quad \text{Eqn. 5.9}$$

where  $\epsilon_\lambda$  is the unit absorptivity of SRFA, determined to be  $1.19 \times 10^{-2} \text{ L.mg}^{-1}.\text{cm}^{-1}$  at 302 nm by the absorbance measurements,  $l$  is the light path length (cm), and  $C_s$  is the concentration of SRFA ( $\text{mg.L}^{-1}$ ). The light path length was taken to be the film thickness, which yields the lower limit of the light screening factor. For the 22  $\mu\text{m}$  film, the light screening factor was close to 1 in the concentration range that we investigated and light filtering by SRFA was negligible due to the small path length. However, light attenuation by SRFA in the 450  $\mu\text{m}$  film was notable. To

get a light screening factor of 0.95, we need a SRFA concentration of  $1700 \text{ mg.L}^{-1}$  for a  $22 \text{ }\mu\text{m}$  film but only  $85 \text{ mg.L}^{-1}$  for a  $450 \text{ }\mu\text{m}$  film. Therefore, light attenuation by SRFA should be taken into account for the  $450 \text{ }\mu\text{m}$  film. The rate constants for the  $450 \text{ }\mu\text{m}$  SRFA aqueous film in this work were corrected based on the light screening factor.

Table 5.2 compares the reaction rate constants for the four products in a typical SRFA aqueous film and pure water film. As shown in Table 5.2, the product formation rate constants in SRFA aqueous films at  $C_S = 18.8 \text{ mg.L}^{-1}$  were smaller than those in pure water films of the same film thickness, indicating an inhibiting effect of SRFA on naphthalene photochemical reactions at  $C_S = 18.8 \text{ mg.L}^{-1}$ . To ascertain the inhibiting effect of SRFA on naphthalene photooxidation, we conducted a series of photoreaction experiments over a wide range of SRFA concentration ( $0\text{-}949 \text{ mg.L}^{-1}$ ). The observed formation rate constant,  $k_{1,\text{obs}}$ , for phthalide and coumarin in a  $450 \text{ }\mu\text{m}$  film as a function of the aqueous phase SRFA concentration is shown in Figure 5.5. Interestingly, it turns out that SRFA has multiple effects on naphthalene photochemical reactions instead of a single inhibiting effect. For both products,  $k_{1,\text{obs}}$  initially decreased with an increase in SRFA concentration until  $C_S$  reached around  $50 \text{ mg.L}^{-1}$ . After that,  $k_{1,\text{obs}}$  began to increase with further addition of SRFA to reach an asymptotic bound.

It has been proposed in the literature that singlet oxygen ( $^1\text{O}_2$ ) is the dominant reaction intermediate in the direct photooxidation of PAHs induced by UV light [5, 110]. The PAH photooxidation mechanism by the singlet oxygen route is briefly described as follows. Under UV light, PAH molecules are excited to their singlet state, which has a very short lifetime usually on the order of  $10 \text{ ns}$  or less [109] and can decay in part to the triplet state through intersystem crossing. Energy transfer from triplet PAH molecules to dioxygen molecules produces highly reactive singlet oxygen, which reacts with ground state PAH molecules to produce oxidation

**Table 5.2.** Kinetic rate constants for product formation in SRFA solution films and pure water films (T=296 K).

	Pure water						SRFA (18.8 mg.L <sup>-1</sup> )					
	450 $\mu\text{m}$			22 $\mu\text{m}$			450 $\mu\text{m}$			22 $\mu\text{m}$		
<i>Compound</i>	$k_1$ /min <sup>-1</sup>	$k_2$ /min <sup>-1</sup>	$R^2$	$k_1$ /min <sup>-1</sup>	$k_2$ /min <sup>-1</sup>	$R^2$	$k_1$ /min <sup>-1</sup>	$k_2$ /min <sup>-1</sup>	$R^2$	$k_1$ /min <sup>-1</sup>	$k_2$ /min <sup>-1</sup>	$R^2$ <sup>(a)</sup>
Coumarin	$3.3 \times 10^{-4}$	$3.6 \times 10^{-3}$	0.945	$4.8 \times 10^{-4}$	$2.7 \times 10^{-3}$	0.969	$4.4 \times 10^{-5}$	$6.6 \times 10^{-5}$	0.976	$1.9 \times 10^{-4}$	$1.1 \times 10^{-3}$	0.945
Phthalide	$1.1 \times 10^{-4}$	--	0.976	$2.8 \times 10^{-4}$	--	0.981	$6.2 \times 10^{-5}$	--	0.930	$2.0 \times 10^{-4}$	--	0.960
1,3-Indandione	$8.7 \times 10^{-5}$	$2.2 \times 10^{-3}$	0.950	$1.1 \times 10^{-4}$	$2.2 \times 10^{-3}$	0.956	$3.0 \times 10^{-5}$	$1.6 \times 10^{-4}$	0.988	$7.3 \times 10^{-5}$	$9.3 \times 10^{-4}$	0.961
1-Naphthol	$4.3 \times 10^{-5}$	$3.1 \times 10^{-3}$	0.952	$7.4 \times 10^{-5}$	$5.2 \times 10^{-3}$	0.927	$1.5 \times 10^{-5}$	$1.3 \times 10^{-3}$	0.948	$3.2 \times 10^{-5}$	$1.8 \times 10^{-3}$	0.952

<sup>(a)</sup>  $R^2$  is the correlation coefficient for the data fit to Equation 3.

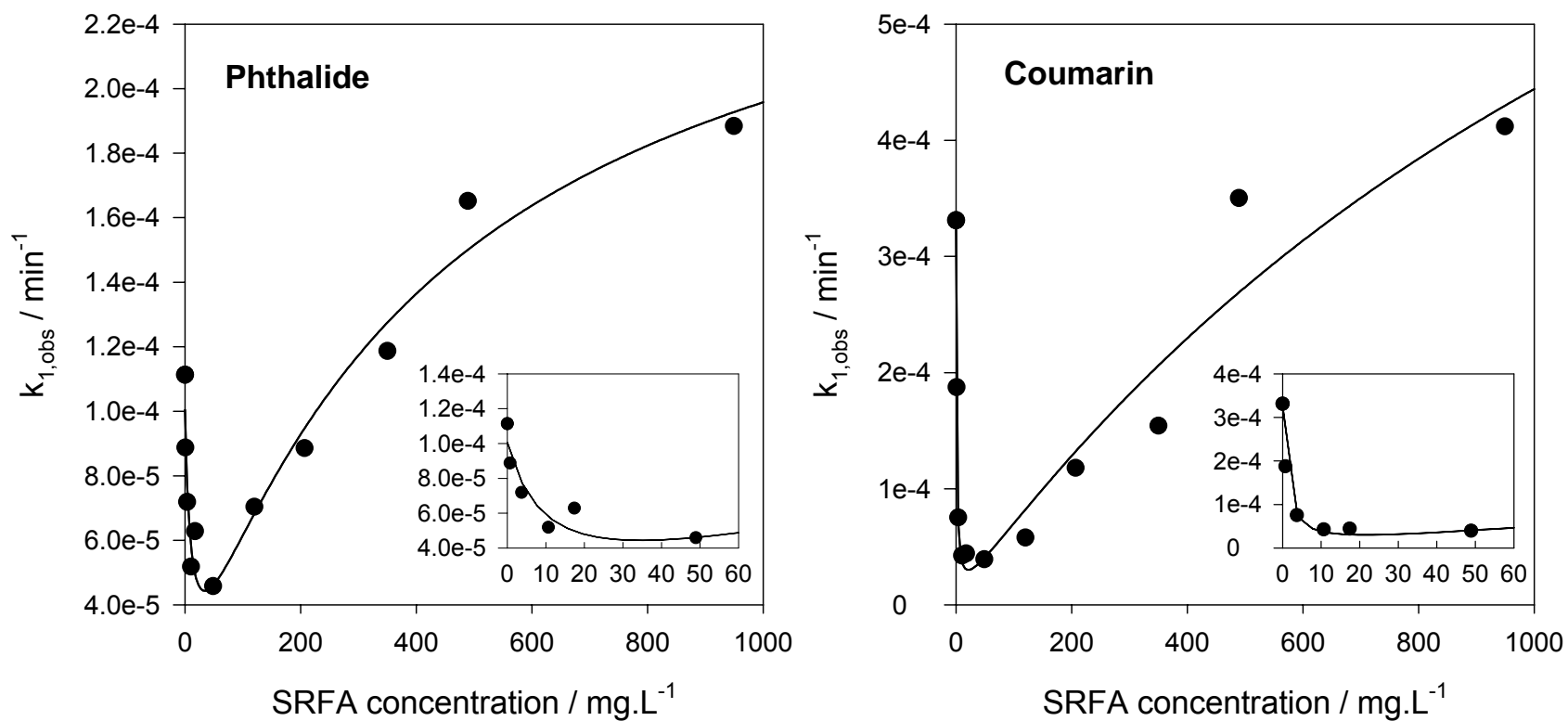


**Figure 5.5.** Effect of SRFA on the observed formation rate constants for phthalide and coumarin in a 450  $\mu\text{m}$  aqueous film. The solid lines represent the theoretical fit to experimental data (Eqn. 5.13). The insets are blowups of the data at small SRFA concentrations.

products. On the other hand, UV-light absorption of humic or fulvic acid molecules can also promote them to their singlet excited state and generate singlet oxygen via the same route as PAHs [109, 111, 112]. Therefore, singlet oxygen involved in the photooxidation of naphthalene in SRFA aqueous solutions can be induced either by naphthalene or by SRFA. Figure 5.6 shows the mechanistic scheme that depicts both self-sensitized and SRFA-sensitized photooxidation of naphthalene in SRFA aqueous solutions. In light of this mechanism, the observed photooxidation rates of naphthalene in SRFA solutions are considered to be a combined result of the self-sensitized process and the SRFA-sensitized process. The kinetic data is analyzed as follows based on this hypothesis.

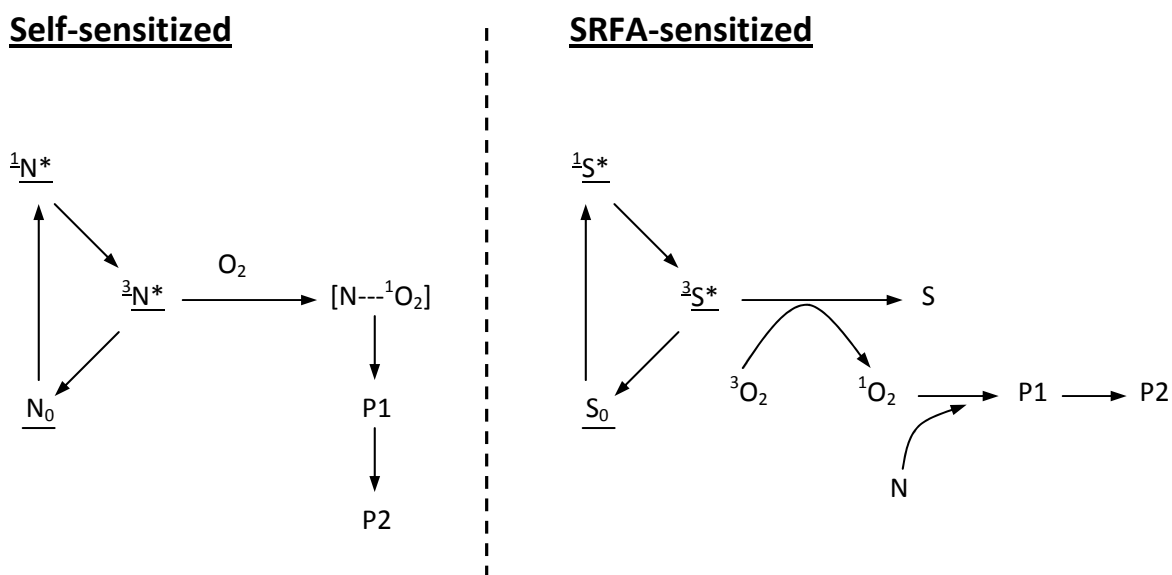


**Figure 5.6.** Mechanistic interpretation of naphthalene oxidation by singlet oxygen via (a) self-sensitized and (b) SRFA-sensitized pathways.

**SRFA-sensitized:**

PAHs are highly hydrophobic and are known to undergo complex formation with humic materials through hydrophobic interactions [113]. As a result of the association between naphthalene and SRFA, naphthalene in SRFA aqueous solutions exists in two regions: the SRFA

region and the bulk aqueous region. Therefore, the product formation rate of naphthalene photooxidation sensitized by SRFA can be expressed by

$$\frac{d[P]}{dt}_{SRFA} = \frac{V_1}{V_{tot}} k_{rxn} [Naph]_1 [^1O_2]_{1,SRFA} + \frac{V_2}{V_{tot}} k_{rxn} [Naph]_2 [^1O_2]_{2,SRFA} \quad \text{Eqn. 5.10}$$

where  $k_{rxn}$  is the bimolecular reaction rate constant of naphthalene with  $^1O_2$  and  $V_1$ ,  $V_2$ , and  $V_{tot}$  are the volumes of the SRFA region, the bulk aqueous region, and the whole solution respectively. The subscript SRFA denotes the contribution from the SRFA-sensitized process and 1 and 2 denote the SRFA and the bulk aqueous phase respectively. The above equation can be coupled with the distribution of naphthalene and SRFA-induced singlet oxygen between the SRFA and the bulk aqueous region to obtain the following equation for product formation (see supporting information in Appendix I for full derivation).

$$\frac{d[P]}{dt}_{SRFA} = (k_{rxn} K_{OM} [^1O_2]_{1,SRFA} + k_{rxn} k_{gen}) \frac{[SRFA]}{1 + K_{OM}[SRFA]} [Naph] \quad \text{Eqn. 5.11}$$

In this equation,  $K_{OM}$  is the partition coefficient of naphthalene to SRFA and  $k_{gen}$  is a kinetic constant describing the concentration of singlet oxygen in the bulk aqueous phase induced by SRFA. The term in the parentheses is a constant.

### **Self-sensitized:**

Although humic substances can induce highly reactive photo-oxidants under UV-visible light [114], they can also quench or scavenge the PAH excited states, free radicals, or other excited species that may be intermediates in the photochemical reactions of PAHs. Considering the self-sensitized photooxidation of naphthalene in the presence of SRFA, the predominant triplet energy of SRFA is estimated to be  $250 \text{ kJ.mol}^{-1}$  [109] and is lower than the triplet energy of naphthalene ( $255 \text{ kJ.mol}^{-1}$  [115]). Therefore, triplet-triplet (T-T) energy transfer occurs between triplet naphthalene and ground state SRFA to give ground state naphthalene and triplet

SRFA. In this way triplet naphthalene is quenched. T-T energy transfer is a spin-allowed process and the quenching normally proceeds at a diffusion-controlled rate [115]. On the other hand, Figure 5.7 shows the fluorescence emission spectrum of naphthalene and the fluorescence excitation spectrum of SRFA in water samples from the fluorescence measurements. Interestingly, we found that both the emission spectrum of naphthalene and the excitation spectrum of SRFA peak at 332 nm. This peak overlap suggests that singlet naphthalene molecules could also transfer their energy to ground state SRFA molecules by fluorescence resonance energy transfer (FRET). Therefore, SRFA can not only quench triplet naphthalene via the T-T energy transfer process but also compete for the energy transferred from singlet naphthalene and inhibit the production of triplet naphthalene. As a result, the production of singlet oxygen induced by triplet naphthalene is inhibited, which consequently slows the self-sensitized photooxidation of naphthalene. Using the Stern-Volmer approach to describe the inhibiting effect of SRFA on the self-sensitized photooxidation of naphthalene, we obtain (see supporting information in Appendix I for full derivation)

$$\frac{d[P]}{dt}_{\text{Naph}} = k_{\text{rxn}}[{}^1\text{O}_2]_0 \frac{1}{(1 + K_{\text{OM}}[\text{SRFA}])(1 + k_q[\text{SRFA}])} [\text{Naph}] \quad \text{Eqn. 5.12}$$

where  $k_q$  is the quenching constant of SRFA and  $[{}^1\text{O}_2]_0$  is the concentration of singlet oxygen in the solution without SRFA.

Combining Equations 5.11 and 5.12, we obtain the following expression that describes the dependence of the observed overall product formation rate constant on the concentration of SRFA.

$$k_{\text{l,obs}} = (k_{\text{rxn}} K_{\text{OM}} [{}^1\text{O}_2]_{\text{SRFA}} + k_{\text{rxn}} k_{\text{gen}}) \frac{[\text{SRFA}]}{1 + K_{\text{OM}}[\text{SRFA}]} + k_{\text{rxn}} [{}^1\text{O}_2]_0 \frac{1}{(1 + K_{\text{OM}}[\text{SRFA}])(1 + k_q[\text{SRFA}])} \quad \text{Eqn. 5.13}$$

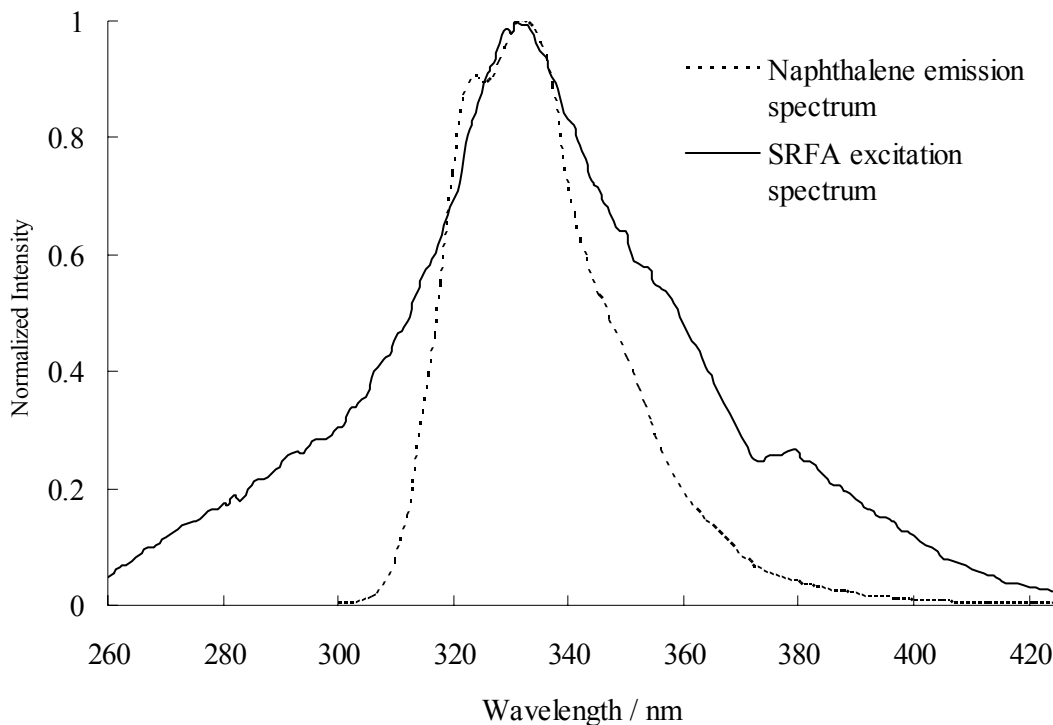


**Figure 5.7.** Fluorescence excitation spectrum of SRFA (4.4 mg.L<sup>-1</sup>, detection emission wavelength: 432 nm) and fluorescence emission spectrum of naphthalene (6.5 mg.L<sup>-1</sup>, excited at 286.5nm).

The formation rate constants of phthalide and coumarin in the 450  $\mu\text{m}$  SRFA aqueous films are fitted to Eqn. 5.13 and the resulting fit parameters are listed in Table 5.3. The correlation coefficients are 0.963 and 0.950 respectively, indicating that the fit is satisfactory. Although the correlation cannot give all the individual constants in Eqn. 5.13, values of  $K_{\text{OM}}$  ( $=C_2$ ) and  $k_q$  ( $=C_4$ ) are obtained. To compare with the value of  $K_{\text{OM}}$  obtained from the data correlation, we also tried to measure the partition coefficient of naphthalene to SRFA by fluorescence quenching. Unfortunately, no detectable fluorescence quenching was observed from the fluorescence measurements after the inner filter effect of SRFA was corrected. Using the average  $K_{\text{OM}}$  value we obtained from the correlation, the Stern-Volmer plot for naphthalene quenching by SRFA would have a slope of  $1.45 \times 10^{-3} \text{ L.mg}^{-1}$ , which indeed is too small to be observed from the fluorescence quenching measurements.

**Table 5.3.** Parameters obtained by fitting the formation rate constant data to Eqn. 5.13 <sup>(a)</sup>.

Source	$C_1$ /L.mg <sup>-1</sup> .min <sup>-1</sup>	$C_2 (=K_{OM})$ / L.mg <sup>-1</sup>	$C_3$ / min <sup>-1</sup>	$C_4 (=k_q)$ / L.mg <sup>-1</sup>	$R^2$ <sup>(b)</sup>
Phthalide	$6.5 \times 10^{-7}$	$2.3 \times 10^{-3}$	$1.0 \times 10^{-4}$	$8.6 \times 10^{-2}$	0.963
Coumarin	$7.1 \times 10^{-7}$	$6.0 \times 10^{-4}$	$3.3 \times 10^{-4}$	$9.5 \times 10^{-1}$	0.950

<sup>(a)</sup> Simplified fit equation:  $k_{obs} = C_1[SRFA]/(1+C_2[SRFA]) + C_3/(1+C_2[SRFA]) + C_4[SRFA]$

<sup>(b)</sup>  $R^2$  is the correlation coefficient.

To represent the typical water film in a fog droplet, we performed experiments on the 22  $\mu\text{m}$  water film with sub-monolayer coverage of SRFA. According to Eqn. 4.2, the surface coverage of SRFA at the highest concentration we used was 77 percent of full monolayer coverage. Figure 5.8 shows the observed formation rate constants for phthalide and coumarin on the 22  $\mu\text{m}$  film. It should be noted that the photooxidation mechanism and kinetics discussed above pertained to the bulk phase photochemical reactions of naphthalene and no surface effects were considered. For the 450  $\mu\text{m}$  film that has been shown in our previous work to exhibit mainly bulk phase behavior [90], the kinetic data was well interpreted by Eqn. 5.13. However, the photochemical reactions of naphthalene on the 22  $\mu\text{m}$  film were predominantly surface reaction limited [90] and it would be inappropriate to fit the kinetic data on the 22  $\mu\text{m}$  film to Eqn. 5.13. Thus, the data shown in Figure 5.8 was not fitted to Eqn. 5.13. Similar to the photooxidation on the 450  $\mu\text{m}$  film, the observed formation rate constants on the 22  $\mu\text{m}$  film also show an initial decrease followed by an increase as the concentration of SRFA increases, consistent with the two-pathway mechanism. Moreover, SRFA exhibits a distinct effect on the surface photochemical reactions of naphthalene. Take the formation of phthalide for example. The ratio of the formation rate constant for phthalide on the 22  $\mu\text{m}$  film to the corresponding rate constant on the 450  $\mu\text{m}$  film increases from 2.5 in pure water to 3.3 at  $C_S = 49 \text{ mg.L}^{-1}$  and then decreases to 1.2 at  $C_S = 980 \text{ mg.L}^{-1}$ , indicating a greater surface reaction enhancement at low

SRFA concentrations than in pure water and a slight or zero surface reaction enhancement at high SRFA concentrations. Heterogeneous reactions at the gas-aqueous interface have been shown to proceed faster than homogeneous reactions in the bulk water phase. The surface reaction enhancement can be attributed to the enhanced surface concentrations of reactive species resulting from the free energy minimum at the interface and the increased quantum yield for photolysis due to decreased solvent-cage effect on the surface [90, 102, 116]. The reasons for the greater surface reaction enhancement in the region of small SRFA concentrations are probably twofold. First, the presence of SRFA increases the surface concentration of naphthalene, which directly enhances the surface reaction rate. Second, as shown earlier, the self-sensitized photooxidation of naphthalene is the dominant reaction pathway at small SRFA concentrations. The presence of SRFA probably decreases the mobility of molecules on the surface and consequently suppresses the diffusion-controlled T-T energy transfer from triplet naphthalene to ground state SRFA. Thereby the quenching effect of SRFA on the self-sensitized process is weakened and the surface reaction rate is enhanced. Unlike under low SRFA concentrations, naphthalene molecules are primarily distributed in the SRFA region at high SRFA concentrations. Humic substances have been pictured to have an open structure with a number of hydrophobic cavities where hydrophobic interactions between humic substances and hydrophobic organic compounds occur[113]. In light of this molecular level binding picture, it is speculated that naphthalene molecules bound to SRFA are “caged” in the SRFA region, regardless of whether they are on the surface or in the bulk phase. As a result, the property of the SRFA micro-region determines the photochemical reactivity of naphthalene at high SRFA concentrations and no difference exists between the surface and the bulk phase reactions.

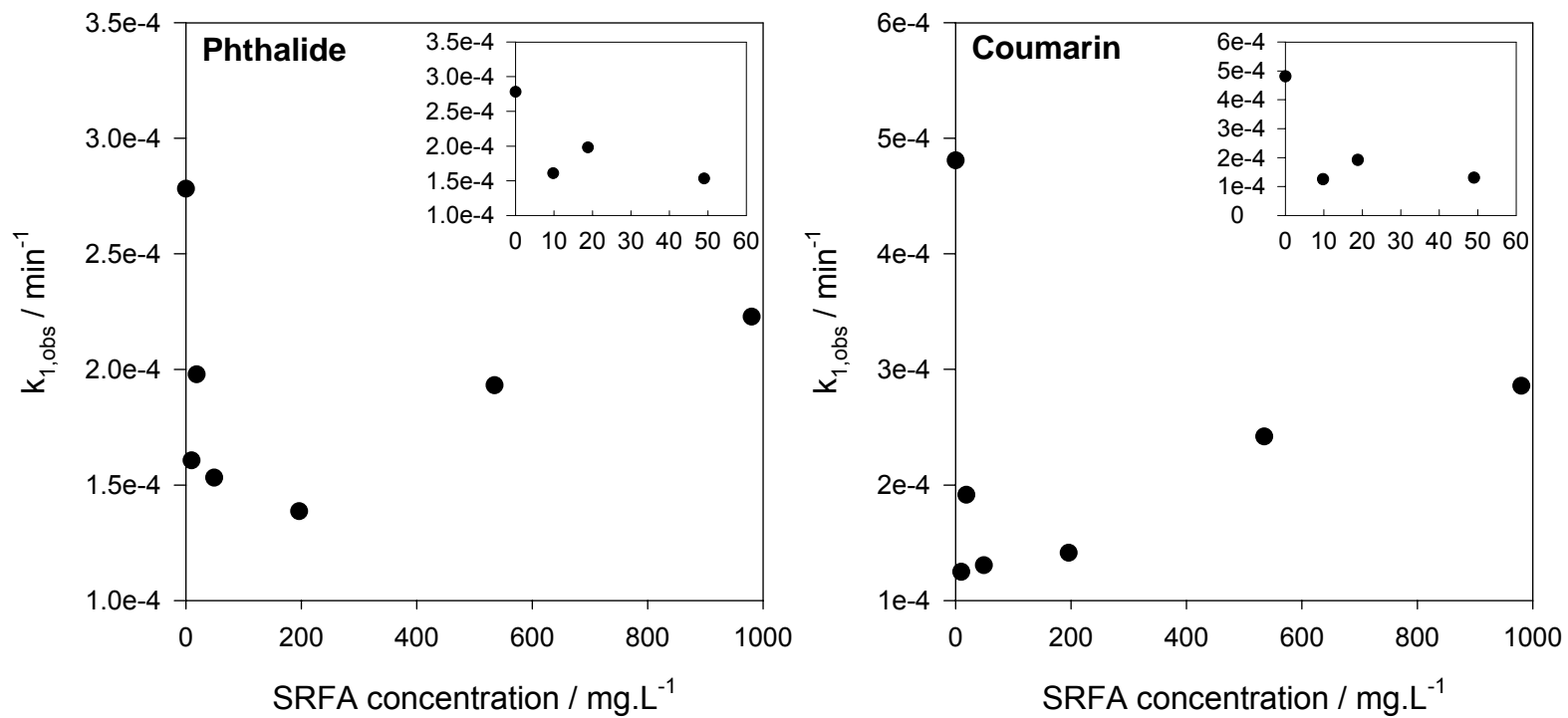


**Figure 5.8.** Effect of SRFA on the observed formation rate constants for phthalide and coumarin in a 22  $\mu\text{m}$  aqueous film. The insets are blowups of the data at small SRFA concentrations.

### 5.3.2.2 Photochemical Reactions of Naphthalene in SDS Aqueous Films

To compare the effect of SRFA with conventional surfactants, photochemical reaction kinetics of naphthalene in the 450  $\mu\text{m}$  SDS aqueous solution film was also investigated. Figure 5.9 shows the observed formation rate constants for phthalide and coumarin in the 450  $\mu\text{m}$  film as a function of the SDS concentration. Unlike SRFA, SDS was photochemically inert under the UV light we used and did not show a significant effect on the photooxidation of naphthalene as SRFA did. Only at SDS concentrations as high as 500  $\text{mg}\cdot\text{L}^{-1}$  was an obvious decrease in the formation rate constants observed. The reason for the suppression of naphthalene photooxidation at high SDS concentrations could be that a considerable portion of naphthalene molecules are bound to SDS molecules at high SDS concentrations and become insusceptible to singlet oxygen attack. The following expression of the formation rate constant is obtained based on this assumption (see supporting information in Appendix I for derivation).

$$k_{1,\text{obs}} = k_{1,\text{obs}}^0 \frac{1}{1 + K_{\text{OM}}[\text{SDS}]} \quad \text{Eqn. 5.14}$$

where  $k_{1,\text{obs}}^0$  is the formation rate constant in pure water. By fitting the kinetic data to this equation, we obtain an average  $K_{\text{OM}}$  value of  $1.31 \times 10^{-3} \text{ L}\cdot\text{mg}^{-1}$  for SDS, equal to  $2.62 \times 10^{-3} \text{ L}\cdot(\text{mg carbon})^{-1}$ , which is in good agreement with the average  $K_{\text{OM}}$  value obtained from SRFA ( $2.77 \times 10^{-3} \text{ L}\cdot(\text{mg carbon})^{-1}$ ). Because of their chemical similarity, the effect of SDS on the photooxidation of naphthalene is suggestive of that of naturally occurring long chain fatty acids [84].

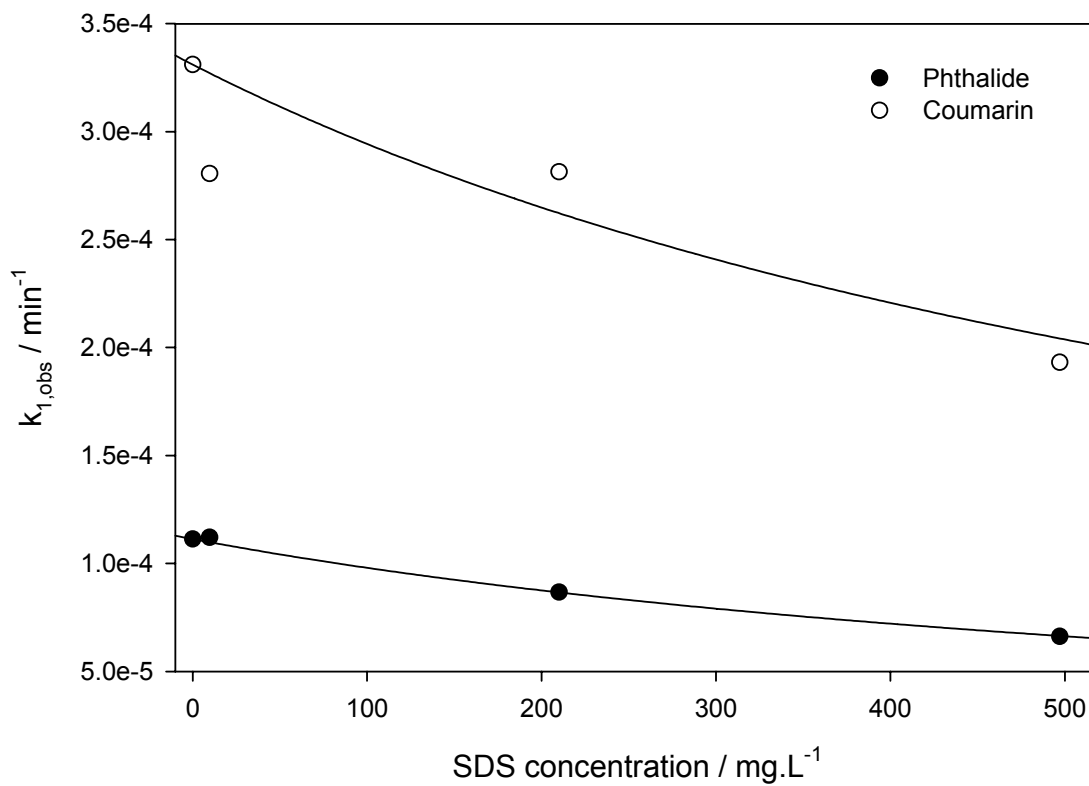


**Figure 5.9.** Effect of SDS on the observed formation rate constants for phthalide and coumarin in a 450  $\mu\text{m}$  aqueous film. The solid lines represent the theoretical fit to experimental data (Eqn. 5.14).

### 5.3.3 Atmospheric Implications

Fog samples collected in the Po Valley of Italy, an area reported to have high levels of pollution, revealed high concentrations of water-soluble organic compounds (WSOC) in fog droplets, ranging between 14-108 mg carbon.L<sup>-1</sup> [117-119]. The humic-like polyacidic compounds were found to represent an average 25% of the WSOC and their concentrations were estimated to range between 3.5-27 mg carbon.L<sup>-1</sup>, corresponding to concentrations of 6.7-51.5 mg. L<sup>-1</sup> for the surrogate SRFA. As shown in our work, SRFA suppresses the photooxidation of naphthalene over this atmospherically relevant concentration range even though the surface reaction enhancement is greater in the presence of SRFA over this range than in pure water. In addition to photochemical reactions, PAHs in thin atmospheric water films are subject to various other oxidation processes initiated by reactive oxygen species in the atmosphere, including, for instance, •OH, •NO<sub>3</sub>, and O<sub>3</sub>. Previous work from our laboratory showed that, contrary to the inhibiting effect of SRFA on the <sup>1</sup>O<sub>2</sub> photooxidation of naphthalene over the atmospherically relevant SRFA concentration range, the presence of SRFA on the surface of micron-size water droplets was conducive to the trapping of O<sub>3</sub> and naphthalene and increased the ozonation rate of naphthalene by approximately one order of magnitude [120]. Although it is difficult to generalize the effect of SRFA on the oxidation of PAHs via different processes, it is doubtless that the presence of SRFA, or HULIS in thin atmospheric water films significantly affects the fate of PAHs in the atmosphere.

## CHAPTER 6

# UV PHOTO-OXIDATION OF GAS-PHASE PHENANTHRENE ON ATMOSPHERIC WATER FILMS

### 6.1 Introduction

Phenanthrene is a 3-ring PAH often detected in the ambient atmosphere. Phenanthrene and other higher molecular weight compounds reside primarily associated with the aerosol phase, whereas the basic 2-ring compound, naphthalene is mostly present in the gas phase. To gain insight of the behavior of more complex organic molecules on atmospheric water films, we stepped forward from naphthalene to phenanthrene and investigated its adsorption, photooxidation reaction and fate process at the air-water interface. Adsorption of phenanthrene on pure water films and surfactant aqueous films has been reported in Chapter 3 and Chapter 4 respectively. In this chapter, we focus on the photooxidation reaction of phenanthrene on both pure water films and surfactant aqueous films.

### 6.2 Experimental Section

#### 6.2.1 Photooxidation of Phenanthrene on Thin Aqueous Films

Photooxidation of phenanthrene on both pure water films and SRFA aqueous films were studied using the flow-tube photo-reactor. The experimental procedure for the photooxidation reactions of phenanthrene was identical to that of naphthalene described in Section 5.2.1. Effect of film thickness on the photooxidation rate of phenanthrene was investigated. The film thickness ranged from 22 to 515  $\mu\text{m}$ . Effect of SRFA on the photooxidation rate of phenanthrene in a 515  $\mu\text{m}$  aqueous film was also investigated and the concentration of SRFA ranged from 2 to 250  $\text{mg}\cdot\text{L}^{-1}$ .

### **6.2.2 Measurement of Singlet Oxygen**

Singlet oxygen has been suggested to be the dominant reaction intermediate in the photooxidation of PAHs induced by UV light [5, 110]. The steady state concentration of singlet oxygen in an illuminated water film with adsorbed phenanthrene was quantified by measuring the loss of low concentrations of furfuryl alcohol in illuminated 100% H<sub>2</sub>O and 50/50 H<sub>2</sub>O/D<sub>2</sub>O films with adsorbed phenanthrene. The concentration change of furfuryl alcohol during illumination was determined using HPLC. The initial concentration of furfuryl alcohol used for the measurement was  $1.2 \times 10^{-6}$  M and the system studied was a 515  $\mu\text{m}$  water film containing  $3.5 \times 10^{-6}$  M adsorbed phenanthrene.

### **6.2.3 Photooxidation of Phenanthrene on Aqueous Films Containing D<sub>2</sub>O**

The decay rate of singlet oxygen in dilute solution is controlled by solvent quenching and there is a considerable water-related H/D isotope effect on the lifetime of singlet oxygen. To investigate the role of singlet oxygen played in the photooxidation of phenanthrene, photooxidation rates of phenanthrene on 515  $\mu\text{m}$  100% H<sub>2</sub>O, 50/50 H<sub>2</sub>O/D<sub>2</sub>O, and 100% D<sub>2</sub>O films were measured.

### **6.2.4 Sample Analysis**

Quantification of phenanthrene and photooxidation products in the aqueous samples was done using the same HPLC and method as described in Section 3.3.1.3. Identification of compounds was achieved by matching retention times of standard solutions within +/- 0.1 min and by matching the UV spectrum of the standards and the sample.

## 6.3 Results and Discussion

### 6.3.1 Photochemical Reactions of Phenanthrene on Thin Aqueous Films

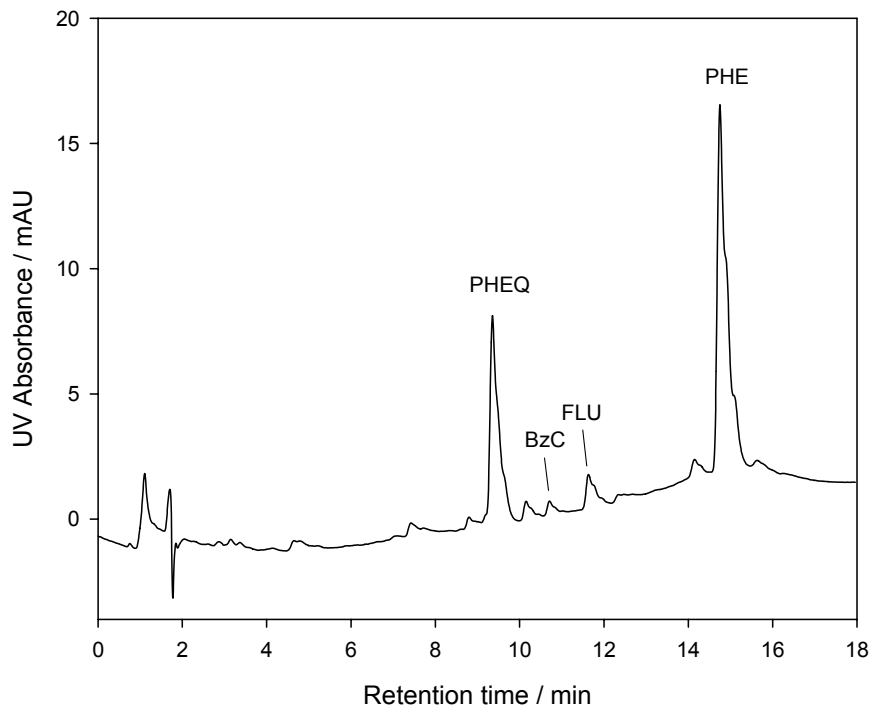
Photochemical reactions of phenanthrene under simulated sunlight conditions were studied after adsorption of phenanthrene onto the film was complete. Figure 6.1 shows the typical HPLC trace of an aqueous film containing adsorbed phenanthrene that was exposed to UV radiation for 12 hours. The chromatogram shows several peaks apart from phenanthrene, among which three compounds with a relatively high abundance were identified and confirmed with pure standards. The products identified were: 9, 10-phenanthrenequinone, 9-fluorenone and 3, 4-benzocoumarin. Note that in the case of the thin film experiments reported in this work we see the three main products in all of our samples.

Figure 6.2 shows the accumulation of the three main products in a 515 $\mu$ m water film as the reaction proceeds. Quantification of the products was done on HPLC.

An overall reaction scheme,  $\text{PHE} \xrightarrow{k_1} \text{P1} \xrightarrow{k_2} \text{P2}$ , was proposed to interpret the kinetic data. As a result, the concentration change of the products during the reaction can be described as

$$C_{\text{P1}}(t) = \frac{k_1}{k_2} \cdot C_{\text{Phe0}} (1 - e^{-k_2 t}) \quad \text{Eqn. 6.1}$$

where  $C_{\text{P1}}$  is the concentration of the product,  $C_{\text{Phe0}}$  is the concentration of phenanthrene,  $k_1$  is the product formation rate constant, and  $k_2$  is the product reaction rate constant. Note that the concentration of phenanthrene,  $C_{\text{Phe0}}$ , was kept constant throughout the reaction because of the continuous supply of phenanthrene from the gas phase. Moreover, since the water-air equilibrium partition constants are high for the oxygenated product compounds, e.g.,  $K_{\text{WA}} = 3.6 \times 10^4$  for 9-fluorenone at 298K [121], we can neglect their gas phase concentrations within the reactor. Separate control experiments with standards of products dissolved in water also showed that the evaporative loss of products from the water film in the reactor was negligible. A detailed



**Figure 6.1.** HPLC trace of a 515  $\mu\text{m}$  aqueous film sample after 12 hours exposure to UV light. The compounds identified are: 9, 10-phenanthrenequinone (PHEQ), 3, 4-benzocoumarin (BzC), 9-fluorenone (FLU), and phenanthrene (PHE).

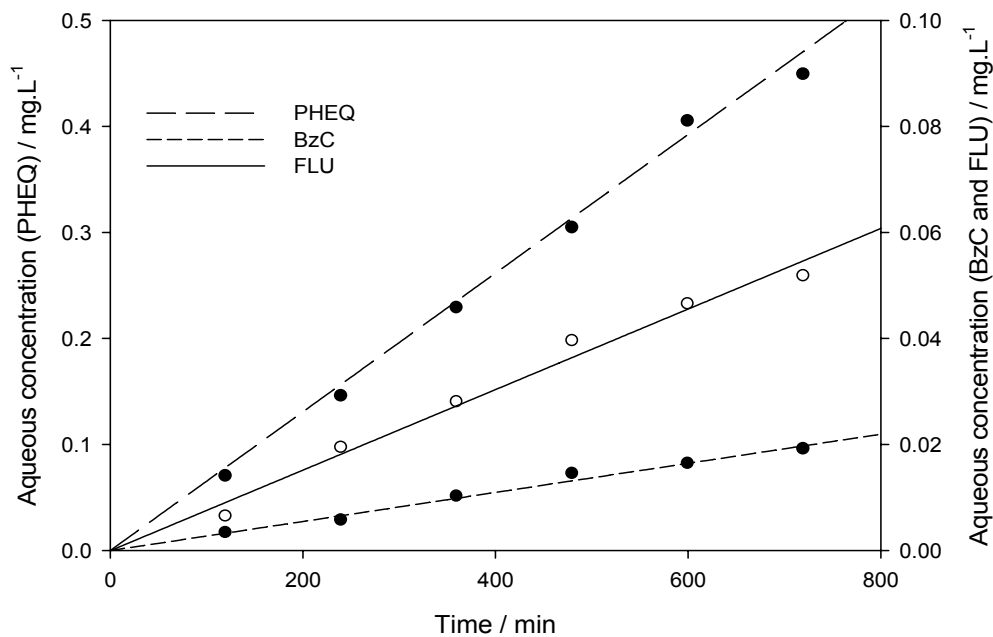


**Figure 6.2.** Accumulation of the three main photooxidation products of phenanthrene in a 515  $\mu\text{m}$  water film.

deduction of Eqn. 6.1 was given in Section 5.2.2. In the case where P1 is a stable product, further degradation of P1 can be neglected and thereby Eqn. 6.1 can be simplified to

$$C_{P1}(t) = k_1 C_{Phe0} t \quad \text{Eqn. 6.2}$$

As shown in Figure 6.2, the concentrations of the products increase linearly with time and the kinetic data fits well to Eqn. 6.2. The formation rate constants for the products were obtained by fitting the kinetic data to Eqn. 6.2.

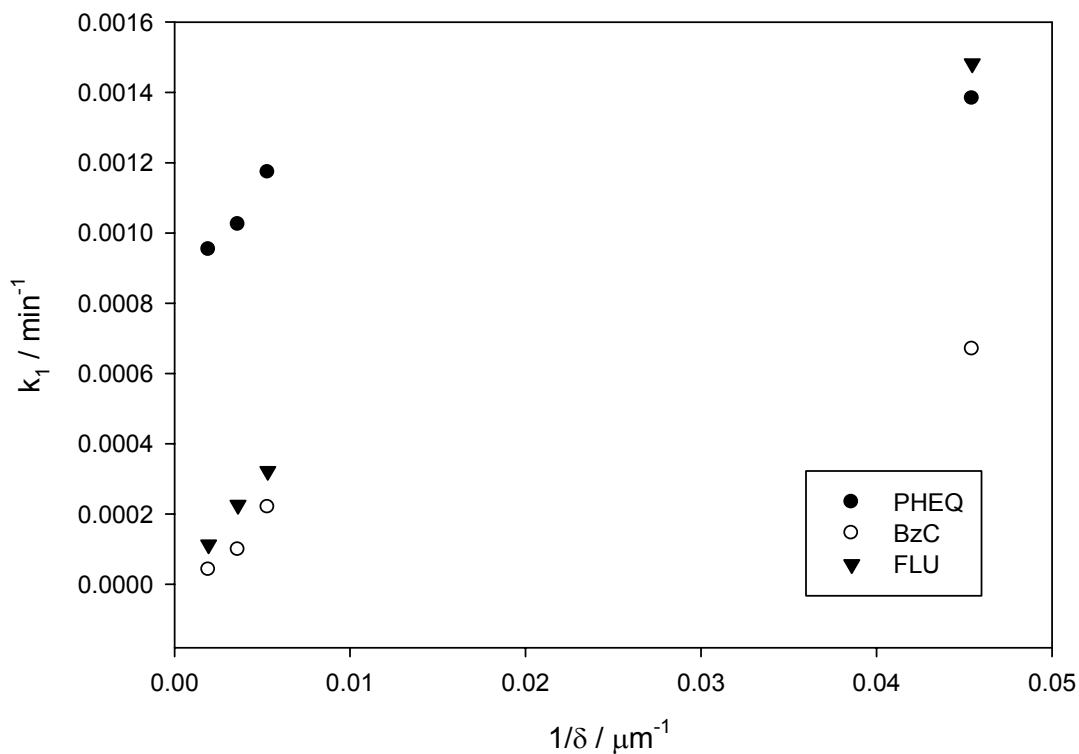
### 6.3.2 Effect of Film Thickness on Reaction Rates

Figure 6.3 shows that the formation rate constants for the three main products from phenanthrene greatly increased as the film thickness decreased. Table 6.1 lists the product formation rate constants measured in water films with both the largest (515  $\mu\text{m}$ ) and the smallest thickness (22  $\mu\text{m}$ ) employed in our experiments. Increases of 47% (9, 10-phenanthrenequinone), 1495% (3, 4-benzocoumarin), and 1264% (9-fluorenone) were observed as the film thickness decreased from 515  $\mu\text{m}$  to 22  $\mu\text{m}$ . Heterogeneous reactions at the gas-aqueous interface have been shown to proceed faster than homogeneous reactions in the bulk water phase [90, 102, 122]. The contribution of surface reaction increases as the surface area per unit volume ( $1/\delta$ ) increases, therefore the measured overall formation rate constants for the products increased with decreasing film thickness. Similar effect of film thickness on the photooxidation rate of naphthalene was shown in our previous work [90]. However, the highest increase in the product formation rate constant for naphthalene was 154% as the film thickness decreased to 22  $\mu\text{m}$ , compared to 1495% for phenanthrene. The reported values of  $K_{IA}$  and  $K_{WA}$  for naphthalene were 21  $\mu\text{m}$  and 86 respectively. Using these values it can be calculated that at equilibrium only 1% of naphthalene is present on the surface of an aqueous film 22  $\mu\text{m}$  thick, whereas 60% of phenanthrene is present on the same aqueous film. Given a fixed film thickness, the proportion

of surface reaction for phenanthrene is higher than for naphthalene, therefore, the measured overall rates for product formation from phenanthrene show a higher increase.

### **6.3.3 Effect of SRFA on Reaction Rates**

It is shown in literature reports that fulvic acid is the most important component of dissolved organic matters in natural waters. It is also shown via molecular characterization that Suwannee River fulvic acid (SRFA) is a good surrogate model to represent polycarboxylic acids in fog waters [79]. In this work, we chose SRFA to study the effect of dissolved surfactants on the photooxidation of phenanthrene in thin water films. Figure 6.4 shows the effect of SRFA on the observed formation rate constants for 9, 10-phenanthrenequinone, 3, 4-benzocoumarin, and 9-fluorenone in a 515  $\mu\text{m}$  aqueous film. Interestingly, the effects of SRFA on the observed formation rate constants for the three main products were totally different. The formation rate constant of 9, 10-phenanthrenequinone decreased monotonically as the concentration of SRFA increased, whereas that of 3, 4-benzocoumarin decreased in the beginning and then increased. Contrary to 3, 4-benzocoumarin, the formation rate constant of 9-fluorenone increased first and then decreased. Literature reports on the effect of SRFA on PAH photodegradation in bulk water have appeared quite conflicting. Fasnacht and Blough reported that photoreactivities of PAHs in bulk water solutions were not affected by SRFA [107]. However, other reports showed that whereas the photodegradation of benzo[a]pyrene and benzo[a]anthracene were slowed by humic-like substances in water, that of naphthalene increased [108]. These seemingly conflicting results are probably attributed to the different reaction mechanisms that different PAHs undergo. In the case of phenanthrene photooxidation in our work, the different effects of SRFA on the formation of the three main products suggest that phenanthrene was photooxidized to the products via different pathways. Effect of SRFA on phenanthrene photooxidation is discussed further in the following section.



**Figure 6.3.** Effect of film thickness on the observed formation rate constants of 9,10-phenanthrenequinone, 3, 4-benzocoumarin, and 9-fluorenone.

**Table 6.1.** Observed Product Formation Rate Constants in Water Films (T=296 K)

<i>Compound</i>	$k_1 / \text{min}^{-1}$ (515 $\mu\text{m}$ film)	$k_1 / \text{min}^{-1}$ (22 $\mu\text{m}$ film)	<i>Percentage increase</i>
PHEQ	$9.5 \times 10^{-4}$	$1.4 \times 10^{-3}$	47%
BzC	$4.2 \times 10^{-5}$	$6.7 \times 10^{-4}$	1495%
FLU	$1.1 \times 10^{-4}$	$1.5 \times 10^{-3}$	1264%

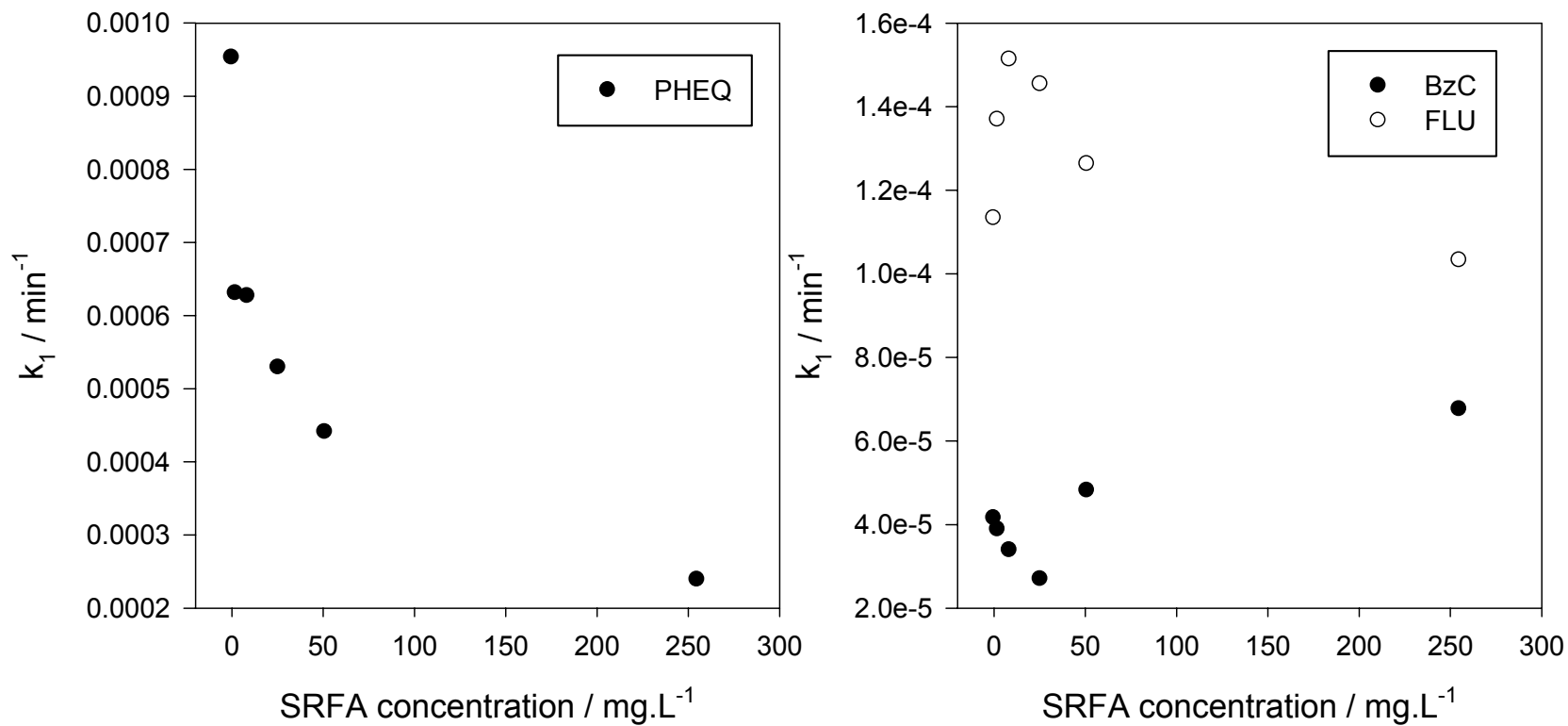


**Figure 6.4.** Effect of SRFA on the observed formation rate constants of 9, 10-phenanthrenequinone, 3, 4-benzocoumarin, and 9-fluorenone in a 515  $\mu\text{m}$  aqueous film.

### 6.3.4 Photooxidation Pathways of Phenanthrene

Three main pathways via which PAHs photodegrade have been proposed in the literature: through radical cation intermediates, via reaction with singlet oxygen ( $^1\text{O}_2$ ), and via reaction with hydroxyl radical ( $\cdot\text{OH}$ ) [38, 107]. Figure 6.5 shows the three possible pathways of PAH photooxidation in oxygen-containing water.

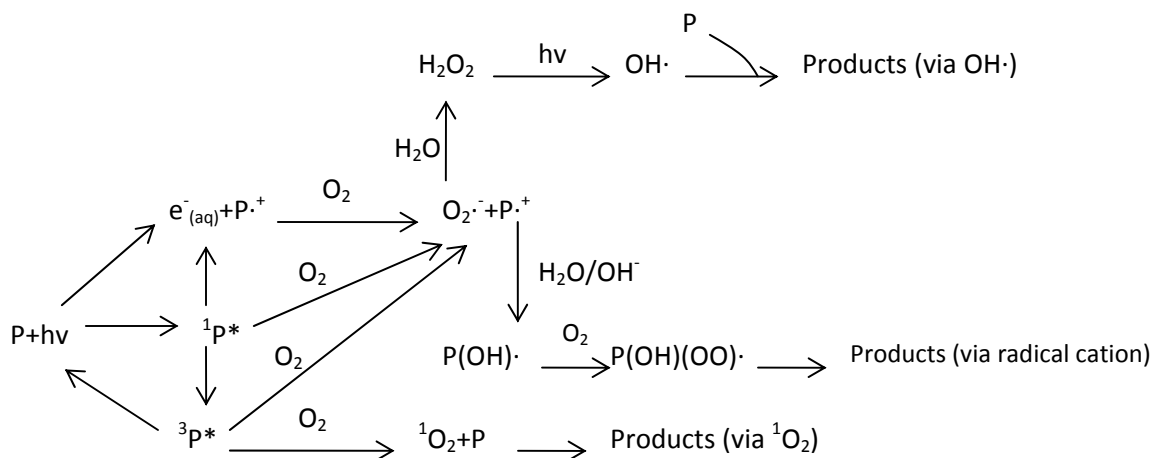


**Figure 6.5** Scheme of photooxidation pathways of PAHs in the  $\text{O}_2/\text{H}_2\text{O}$  system [38, 107].

It has been proposed in the literature that singlet oxygen is the dominant reaction intermediate in the direct photooxidation of PAHs induced by UV light [5, 110]. In our work, we used furfuryl alcohol (FFA), an efficient  $^1\text{O}_2$ -selective trapping agent, to quantify the steady state concentration of singlet oxygen in the illuminated 515  $\mu\text{m}$  water film with adsorbed phenanthrene. The steady state concentration of singlet oxygen was determined by [123]

$$[{}^1\text{O}_2]_{\text{ss}} = \frac{k_{\text{exp,D}_2\text{O}} - k_{\text{exp,H}_2\text{O}}}{k_{\text{FFA},{}^1\text{O}_2} \left[ \frac{k_{\text{H}_2\text{O}}}{k_{\text{H}_2\text{O}}\chi_{\text{H}_2\text{O}} + k_{\text{D}_2\text{O}}\chi_{\text{D}_2\text{O}}} - 1 \right]} \quad \text{Eqn. 6.3}$$

Detailed description of Eqn. 6.3 and values of the constants can be found in the references [123, 124]. The apparent first-order kinetic rate constants for the loss of FFA in 100%  $\text{H}_2\text{O}$  and 50/50  $\text{H}_2\text{O}/\text{D}_2\text{O}$  films with adsorbed phenanthrene ( $k_{\text{exp,H}_2\text{O}}$  and  $k_{\text{exp,D}_2\text{O}}$ ) were determined to be

$2.0 \times 10^{-5} \text{ s}^{-1}$  and  $2.5 \times 10^{-5} \text{ s}^{-1}$  respectively. Knowing all the values of the parameters on the right-hand side of Eqn. 6.3, the steady state concentration of singlet oxygen in the illuminated 515  $\mu\text{m}$  water film with adsorbed phenanthrene can be calculated and the value determined was  $4.9 \times 10^{-14} \text{ M}$ .

The decay rate of singlet oxygen in dilute solution is controlled by solvent quenching. Water-related deuterium isotope shows a considerable effect on the lifetime of singlet oxygen and there is evidence in the literature that the lifetime of singlet oxygen is longer in D<sub>2</sub>O than in H<sub>2</sub>O [125]. Therefore, it is anticipated that the photooxidation of phenanthrene would proceed faster in D<sub>2</sub>O. However, as shown in Figure 6.6, 3, 4-benzocoumarin was the only one of the three main products that had an increasing formation rate constant as the amount of D<sub>2</sub>O in the film increased, confirming its formation route via singlet oxygen. Unlike 3, 4-benzocoumarin, the formation rate constant of 9, 10-phenanthrenequinone decreased with increasing D<sub>2</sub>O and that of 9-fluorenone increased first and then decreased. The different effects of D<sub>2</sub>O on the formation rate constants of the three products further confirmed that phenanthrene was photooxidized to the products via different pathways. D<sub>2</sub>O is a more ordered liquid than H<sub>2</sub>O, thus the lifetimes of reactive species are longer in D<sub>2</sub>O. However, D<sub>2</sub>O exhibits stronger hydrogen bonds than H<sub>2</sub>O, which makes it more difficult to generate deuteroyl radical while illuminated by UV light. Literature reports also show that the yields of radicals and molecular products in the radiolysis of D<sub>2</sub>O are lower than in H<sub>2</sub>O [126, 127]. Therefore, the concentration of hydroxyl or deuteroyl radical in the illuminated water film with adsorbed phenanthrene decreases with increasing amount of D<sub>2</sub>O thus the photooxidation process of phenanthrene via the hydroxyl radical pathway becomes slower. The effect of D<sub>2</sub>O on the formation rate constant of 9, 10-phenanthrenequinone coincided with this phenomenon, suggesting that 9, 10-phenanthrenequinone was formed via the hydroxyl radical pathway. As shown in Figure 6.5,

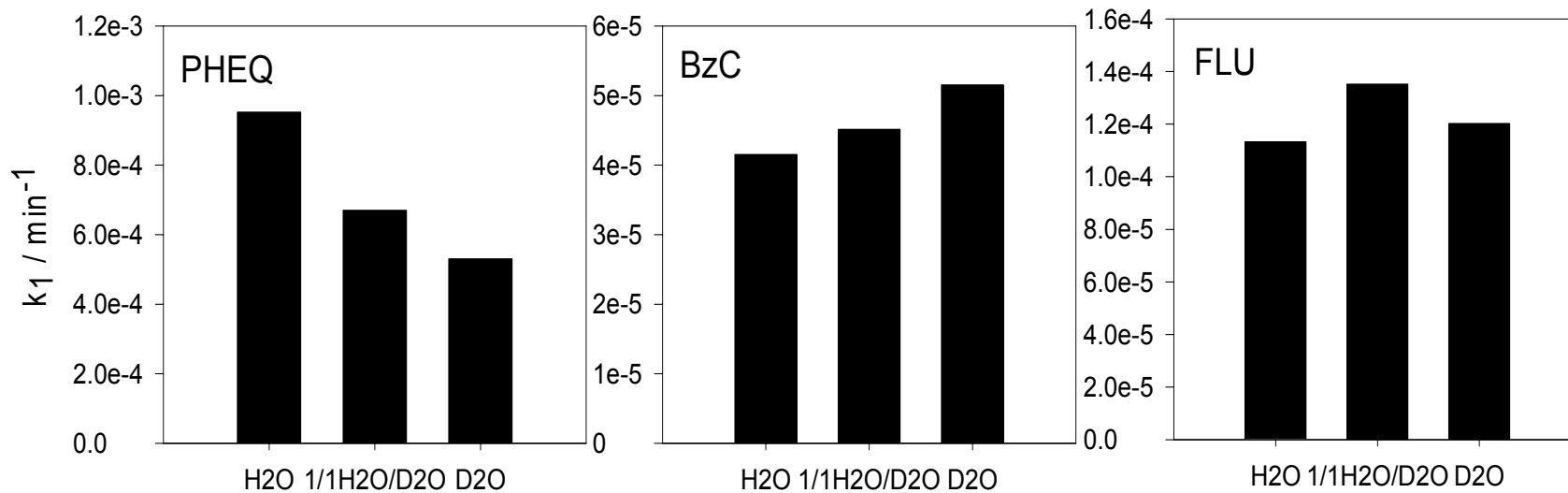


**Figure 6.6.** Observed formation rate constants of 9, 10-phenanthrenequinone, 3,4-benzocoumarin, and 9-fluorenone in 515  $\mu\text{m}$  100%  $\text{H}_2\text{O}$ , 50/50  $\text{H}_2\text{O}/\text{D}_2\text{O}$ , and 100%  $\text{D}_2\text{O}$  films.

photooxidation of phenanthrene via the radical cation pathway involves both water and reactive species transformed from phenanthrene. Reactivity of water decreases with increasing D<sub>2</sub>O, whereas the lifetime of reactive species transformed from phenanthrene increases. The two opposite effects of D<sub>2</sub>O would result in a complex effect of D<sub>2</sub>O on phenanthrene photooxidation via the radical cation pathway. It is hypothesized that 9-fluorenone was formed from phenanthrene via the radical cation pathway.

Now let us look back at the effects of SRFA on phenanthrene photooxidation. SRFA can quench or scavenge the PAH excited states, free radicals, or other excited species that may be intermediates in the photochemical reactions of PAHs. Therefore, the formation rate constant of 9, 10-phenanthrenequinone, which was produced via the hydroxyl radical pathway, decreased with SRFA. On the other hand, UV-light absorption of fulvic acid molecules can also promote them to their singlet excited state and generate singlet oxygen via the same route as PAHs [109, 111, 112]. It was shown in our previous work that photooxidation rate of naphthalene via the singlet oxygen pathway decreased first and then increased with SRFA [128], which was identical to the case of 3, 4-benzocoumarin. The effect of SRFA on the formation of 9-fluorenone is more complex than the other two and needs further investigation.

### **6.3.5 Comparison of Reaction Rates via Radical Cations, <sup>1</sup>O<sub>2</sub>, and •OH**

As shown in Table 6.1, the formation rate constant of 9, 10-phenanthrenequinone is one order of magnitude higher than that of 9-fluorenone and 3, 4-benzocoumarin in the 515 μm water film, indicating that photooxidation via hydroxyl radical is the most favorable reaction pathway for phenanthrene in bulk water under the simulated sunlight conditions employed in our experiments. However, the formation rate constants of 9-fluorenone and 3, 4-benzocoumarin increased much faster than that of 9, 10-phenanthrenequinone as the film thicknesses decreased. The formation rate constant of 9-fluorenone was even higher than that of 9,

10-phenanthrenequinone in the 22  $\mu\text{m}$  water film. Therefore, it can be concluded that photooxidation via the radical cation and  $^1\text{O}_2$  pathways are more favorable than via the hydroxyl radical pathway for the surface reaction of phenanthrene.

## 6.4 Conclusions

Surface processes are significant for the transport and transformations of PAHs in the atmospheric condensed phases (e.g., aerosols, fog and cloud droplets). It is fairly well documented that the behavior of pollutants in fogs is extremely size dependent. The study on the adsorption and UV photo-oxidation of gas-phase phenanthrene on atmospheric water films was intended to provide insight into the behavior of PAHs in the atmospheric environment where thin water films are ubiquitous. Completion of this study enabled us to draw the following conclusions.

The total aqueous concentration of adsorbed phenanthrene increased linearly with the surface area per unit volume ( $1/\delta$ ) of the water film. Bulk and interface air-water partition constants for phenanthrene can be determined by measuring the dependence of the total aqueous concentration of adsorbed phenanthrene on  $1/\delta$ . The interfacial air-water partition constant of phenanthrene increased greatly in the presence of SRFA and SDS, indicating that the presence of surface active materials in the aqueous phase at substantial concentrations effectively increased the equilibrium partitioning to the air-water interface and uptake by the water film.

9, 10-phenanthrenequinone, 3, 4-benzocoumarin and 9-fluorenone were identified as the three main photooxidation products of phenanthrene. The surface reaction of phenanthrene proceeded faster than the reaction in bulk water. Phenanthrene photodegraded through three different pathways under simulated sunlight conditions: through radical cation intermediates, via reaction with singlet oxygen ( $^1\text{O}_2$ ), and via reaction with hydroxyl radical ( $\cdot\text{OH}$ ). Photooxidation via  $\cdot\text{OH}$  was the most favorable reaction pathway for phenanthrene in bulk water, whereas

photooxidation via the radical cation and  $^1\text{O}_2$  pathways were more favorable for the surface reaction.

# **CHAPTER 7**

## **SUMMARY AND RECOMMENDATIONS FOR FUTURE RESEARCH**

### **7.1 Summary**

The processing of PAHs in fog can lead to more harmful oxy- and nitro-PAHs. Hence, the adsorption and photochemical transformations of gas-phase PAH vapor were studied in a flow-tube reactor with a view to understanding the transport and transformation processes of gas-phase PAHs occurring on thin atmospheric water films such as those of aerosols and fog.

The equilibrium uptake of naphthalene and phenanthrene was dependant on water film thickness. Bulk water-air and air-to-interface partition constants of naphthalene and phenanthrene were estimated from the experiments based on the dependence of the equilibrium uptake on the water film thickness. The air-to-interface partition constant of phenanthrene is three orders of magnitude higher than that of naphthalene, showing that phenanthrene is more surface active than naphthalene. Theoretical computations of molecular dynamics of PAHs show a deep free energy minimum at the air-water interface for PAHs entering water phase from the air. As a result, PAH molecules accumulate at the air-water interface and show substantial surface enrichments.

Suwannee River fulvic acid (SRFA) was chosen as a surrogate for the surface active humic-like substances present in atmospheric water films. The effect of SRFA on the equilibrium partitioning of PAHs to the air-water interface was investigated. To compare with SRFA, the effect of a conventional surfactant, sodium dodecyl sulfate, was also studied. The presence of surface active materials in the aqueous phase at substantial concentrations effectively increase

the overall equilibrium partitioning of PAHs to the air-water interface and uptake by the water film.

Several photooxidation products of naphthalene and phenanthrene were identified in the water films and the mechanism of photooxidation was assessed. Singlet oxygen is an important reaction intermediate during the photooxidation of PAHs and photooxidation via singlet oxygen was proposed as the major photooxidation route for naphthalene. However, the photooxidation of PAHs can be very complex, especially for PAHs with several aromatic rings. It was proposed that phenanthrene photodegraded via three different pathways: through radical cation intermediates, via reaction with singlet oxygen, and via reaction with hydroxyl radical.

The rate of photo-oxidation was substantially higher in the thin water film as compared to the bulk phase reaction. Surface reactions proceed faster than reactions in the bulk water. The surface reaction enhancement can be attributed to the enhanced surface concentrations of reactive species resulting from the free energy minimum at the interface and the increased quantum yield for photolysis due to decreased solvent-cage effect on the surface. The contribution of surface reaction increases as the surface area per unit volume ( $1/\delta$ ) increases, therefore the photooxidation rate increased with decreasing film thickness.

Effects of SRFA on the photooxidation of naphthalene and phenanthrene were investigated to give insight into the photooxidation process of PAHs in fog droplets in which surface active compounds are present. SRFA shows complex effects on the photooxidation of PAHs. These were characterized via a dual mechanism of self-sensitized and SRFA-sensitized pathways for reaction. The effect of SRFA changes as the concentration of SRFA and the PAH molecule under investigation change. However, SRFA suppresses the photooxidation of naphthalene and phenanthrene over its atmospherically relevant concentration range (0-51.5 mg. L<sup>-1</sup>).

## 7.2 Recommendations for Future Work

During the photooxidation of PAHs in the flow-tube photo-reactor, only the water samples were taken for composition analysis. The vapor phase losses of the photooxidation products were assumed to be negligible due to their high water-air equilibrium partition constants. However, release of surface bound heterogeneous reaction products into the gas phase has been recognized and reported in the literature [129]. The make-up of the atmosphere is influenced by the release of the surface bound reaction products. Therefore, a careful examination of the composition of the gas phase during photooxidation of PAHs on thin water films is suggested to better understand the effect of the heterogeneous reactions taking place at the air-water interface on the composition of the atmosphere.

Chemical reactions occurring on atmospheric ice particles have received increased attention as to their influence on the climate change. Also, ice surface is an important medium for atmospheric chemistry in cold areas. It has been found that the ionization energy of PAHs can be significantly reduced in an ice matrix. While ionizing gas-phase PAHs requires VUV radiation ( $\lambda < 200\text{nm}$ ), PAHs frozen in ice could readily be ionized by near-UV radiation ( $\lambda < 300\text{nm}$ ) [130-132]. As a result, photoionization may compete with photolysis during the photochemical transformations of PAHs on ice surface under natural sunlight conditions. Therefore, study on the photochemical transformations of PAHs on ice surface under sunlight conditions is proposed with an emphasis on exploring the possible difference in the reaction mechanism between air-water interface and ice surface.

## REFERENCES

1. Bernstein, M.P., Sandford, S. A., Allamandola, L. J., *Life's Far-Flung Raw Materials*. Scientific American, 1999. **281**(1): p. 42-49.
2. Vacha, R., Jungwirth, P., Chen, J., Valsaraj, K. T., *Adsorption of Polycyclic Aromatic Hydrocarbons at the Air-water Interface: Molecular Dynamics Simulations and Experimental Atmospheric Observations*. Phys. Chem. Chem. Phys., 2006. **8**: p. 4461-4467.
3. Hafner, W.D.C., D. L.; Hites, R. A., *Influence of Local Human Population on Atmospheric Polycyclic Aromatic Hydrocarbon Concentrations*. Environ. Sci. Technol., 2005. **39**: p. 7374-7379.
4. Raja, S., Yacone, F. S., Ravikrishna, R., Valsaraj, K. T., *Thermodynamic Parameters for the Adsorption of Aromatic Hydrocarbon Vapors at the Gas-water Interface*. J. Chem. Eng. Data, 2002. **47**: p. 1213-1219.
5. Suzdorf, A.R., Morozov, S. V., Kuzubova, L. I., Anshits, N. N., Anshits, A. G., *Polycyclic Aromatic Hydrocarbons in the Environment: Sources, Profiles and Conversion Routes*. Chem. Sust. Dev., 1994. **2-3**: p. 449-473.
6. McConkey, B.J., Duxbury, C.L., Dixon, D.G., Greenberg, B.M., *Toxicity of a PAH Photo-oxidation Product to the Bacteria Photobacterium Phosphoreum and the Duckweed Lemna Gibba: Effects of Phenanthrene and its Primary Photoproduct, Phenanthrenequinone*. Environ. Toxicol. Chem., 1997. **16**: p. 892-899.
7. Capel, P.D., Luenberger, C., Giger, W., *Hydrophobic Organic Chemicals in Urban Fog*. Atmos. Environ., 1991. **25**: p. 1335-1346.
8. Aneja, V.P., *Organic Compounds in Cloudwater and their Deposition at a Remote Continental Site*. J. Air Waste Manag. Assoc., 1993. **43**: p. 1239-1244.
9. Raja, S., Raghunathan, R., Yu, X.-Y., Lee, T., Chen, J., Kommalapati, R. R., Murugesan, K., Shen, X., Qingzhong, Y., Valsaraj, K. T., Collett Jr., J. L., *Fog Chemistry in the Texas - Louisiana Gulf Coast Corridor*. Atmos. Environ., 2008. **42**: p. 2048-2061.
10. Rauber, R.M., *Microphysical Processes in the Atmosphere*, in *Handbook of Weather, Climate and Water*. 2003, John Wiley and Sons, Inc.: Hoboken, NJ. p. 255-299.
11. Pandis, S.N., Seinfeld, J. H., Pilinis, C., *Chemical Composition Differences in Fog and Cloud Droplets of Different Sizes*. Atmos. Environ., 1990. **24A**: p. 1957-1969.
12. Pandis, S.N., Seinfeld, J. H., *Should Bulk Cloudwater or Fogwater Samples Obey Henry's Law*. J. Geophys. Res., 1991. **96(D6)**: p. 10791-10798.

13. Munger, J.W., Collett, J., Daube, B., Hoffmann, M. R., *Chemical Composition of Coastal Stratus Clouds: Dependence on Droplet Size and Distance from the Coast*. Atmos. Environ., 1989. **23**: p. 2305-2320.
14. Valsaraj, K.T., Thoma, G. J., Reible, D. D., Thibodeaux, L., *On the Enrichment of Hydrophobic Organic Compounds in Fog Droplets*. Atmos. Environ., 1993. **27**: p. 203-210.
15. Ewing, G.W., *Ambient Thin Film Water on Insulator Surfaces*. Chem. Rev., 2006. **106**: p. 1511-1526.
16. Hunt, S.W., Roeselova, M., Wang, W., Wingen, L. M., Knipping, E. M., Tobias, D. J., Dabdub, D., Finlayson-Pitts, B. J., *Formation of Molecular Bromine from the Reaction of Ozone with Deliquesced NaBr Aerosol: Evidence for Interface Chemistry*. J. Phys. Chem. A, 2004. **108**: p. 11559-11572.
17. Sumner, A.L., Menke, E. J., Dubowski, Y., Newberg, J. T., Penner, R. M., Hemminger, J. C., Wingen, L. M., Brauers, T., Finlayson-Pitts, B. J., *The Nature of Water on Surfaces of Laboratory Systems and Implications for Heterogeneous Chemistry in the Troposphere*. Phys. Chem. Chem. Phys. , 2004. **6**: p. 604-613.
18. Streckowski, R.S., Remorov, R., George, C., *Direct Kinetic Study of the Reaction of Cl<sub>2</sub>-Radical Anions with Ethanol at the Air-Water Interface*. J. Phys. Chem. A, 2003. **107**: p. 2497-2504.
19. Blando, J.D., Turpin, B. J., *Secondary Organic Aerosol Formation in Cloud and Fog Droplets: A Literature Evaluation of Plausibility*. Atmos. Environ., 2000. **34**: p. 1623-1632.
20. Domine, F., Shepson, P. B., *Air-Snow Interactions and Atmospheric Chemistry*. Science, 2002. **297**: p. 1506-1510.
21. Dubowski, Y., Colussi, A. J., Hoffman, M. R., *Photochemical Transformation in Ice: Implications for the Fate of Chemical Species*. Geophys. Res. Lett., 2000. **27**(20): p. 3321-3324.
22. Klanova, J., Klan, P., Nosek, J., Holoubek, I., *Environmental Ice Photochemistry: Monochlorophenols*. Environ. Sci. Technol., 2003. **37**: p. 1568-1574.
23. Nikolaou, K., Masclet, P., Mouvier, G., *Sources and Chemical Reactivity of Polynuclear Aromatic Hydrocarbons in the Atmosphere - a Critical Review*. Sci. Total Environ., 1984. **32**: p. 103-132.
24. Raja, S., Valsaraj, K. T., *Adsorption and Transport of Gas-phase Naphthalene on Micron-size Fog Droplets in Air*. Environ. Sci. Technol. , 2004. **38**: p. 763-768.
25. Girardet, C., Toubin, C., *Molecular Atmospheric Pollutant Adsorption on Ice: A Theoretical Survey*. Surface Science Reports, 2001. **44**: p. 159-238.

26. Blank, M., Ottewill, R. H., *The Adsorption of Aromatic Vapors in Water Surfaces*. J. Phys. Chem., 1964. **68**: p. 2206-2211.
27. Karger, B.L., Castells, R. C., Sewell, P. A., Hartkopf, A., *Study of the Adsorption of Insoluble and Sparingly Soluble Vapors at the Gas-Liquid Interface of Water by Gas Chromatography*. J. Phys. Chem., 1971. **75**: p. 3870-3879.
28. Nathanson, G.M., Fsvidovits, P., Worsnop, D. R., Kolb, C. E., *Dynamics and Kinetics at the Gas-Liquid Interface*. J. Phys. Chem., 1996. **100**: p. 13007-13020.
29. Posner, A.M., Anderson, J. R., Alexander, A. E., *The Surface Tension and Surface Potential of Aqueous Solutions of Normal Aliphatic Alcohols*. J. Colloid Interface Sci., 1952. **7**: p. 623-644.
30. Hoff, J.T., Mackay, D., Gillham, R., Shiu, W. Y., *Partitioning of Organic Chemicals at the Air-Water Interface in Environmental Systems*. Environ. Sci. Technol., 1993. **27**: p. 2174-2180.
31. Davidovits, P., Hu, J. H., Worsnop, D. R., Zahniser, M. S., Kolb, C. E., *Entry of Gas Molecules into Liquids*. Faraday Discuss., 1995. **100**: p. 65-82.
32. MacKay, D., Shiu, W.Y., Valsaraj, K.T., Thibodeaux, L. J., *Air-Water Transfer: The Role of Partitioning*, in *Air-water Mass Transfer*, S.C. Wilhelms, Gulliver, J. S., Editor. 1991, American Society for Civil Engineers: New York.
33. Debestani, R., Ivanov, I. N., *A Compilation of Physical, Spectroscopic and Photophysical Properties of Polycyclic Aromatic Hydrocarbons*. Photochem. Photobiol., 1999. **70**: p. 10-34.
34. Finalayson-Pitts, B.J., Pitts, J. N., Jr., *Tropospheric Air Pollution: Ozone, Airborne Toxics, Polycyclic Aromatic Hydrocarbons and Particles*. Science, 1997. **276**: p. 1045-1051.
35. Beltran, F.J., Gonzalez, M., Rivas, J., *Advanced Oxidation of Polynuclear Aromatic Hydrocarbons in Natural Waters*. J. Env. Sci. Health, 1996. **A31**: p. 2193-2210.
36. Beltran, F.J., Ovejero, G., Rivas, J., *Oxidation of Polynuclear Aromatic Hydrocarbons in Water. 3. UV Radiation Combined with Hydrogen Peroxide*. Ind. Eng. Chem. Res., 1996. **35**: p. 883-890.
37. Beltran, F.J., Ovejero, G., Garcia-Araya, J. F., Rivas, J., *Oxidation of Polynuclear Aromatic Hydrocarbons in Water. 2. UV Radiation and Ozonation in the Presence of UV Radiation*. Ind. Eng. Chem. Res., 1995. **34**: p. 1607-1615.
38. Miller, J.S., Olejnik, D., *Photolysis of Polycyclic Aromatic Hydrocarbons in Water*. Wat. Res., 2001. **35**(1): p. 233-243.

39. Mahajan, T.B., Elsila, J. E., Deamer, D. W., Zare, R. N., *Formation of Carbon-Carbon Bonds in the Photochemical Alkylation of Polycyclic Aromatic Hydrocarbons*. *Origins of Life and Evolution of the Biosphere*, 2003. **33**: p. 17-35.
40. McConkey, B.J., Hewitt, L. M., Dixon, D. G., Greenberg, B. M., *Natural Sunlight Induced Photooxidation of Naphthalene in Aqueous Solution*. *Water, Air and Soil Pollution*, 2002. **136**: p. 347-359.
41. Arey, J.A., R.; Harger, W. P.; Helmig, D.; Sasaki, J., *Formation of Mutagens from the Atmospheric Photooxidation of PAH and Their Occurrence in Ambient Air*. 1994, Statewide Air Pollution Research Center, University of California: Riverside, CA.
42. Bernstein, M.P., Sandford, S. A., Allamandola, L. J., Gillette, J. S., Clemett, S. J., and Zare, R. N., *UV Irradiation of Polycyclic Aromatic Hydrocarbons in Ices: Production of Alcohols, Quinones, and Ethers*. *Science*, 1999. **283**: p. 1135-1138.
43. Mmereki, B.T., Donaldson, D. J., Gilman, J. B., Eliason, T. L., Vaida, V., *Kinetics and Products of the Reaction of Gas-phase Ozone with Anthracene Adsorbed at the Air-aqueous Interface*. *Atmos. Environ.*, 2004. **38**: p. 6091-6103.
44. Mmereki, B.T., Donaldson, D. J., *Direct Observation of the Kinetics of an Atmospherically Important Reaction at the Air-aqueous Interface*. *J. Phys. Chem. A* 2003. **107**: p. 11038-11042.
45. Finlayson-Pitts, B.J., Pitts, J. N. , *Chemistry of the Upper and Lower Atmosphere*. 2000, San Diego, California: Academic Press.
46. Clegg, S.M., Abbatt, J. P. D., *Uptake of Gas-Phase SO<sub>2</sub> and H<sub>2</sub>O<sub>2</sub> by Ice Surfaces: Dependence on Partial Pressure, Temperature, and Surface Acidity*. *J. Phys. Chem. A*, 2001. **105**(27): p. 6630-6636.
47. Abbatt, J.P.D., Beyer, K. D., Fucaloro, A. F., McMahon, J. R., Wooldridge, P. J., Zhang, R., Molina, M. J., *Interaction of HCl Vapor with Water-Ice: Implications for the Stratosphere*. *J. Geophys. Res.*, 1992. **97**(D14): p. 15,819-15,826.
48. Arora, O.P., Cziczo, D. J., Morgan, A. M., Abbatt, J. P. D., *Uptake of Nitric Acid by Sub-Micron-Sized Ice Particles*. *Geophysical Research Letters*, 1999. **26**(24): p. 3621-3624.
49. Shi, Q., Li, Y. Q., Davidovits, P., Jayne, J. T., Worsnop, D. R., Mozurkewich, M., Kolb, C. E., *Isotope Exchange for Gas-Phase Acetic Acid and Ethanol at Aqueous Interfaces: A Study of Surface Reactions*. *J. Phys. Chem. B*, 1999. **103**: p. 2417-2430.
50. Goss, K.U., *The air/surface adsorption equilibrium of organic compounds under ambient conditions*. *Critical Reviews in Environmental Science and Technology*, 2004. **34**(4): p. 339-389.

51. Mmereki, B.T., S.R. Chaudhuri, and D.J. Donaldson, *Enhanced uptake of PAHs by organic-coated aqueous surfaces*. Journal of Physical Chemistry A, 2003. **107**(13): p. 2264-2269.
52. Mmereki, B.T. and D.J. Donaldson, *Laser induced fluorescence of pyrene at an organic coated air-water interface*. Physical Chemistry Chemical Physics, 2002. **4**(17): p. 4186-4191.
53. Mmereki, B.T., J.M. Hicks, and D.J. Donaldson, *Adsorption of atmospheric gases at the air-water interface. 3: Methylamines*. Journal of Physical Chemistry A, 2000. **104**(46): p. 10789-10793.
54. Donaldson, D.J., *Adsorption of atmospheric gases at the air-water interface. I. NH<sub>3</sub>*. Journal of Physical Chemistry A, 1999. **103**(1): p. 62-70.
55. Demou, E. and D.J. Donaldson, *Adsorption of atmospheric gases at the air-water interface. 4: The influence of salts*. Journal of Physical Chemistry A, 2002. **106**(6): p. 982-987.
56. Donaldson, D.J. and D. Anderson, *Adsorption of atmospheric gases at the air-water interface. 2. C-1-C-4 alcohols, acids, and acetone*. Journal of Physical Chemistry A, 1999. **103**(7): p. 871-876.
57. Raja, S., et al., *Thermodynamic parameters for the adsorption of aromatic hydrocarbon vapors at the gas-water interface*. Journal of Chemical and Engineering Data, 2002. **47**(5): p. 1213-1219.
58. Raja, S. and K.T. Valsaraj, *Adsorption and transport of gas-phase naphthalene on micron-size fog droplets in air*. Environmental Science & Technology, 2004. **38**(3): p. 763-768.
59. Raja, S. and K.T. Valsaraj, *Heterogeneous oxidation by ozone of naphthalene adsorbed at the air-water interface of micron-size water droplets*. Journal of the Air & Waste Management Association, 2005. **55**(9): p. 1345-1355.
60. Donaldson, D.J., et al., *Uptake and reaction of atmospheric organic vapours on organic films*. Faraday Discussions, 2005. **130**: p. 227-239.
61. Mmereki, B.T., et al., *Kinetics and products of the reaction of gas-phase ozone with anthracene adsorbed at the air-aqueous interface*. Atmospheric Environment, 2004. **38**(36): p. 6091-6103.
62. Mmereki, B.T. and D.J. Donaldson, *Direct observation of the kinetics of an atmospherically important reaction at the air-aqueous interface*. Journal of Physical Chemistry A, 2003. **107**(50): p. 11038-11042.

63. Valsaraj, K.T., *Adsorption of Polycyclic Aromatic Hydrocarbons at the Air-water Interface and its Role in Atmospheric Deposition by Fog Droplets*. Environ. Toxicol. Chem., 2004. **23**(10): p. 2318-2323.
64. Subramanyam, V., Valsaraj, K. T., Thibodeaux, L. J., Reible, D., *Gas-to-Particle Partitioning of PAHs in an Urban Atmosphere*. Atmos. Environ., 1994. **28**: p. 3083-3091.
65. Montgomery, J.H., *Groundwater Chemicals: Desk Reference*. 2nd ed. 1996, Boca Raton, FL: CRC Press/Lewis Publishers.
66. Streckowski, R.S., George, C., *Measurement of Henry's Law Constants for Acetone, 2-Butanone, 2,3-Butanedione, and Isobutyraldehyde Using a Horizontal Flow Reactor*. J. Chem. Eng. Data, 2005. **50**: p. 804-810.
67. Smith, J.H., Bomberger, D. C., Haynes, D. L., *Predication of the Volatilization Rate of Intermediate and Low Volatility Chemicals from Natural Water Bodies*. Chemosphere, 1981. **10**: p. 281-289.
68. Sander, R., *Henry's Law data*. 69th ed. NIST Chemistry WebBook, NIST Standard Reference Database, ed. P.J. Lindstrom, Mallard, W. G. 2005, Gaithersburg, MD: U.S. Department of Commerce.
69. Alaei, M., Whittall, R. M., Strachan, W. M. J., *The Effect of Water Temperature and Composition on Henry's Law Constant for Various PAH's*. Chemosphere, 1996. **32**: p. 1153-1164.
70. Hung, H.H., Blanchard, P., Halsall, C. J., Bidleman T. F., Stern, G. A., Fellin, P., Muir, D. C. G., Barrie, L. A., Jantunen, L. M., Helm, P. A., Ma, J., Konoplev, A., *Temporal and Spatial Variability of Atmospheric POPs in the Canadian Arctic: Results from a Decade of Monitoring*. Sci. Total Environ., 2005. **342**: p. 119-144.
71. Li, X., Chen, J., Zhang, L., Qiao, X., Huang, L., *The Fragment Constant Method for Predicting Octanol-Air Partition Coefficients of Persistent Organic Pollutants at Different Temperatures*. J. Phys. Chem. Ref. Data, 2006. **35**(3): p. 1365-1384.
72. Sander, R., *Compilation of Henry's Law Constants for Inorganic and Organic Species of Potential Importance in Environmental Chemistry (Version 3)*. 1999.
73. Ben Naim, A. and Y. Marcus, *Solvation Thermodynamics of Nonionic Solutes*. Journal of Chemical Physics, 1984. **81**(4): p. 2016-2027.
74. Vacha, R., et al., *Adsorption of atmospherically relevant gases at the air/water interface: Free energy profiles of aqueous solvation of N-2, O-2, O-3, OH, H2O, HO2, and H2O2*. Journal of Physical Chemistry A, 2004. **108**(52): p. 11573-11579.
75. Dobson, C.M., Ellison, G. B., Tuck, A. F., Vaida, V., *Atmospheric Aerosols as Prebiotic Chemical Reactors*. Proc. Nat. Acad. Sci., 2000. **97**(2): p. 11864-11868.

76. Gill, P.S., Graedel, T. E., Weschler, C. J., *Organic Films on Atmospheric Aerosols Particles, Fog Droplets, Cloud Droplets, Raindrops, and Snowflakes*. Rev. Geophys. Space Phys., 1983. **21**: p. 903-920.
77. Seidl, W., *Model for a Surface Film of Fatty Acids on Rain Water and Aerosol Particles*. Atmos. Environ. , 2000. **34**: p. 4917-4932.
78. Latif, M.T., Brimblecombe, P., *Surfactants in Atmospheric Aerosols*. Environ. Sci. Technol., 2004. **38**: p. 6501-6506
79. Cappiello, A., De Simoni, E., Fiorucci, C., Mangani, F., Palma, P., Trufelli, H., Decesari, S., Facchini, M. C., Fuzzi, S., *Molecular Characterization of the Water-soluble Organic Compounds in Fogwater by ESIMS/MS*. Environ. Sci. Technol., 2003. **37**: p. 1229-1240.
80. Capel, P.D., Gunde, R., Zurcher, F., Giger, W., *Carbon Speciation and Surface Tension of Fog*. Environ. Sci. Technol., 1990. **24**(5): p. 722-727.
81. Donaldson, D.J., Vaida, V., *The Influence of Organic Films at the Air-aqueous Boundary on Atmospheric Processes*. Chem. Rev. , 2006. **106**: p. 1445-1461.
82. Davies, J.T., Rideal, E. K., *Interfacial Phenomena*. 2nd ed. 1961, New York, NY: Academic Press, Inc.
83. Thornton, J.A., Abbatt, J. P. D., *N<sub>2</sub>O<sub>5</sub> Reaction on Submicron Sea Salt Aerosol: Kinetics, Products, and the Effect of Surface Active Organics*. J. Phys. Chem. A, 2005. **109**: p. 10004-10012.
84. McNeill, V.F., Patterson, J., Wolfe, G. M., Thornton, J. A., *The Effect of Varying Levels of Surfactant on the Reactive Uptake of N<sub>2</sub>O<sub>5</sub> to Aqueous Aerosol*. Atmos. Chem. Phys. , 2006. **6**: p. 1635-1644.
85. Eliason, T.L., Gilman, J. B., Vaida, V., *Oxidation of Organic Films Relevant to Atmospheric Aerosols*. Atmos. Environ., 2003. **38**: p. 1367-1378.
86. Rana, D., Neale, G.H., and Hornof, V., *Surface Tension of Mixed Surfactant Systems: Lignosulfonate and Sodium Dodecyl Sulfate*. Colloid Polym. Sci., 2002. **280**: p. 775-778.
87. Browne, B.A., and Driscoll, C. T., *pH-Dependent Binding of Aluminum by a Fulvic Acid*. Environ. Sci. Technol., 1993. **27**: p. 915-922.
88. Thorn, K.A., Folan, D. W., and MacCarthy P., *Characterization of the International Humic Substances Society Standard and Reference Fulvic and Humic Acids by Solution State Carbon-13 (<sup>13</sup>C) and Hydrogen-1 (<sup>1</sup>H) Nuclear Magnetic Resonance Spectrometry*. 1989, U.S. Geological Survey, Water-Resources Investigations Report 89-4196: Denver, CO. p. 93.
89. Hayase, K., Tsubota, H., *Sedimentary Humic Acid and Fulvic Acid as Surface Active Substances*. Geochim. Cosmochim. Acta, 1983. **47**: p. 947-952.

90. Chen, J., Ehrenhauser, F. S., Valsaraj, K. T., Wornat, M. J., *Uptake and UV-photooxidation of Gas-phase PAHs on the Surface of Atmospheric Water Films. I. Naphthalene*. J. Phys. Chem. A, 2006. **110**: p. 9161-9168.
91. Valsaraj, K.T., *Elements of Environmental Engineering: Thermodynamics and Kinetics*. 2nd ed. 2000, Boca Raton, FL: CRC Press/Lewis Publishers.
92. Kahan, T.F., Donaldson, D. J., *Photolysis of Polycyclic Aromatic Hydrocarbons on Water and Ice Surfaces*. J. Phys. Chem. A, 2007. **111**(7): p. 1277-1285.
93. Kwamena, N.-O.A., Thornton, J.A., Abbatt, J.P.D., *Kinetics of Surface-Bound Benzo[a]pyrene and Ozone on Solid Organic and Salt Aerosols*. J. Phys. Chem. A, 2004. **108**(52): p. 11626 -11634.
94. Perraudin, E., Budzinski, H., Villenave, E., *Identification and Quantification of Ozonation Products of Anthracene and Phenanthrene Adsorbed on Silica Particles*. Atmos. Environ., 2007. **41**(28): p. 6005-6017.
95. Fasnacht, M.P., Blough, N. V., *Mechanisms of the Aqueous Photodegradation of Polycyclic Aromatic Hydrocarbons*. Environ. Sci. Technol., 2003. **37**: p. 5767-5772.
96. Karthikeyan, K.G., Chorover, J., *Effects of Solution Chemistry on the Oxidative Transformation of 1-Naphthol and Its Complexation with Humic Acid*. Environ. Sci. Technol., 2000. **34**: p. 2939-2946.
97. Hammond, G.S., Stout, C. A., Lamola, A. A., *Mechanisms of Photochemical Reactions in Solution. XXV. The Photodimerization of Coumarin*. J. Amer. Chem. Soc., 1964. **86**: p. 3103-3106.
98. Pramauro, E., Prevot, A. B., Vincenti, M., Brizzolesi, G., *Photocatalytic Degradation of Carbaryl in Aqueous Solutions Containing TiO<sub>2</sub> Suspensions*. Environ. Sci. Technol., 1997. **31**: p. 3126-3131.
99. Vacha, R., Slavicek, P., Mucha, M., Finlayson-Pitts, B. J., Jungwirth, P., *Adsorption of Atmospherically Relevant Gases at the Air/Water Interface: Free Energy Profiles of Aqueous Solvation of N-2, O-2, O-3, OH, H<sub>2</sub>O, HO<sub>2</sub>, and H<sub>2</sub>O<sub>2</sub>*. J. Phys. Chem. A, 2005. **108**: p. 11573-11579.
100. Poschl, U., Letzel, T., Kramer, L., Niessner, R., *The Reaction of Benzo[A]pyrene-Coated Soot Particles with Ozone: Products, Reaction Kinetics and Condensation Properties*. J. Aerosol Sci., 1999. **30**: p. S871-S872.
101. Levenspiel, O., *Chemical Reaction Engineering*. Ind. Eng. Chem. Res., 1999. **38**: p. 4140-4143.

102. Nissenson, P., Knox, C. J. H., Finlayson-Pitts, B. J., Phillips, L. F., Dabdub, D., *Enhanced Photolysis in Aerosols: Evidence for Important Surface Effects*. Phys. Chem. Chem. Phys., 2006. **8**: p. 4700-4710.
103. Wayne, R.P., *Chemistry of Atmospheres*. 3 ed. 2000, New York: Oxford University Press.
104. Bertram, A.I., A. V.; Hunter, M.; Molina, L. T.; Molina, M. J., *The Reaction Probability of OH on Organic Surfaces of Tropospheric Interest* J. Phys. Chem. A, 2001. **105**: p. 9415-9421.
105. Gilman, J.B., Vaida, V., *Permeability of Acetic Acid through Organic Films at the Air-aqueous Interface*. J. Phys. Chem. A, 2006. **110**: p. 7581-7587.
106. Donaldson, D.J., Mmereki, B. T., Chaudhuri, S. R., Handley, S., Oh, M., *Uptake and Reaction of Atmospheric Organic Vapours on Organic Films*. Faraday Discuss., 2005. **130**: p. 1-13.
107. Fasnacht, M.P., Blough, N. V., *Aqueous Photodegradation of Polycyclic Aromatic Hydrocarbons*. Environ. Sci. Technol., 2002. **36**: p. 4364-4369.
108. Bertilsson, S., Widenfalk, A., *Photochemical Degradation of PAHs in Freshwaters and Their Impact on Bacterial Growth - Influence of Water Chemistry*. Hydrobiologia, 2002. **469**: p. 23-32.
109. Zepp, R.G., Schlotzhauer, P. F., Sink, R. M., *Photosensitized Transformations Involving Electronic Energy Transfer in Natural Waters: Role of Humic Substances*. Environ. Sci. Technol., 1985. **19**: p. 74-81.
110. Vione, D., Maurino, V., Minero, C., Pelizzetti, E., Harrison, M. A. J., Olariu, R. I., Arsene, C., *Photochemical Reactions in the Tropospheric Aqueous Phase and on Particulate Matter*. Chem. Soc. Rev., 2006. **35**: p. 441-453.
111. Haag, W.R., Hoigne, J., *Singlet Oxygen in Surface Waters. 3. Photochemical Formation and Steady-State Concentrations in Various Types of Waters*. Environ. Sci. Technol., 1986. **20**: p. 341-348.
112. Latch, D.E., McNeill, K., *Microheterogeneity of Singlet Oxygen Distributions in Irradiated Humic Acid Solutions*. Science, 2006. **311**: p. 1743-1747.
113. Schlautman, M.A., Morgan, J. J., *Effects of Aqueous Chemistry on the Binding of Polycyclic Aromatic Hydrocarbons by Dissolved Humic Materials*. Environ. Sci. Technol., 1993. **27**: p. 961-969.
114. Canonica, S., Hoigne, J., *Enhanced Oxidation of Methoxy Phenols at Micromolar Concentration Photosensitized by Dissolved Natural Organic Material*. Chemosphere, 1995. **30**(12): p. 2365-2374.

115. Murov, S.L., Carmichael, I., Hug, G. L., *Handbook of photochemistry*. 2nd ed. 1993, New York: Marcel Dekker.
116. Remorov., R.G., George, C., *Analysis of Chemical Kinetics at the Gas-aqueous interface for submicron aerosols*. Phys. Chem. Chem. Phys., 2006. **8**: p. 4897-4901.
117. Facchini, M.C., Mircea, M., Fuzzi, S., Charlson, R. J., *Cloud Albedo Enhancement by Surface-Active Organic Solutes in Growing Droplets*. Nature, 1999. **401**: p. 257-259.
118. Gelencser, A., Sallai, M., Krivacsy, Z., Kiss, G., Meszaros, E., *Voltammetric Evidence for the Presence of Humic-Like Substances in Fog Water*. Atmos. Res., 2000. **54**: p. 157-165.
119. Facchini, M.C., Decesari, S., Mircea, M., Fuzzi, S., Loglio, G., *Surface Tension of Atmospheric Wet Aerosol and Cloud/Fog Droplets in Relation to Their Organic Carbon Content and Chemical Composition*. Atmos. Environ., 2000. **34**: p. 4853-4857.
120. Raja, S., Valsaraj, K. T., *Heterogeneous Oxidation by Ozone of Naphthalene Adsorbed at the Air-water Interface of Micron-size Water Droplets*. J. Air & Waste Manage. Assoc., 2005. **55**: p. 1345-1355.
121. Meyer, D., Dressler, H., Ruck, W., *Improvement of GC Sensitivity for Polar and Nonpolar PAHs by Using a Deactivated Liner*. LCGC North America, 2007. **25**(2): p. 180-190.
122. Remorov, R.G., George, C., *Analysis of Chemical Kinetics at the Gas-aqueous interface for submicron aerosols*. Phys. Chem. Chem. Phys., 2006. **8**: p. 4897-4901.
123. Anastasio, C., McGregor, K. G., *Chemistry of Fog Waters in California's Central Valley: I. In Situ Photoformation of Hydroxyl Radical and Singlet Molecular Oxygen*. Atmos. Environ., 2001. **35**: p. 1079-1089.
124. Allen, J.M., Gossett, C. J., Allen, S. K., *Photochemical Formation of Singlet Molecular Oxygen ( $^1O_2$ ) in Illuminated Aqueous Solutions of p-Aminobenzoic Acid (PABA)*. J. Photochem. Photobiol. B: Biol., 1996. **32**: p. 33-37.
125. Kajiwarra, T., Kearns, D. R., *Direct Spectroscopic Evidence for a Deuterium Solvent Effect on the Lifetime of Singlet oxygen in Water*. J. Am. Chem. Soc., 1973. **95**(18): p. 5886-5890.
126. Hayon, E., *Radiolysis of Heavy Water in the pD Range 0-14*. J. Phys. Chem. , 1965. **69**(8): p. 2628-2632.
127. Gauduel, Y., Pommeret, S., Antonetti, A., *Early Formation of Electron-Radical Pairs in a Polar Protic Liquid: Evidence of Ultrafast Concerted Electron-Proton Transfers*. J. Phys. Chem., 1993. **97**(1): p. 134-142.

128. Chen, J., Valsaraj, K.T., *Uptake and UV-Photooxidation of Gas-Phase Polyaromatic Hydrocarbons on the Surface of Atmospheric Water Films. 2. Effects of Dissolved Surfactants on Naphthalene Photooxidation*. J. Phys. Chem. A, 2007. **111**: p. 4289-4296.
129. Thomas, E.R., Frost, G. J., Rudich, Y., *Reactive Uptake of Ozone by Proxies for Organic Aerosols: Surface-Bound and Gas Phase Products*. Journal of Geophysical Research - Atmospheres, 2001. **106**: p. 3045-3056.
130. Woon, D.E., Park, J. Y., *Photoionization of Benzene and Small Polycyclic Aromatic Hydrocarbons in Ultraviolet-processed Astrophysical Ices: A Computational Study*. The Astrophysical Journal, 2004. **607**(1): p. 342-345.
131. Gudipati, M.S., Allamandola, L. J., *Polycyclic Aromatic Hydrocarbon Ionization Energy Lowering in Water Ices*. The Astrophysical Journal, 2004. **615**(2): p. L177-L180.
132. Gudipati, M.S., Allamandola, L. J., *Facile Generation and Storage of Polycyclic Aromatic Hydrocarbon Ions in Astrophysical Ices*. The Astrophysical Journal, 2003. **596**(2): p. L195-L198.

## APPENDIX I SUPPORTING INFORMATION FOR SECTION 5.3.2

### Derivation of the product formation rate via the SRFA-sensitized pathway

The amount of naphthalene partitioned into the SRFA region is a function of the SRFA concentration and is given by

$$N_{\text{Naph},1} = \frac{K_{\text{OM}}[\text{SRFA}]}{1 + K_{\text{OM}}[\text{SRFA}]} N_{\text{Naph,tot}} \quad \text{Eqn. S.1}$$

where  $K_{\text{OM}}$  is the partition coefficient of naphthalene to SRFA. Thus, naphthalene concentration in the SRFA region,  $[\text{Naph}]_1$ , can be given by

$$[\text{Naph}]_1 = \frac{N_{\text{Naph},1}}{V_1} = \frac{1}{V_1} \frac{K_{\text{OM}}[\text{SRFA}]}{1 + K_{\text{OM}}[\text{SRFA}]} N_{\text{Naph,tot}} \quad \text{Eqn. S.2}$$

Similarly,

$$[\text{Naph}]_2 = \frac{N_{\text{Naph},2}}{V_2} = \frac{1}{V_2} \frac{1}{1 + K_{\text{OM}}[\text{SRFA}]} N_{\text{Naph,tot}} \quad \text{Eqn. S.3}$$

Substituting Eqn. S.2 and Eqn. S.3 into Eqn. 5.10 shown in the text and noting that  $N_{\text{Naph,tot}}/V_{\text{tot}}=[\text{Naph}]$ , we obtain

$$\frac{d[\text{P}]}{dt}_{\text{SRFA}} = k_{\text{rxn}} \frac{K_{\text{OM}}[\text{SRFA}]}{1 + K_{\text{OM}}[\text{SRFA}]} [\text{Naph}][^1\text{O}_2]_{1,\text{SRFA}} + k_{\text{rxn}} \frac{1}{1 + K_{\text{OM}}[\text{SRFA}]} [\text{Naph}][^1\text{O}_2]_{2,\text{SRFA}} \quad \text{Eqn. S.4}$$

In their recent work, Latch and McNeill found that microheterogeneity of singlet oxygen distributions exist in irradiated humic acid solutions [112], suggesting a constant singlet oxygen concentration in the humic substance region and a linear dependence of the aqueous region singlet oxygen concentration on the concentration of the humic substances. According to this finding,  $[^1\text{O}_2]_{1,\text{SRFA}}$  in Eqn. S.4 is assumed to be constant and  $[^1\text{O}_2]_{2,\text{SRFA}}$  is expressed by  $[^1\text{O}_2]_{2,\text{SRFA}}=k_{\text{gen}}[\text{SRFA}]$ , where  $k_{\text{gen}}$  is a kinetic constant describing the concentration of singlet

oxygen in the bulk aqueous phase induced by SRFA. Rewriting Eqn. S.4 accordingly gives Eqn. 5.11 shown in the text.

### **Derivation of the product formation rate via the self-sensitized pathway**

The concentration of singlet oxygen in the bulk aqueous phase associated with the self-sensitized process is described using the Stern-Volmer approach by

$$[{}^1\text{O}_2]_{2,\text{Naph}} = \frac{[{}^1\text{O}_2]_0}{1 + k_q[\text{SRFA}]} \quad \text{Eqn. S.5}$$

where  $k_q$  is the quenching constant of SRFA and  $[{}^1\text{O}_2]_0$  is the concentration of singlet oxygen in the solution without SRFA. Although used to describe the concentration of singlet oxygen, the quenching constant  $k_q$  reflects the total quenching effect of SRFA on naphthalene excited states and does not imply the direct quenching of singlet oxygen by SRFA. Since the diffusion-controlled T-T energy transfer from triplet naphthalene to ground state SRFA is fast in the SRFA region, the self-sensitized process in the SRFA region is neglected and we obtain the product formation rate of the self-sensitized process as

$$\frac{d[\text{P}]}{dt}_{\text{Naph}} = \frac{V_2}{V_{\text{tot}}} k_{\text{rxn}} [\text{Naph}]_2 [{}^1\text{O}_2]_{2,\text{Naph}} \quad \text{Eqn. S.6}$$

Substituting Eqn. S.3 and Eqn. S.5 into Eqn. S.6 gives Eqn. 5.12 shown in the text.

### **Derivation of the product formation rate in the presence of SDS**

Based on the assumption that naphthalene molecules bound to SDS are not subject to the reaction with singlet oxygen, the product formation rate is expressed by

$$\frac{d[\text{P}]}{dt} = \frac{V_2}{V_{\text{tot}}} k_{\text{rxn}} [\text{Naph}]_2 [{}^1\text{O}_2] \quad \text{Eqn. S.7}$$

The distribution of naphthalene in the SDS aqueous solution is similar to that in the SRFA solution. Thus,

$$\frac{d[P]}{dt} = k_{\text{rxn}} \frac{1}{1 + K_{\text{OM}}[\text{SDS}]} [\text{Naph}][^1\text{O}_2] = k_{1,\text{obs}} [\text{Naph}] \quad \text{Eqn. S.8}$$

Noting that  $k_{\text{rxn}} \cdot [^1\text{O}_2] = k_{1,\text{obs}}^0$ , we obtain Eqn. 5.14 shown in the text.

## **APPENDIX II COPYRIGHT PERMISSION FOR PUBLISHED MATERIAL**

Chapters 3, 4, and 5 are based on two journal articles both published in the Journal of Physical Chemistry A, copyright by the American Chemical Society. Permission to include the published material in the dissertation has been extended by the American Chemical Society. A copy of the letter of copyright permission from the American Chemical Society is attached as follows.

## American Chemical Society's Policy on Theses and Dissertations

**If your university requires a signed copy of this letter see contact information below.**

Thank you for your request for permission to include **your** paper(s) or portions of text from **your** paper(s) in your thesis. Permission is now automatically granted; please pay special attention to the implications paragraph below. The Copyright Subcommittee of the Joint Board/Council Committees on Publications approved the following:

### Copyright permission for published and submitted material from theses and dissertations

ACS extends blanket permission to students to include in their theses and dissertations their own articles, or portions thereof, that have been published in ACS journals or submitted to ACS journals for publication, provided that the ACS copyright credit line is noted on the appropriate page(s).

### Publishing implications of electronic publication of theses and dissertation material

Students and their mentors should be aware that posting of theses and dissertation material on the Web prior to submission of material from that thesis or dissertation to an ACS journal may affect publication in that journal. Whether Web posting is considered prior publication may be evaluated on a case-by-case basis by the journal's editor. If an ACS journal editor considers Web posting to be "prior publication", the paper will not be accepted for publication in that journal. If you intend to submit your unpublished paper to ACS for publication, check with the appropriate editor prior to posting your manuscript electronically.

If your paper has not yet been published by ACS, we have no objection to your including the text or portions of the text in your thesis/dissertation in **print and microfilm formats**; please note, however, that electronic distribution or Web posting of the unpublished paper as part of your thesis in electronic formats might jeopardize publication of your paper by ACS. Please print the following credit line on the first page of your article: "Reproduced (or 'Reproduced in part') with permission from [JOURNAL NAME], in press (or 'submitted for publication'). Unpublished work copyright [CURRENT YEAR] American Chemical Society." Include appropriate information.

If your paper has already been published by ACS and you want to include the text or portions of the text in your thesis/dissertation in **print or microfilm formats**, please print the ACS copyright credit line on the first page of your article: "Reproduced (or 'Reproduced in part') with permission from [FULL REFERENCE CITATION.] Copyright [YEAR] American Chemical Society." Include appropriate information.

**Submission to a Dissertation Distributor:** If you plan to submit your thesis to UMI or to another dissertation distributor, you should not include the unpublished ACS paper in your thesis if the thesis will be disseminated electronically, until ACS has published your paper. After publication of the paper by ACS, you may release the entire thesis (**not the individual ACS article by itself**) for electronic dissemination through the distributor; ACS's copyright credit line should be printed on the first page of the ACS paper.

**Use on an Intranet:** The inclusion of your ACS unpublished or published manuscript is permitted in your thesis in print and microfilm formats. If ACS has published your paper you may include the manuscript in your thesis on an intranet that is not publicly available. Your ACS article cannot be posted electronically on a publicly available medium (i.e. one that is not password protected), such as but not limited to, electronic archives, Internet, library server, etc. The only material from your paper that can be posted on a public electronic medium is the article abstract, figures, and tables, and you may link to the article's DOI or post the article's author-directed URL link provided by ACS. This paragraph does not pertain to the dissertation distributor paragraph above.

Questions? Call +1 202/872-4368/4367. Send e-mail to [copyright@acs.org](mailto:copyright@acs.org) or fax to +1 202-776-8112. 10/10/03, 01/15/04, 06/07/06

## VITA

Jing Chen was born in 1981 in the People's Republic of China. She received her Bachelor of Science degree from Fudan University in June 2003. In August 2003, she came to Louisiana State University to pursue her doctoral degree.

Her list of publications and presentations that resulted from this project thus far includes:

J. Chen, F. S. Ehrenhauser, K. T. Valsaraj, and M. J. Wornat, "Uptake and UV-Photooxidation of Gas-Phase PAHs on the Surface of Atmospheric Films. 1. Naphthalene", *Journal of Physical Chemistry A*, 110, 9161-9168 (2006).

R. Vacha, P. Jungwirth, J. Chen, and K. T. Valsaraj, "Adsorption of Polycyclic Aromatic Hydrocarbons at the Air-Water Interface: Molecular Dynamics Simulations and Experimental Atmospheric Observations", *Physical Chemistry Chemical Physics*, 8, 4461-4467 (2006).

J. Chen and K. T. Valsaraj, "Uptake and UV-Photooxidation of Gas-Phase PAHs on the Surface of Atmospheric Films. 2. The Effects of Dissolved Surfactants on Naphthalene Photooxidation", *Journal of Physical Chemistry A*, 111, 4289-4296 (2007).

S. Raja, R. Raghunathan, X. Y. Yu, T. Lee, J. Chen, R. R. Kommalapati, K. Murugesan, X. Shen, Q. Yuan, K. T. Valsaraj and J. L. Collett, "Fog Chemistry in the Texas-Louisiana Gulf Coast Corridor", *Atmospheric Environment*, 42, 2048-2061 (2008).

J. Chen, F. S. Ehrenhauser, K. T. Valsaraj, and M. J. Wornat, "Adsorption and UV Photo-Oxidation of Gas-Phase Phenanthrene on Atmospheric Films", in ACS Symposium Series: Atmospheric Aerosols: Characterization, Chemistry and Modeling, K. T. Valsaraj and R. R. Kommalapati (editors), ACS Books Department, Washington, D. C., 2008 (Submitted).

J. Chen and K. T. Valsaraj, Proc. 99th AWMA Ann. Conf., Paper # 162, New Orleans, LA, 2006.

K. T. Valsaraj and J. Chen, 233rd ACS National Meeting, Paper # 1029723, Chicago, IL, 2007.

J. Chen and K. T. Valsaraj, 234th ACS National Meeting, Paper # 1069531, Boston, MA, 2007.